Title

EXPERIMENTAL SITUATION OF NUCLEON TRANSFER BETWEEN HEAVY IONS, ELASTIC AND INELASTIC SCATTERING OF HEAVY IONS

Author

Becchetti, F.D.

Publication Date

1972-06-01

Talk presented at the ORNL Heavy-Ion
Summer Study, Oak Ridge, TN,
June 12-23, 1972

LBL-1208

EXPERIMENTAL SITUATION OF NUCLEON TRANSFER BETWEEN HEAVY IONS, ELASTIC AND INELASTIC SCATTERING OF HEAVY IONS

F. D. Becchetti

June 1972

AEC Contract No. W-7405-eng-48

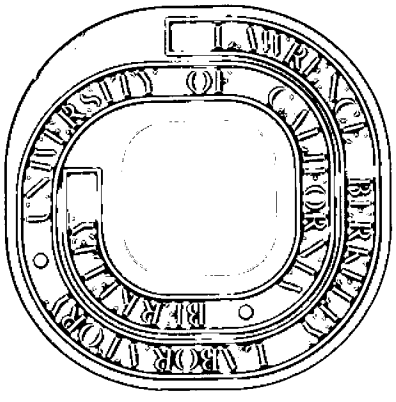

LBL-1208

DISCLAIMER

LBL-1208

EXPERIMENTAL SITUATION OF NUCLEON TRANSFER BETWEEN HEAVY IONS, ELASTIC AND INELASTIC SCATTERING OF HEAVY IONS*

F. D. Becchetti

Department of Chemistry
and Lawrence Berkeley Laboratory
University of California
Berkeley, California 94720

June 1972

BECCHETTI:

Well, today experimentalists strike back. I am going to show a lot of data. I hope I don't bore the theoreticians too much. I have also taken the liberty of introducing a bit of theory, but it is rather painless. The data I will be showing are from five or six sources: the Niels Bohr Institute (NBI) (the data are mostly 60 MeV oxygen and carbon on various nuclei between calcium and molybdenum); then there's some data from Berkeley (LBL) which are at $\sim$ 100 MeV on a number of nuclei; and then there are data from Argonne (ANL) and Saclay (CEN) which are at lower energies, 40 to 50 MeV. There are also data from BNL, Orsay, and Oxford, which I will slip in occasionally. So please excuse me if I don't reference all the data properly.

I refer you to some conference proceedings: the Heidelberg heavy ion conference[1] which was held in 1969; the Dubna conference[2] which was held in February, 1971; the Saclay conference[3] which was held last September (1971) and published in a supplement of Journal de Physique;[3] and the current meeting in France at Aix-en-Provence,[4] which will also have a heavy ion session.

---

*A talk presented at the ORNL Heavy-Ion Summer Study, June 12-23, 1972

Work done under the auspices of the U.S. Atomic Energy Commission.

There are a number of features of heavy ion reactions, and I will attempt at the end to show why one might use heavy ions rather than light ions. It is sort of an after-the-fact justification, of course, but there are a number of unique features that do appear, although these were not apparent at the beginning. I will start first by talking about nucleon transfer, the sort of cross sections one expects, and then say something about kinematics, because they play a very dominant role, and then give a semi-classical interpretation of the data which allows one to extract a good deal of information. I will also say something about the quantitative information one obtains, i.e. what can one learn about structure? Finally I will talk about DWBA and elastic and inelastic scattering.

Figure 1 shows what happens when one bombards calcium with 70 MeV ^{16}O, as was done at Stanford.[5] This is looking with a counter telescope with time of flight, so the mass separation is good. Figure 1 shows the number of particles transferred to the projectile. What one observes is a Gaussian distribution, skewed, depending on the reaction, i.e. stripping or pick up. This is a consequence of some kinematic effects which I will discuss later. The essential thing is that the cross sections are millibarns for the one nucleon transfers and then drop between a factor of $\sim$ 3-10 with succeeding nucleon transfers. However, even for multi-nucleon transfers the cross sections are still measurable. There are some anamolies. In particular, for ^{16}O projectiles this occurs for carbon 12, which indicates a special process. I will discuss this later.

GREINER: The ^{24}Mg - is this pick up or a spallation process?

BECCHETTI: One could think of that as a spallation of the target, I would think. We have done some measurements at Berkeley on target spallation and this is possible.

Figure 2 shows data for argon on thorium. These are the well known experiments done at Dubna using a spectrometer with a counter-telescope in the focal plane.[6] These data are at the grazing angle so these are, at least partially, direct transfers. Again one observes, looking at the yields, a factor of 3 to 10 between successive nucleon transfers. Apparently one can extrapolate down and make a fairly good estimate of the cross sections for multi-nucleon transfers.

In Fig. 3 we show some spectra. This happens to be oxygen on iron.[7] This target is, for some reason, one of the chosen targets where just about all heavy ion reactions proceed with very nice cross sections. In this case, we have single proton stripping from ^{16}O, so it should be compared with (d,n), (α,t) or (^{3}He,d). (^{3}He,d) spectroscopic factors are shown here. One can in general make a correspondence, particularly with the high spin states, between the two reactions. Concurrently, one obtains (^{16}O,^{14}N), which is a proton neutron transfer. The ground state is calculated to be channel 157, and isn't seen. The strongest states are at 0.6 MeV and 3.8 MeV. These happen to be states of a certain configuration and indicate some selectivity for this particular reaction.

Figure 4 shows the carbon spectra one obtains -- this also happen to be on iron. $^{54}Fe(^{16}O,^{12}C)$, of course, is one of the experiments that started the whole game, done originally at Saclay.[8] The data shown are at 60 MeV. In Fig. 1 ^{12}C was the particle that showed the anomalous increase from the systematics. The large bump corresponds (at least I believe and a lot of other people believe) to a break-up spectrum of the projectile into ^{12}C plus alpha. The bump starts essentially at the break-up Q-value ($\sim$8 MeV), is relatively independent of

target, and has many of the characteristics one would expect of break up, although not necessarily Coulomb break up. Superimposed on this are a number of sharp states. The ground state is weakly populated, and then there are a number of states that correspond to collective levels (the 3^- in particular here). At the top we have (^{16}O,^{14}C) which is a very useful experiment since the equivalent is (^{3}He,n). In (^{16}O,^{14}C) we again populate some selected levels.

A serious problem is the projectile break up which is inherent to heavy ions. One way to avoid it is by carefully choosing bombarding energies -- this is shown in Fig. 5.

D. THOMAS: How do you know this is break up and not actual transfer of the nucleons?

BECCHETTI: Well, there do not appear to be any states. At least the density of the states would have to be extremely large, and would have to be the same for most nuclei. The states would have to be at different excitation energies, but at about the same Q value for all nuclei. Also, the angular distributions are different than those for the resolved states.

At Saclay they have shown that if one comes down closer to the barrier, then most of what I call break up (the mechanism is not completely understood), can be avoided and one obtains relatively clean ^{12}C spectra.[9] As one goes up in energy, the "break up" increases and eventually, as shown in Fig. 6, will dominate the (^{16}O,^{12}C) spectrum.

Another way to avoid the break-up problem is to choose a different projectile, one that doesn't like to break up into the particular channel one is looking at. Figure 7 shows some recent data from Saclay[10] for (^{18}O,^{14}C) and

(^{14}N,^{10}B). As one can note, the cross section is down a great deal from (^{16}O,^{12}C). They see a number of states populated in both reactions and are able to answer one particular question: A group at 4.4 MeV seen in $^{54}Fe(^{16}O,^{12}C)^{58}Ni$ (Fig. 5) could be the carbon-12 first excited state. In Fig. 7 one sees this group in both of the reactions, so it doesn't appear to be due to the excited state of carbon-12 in (^{16}O,^{12}C) but to a state in ^{58}Ni.

I should say something about the single-nucleon transfers since these show some interesting properties. Figure 8 shows data taken at Berkeley with a spectrometer and a focal plane counter.[11] The abscissa is now focal plane position. This is for ^{54}Fe, the standard target. Here we compare three different reactions[12] -- at the top, (^{12}C,^{11}B) to ^{55}Co, (^{16}O,^{15}N) to ^{55}Co, (note the differences) and (^{16}O,^{15}O) to ^{55}Fe. In the latter case I have lined up the $p_{3/2}$ neutron state with the $p_{3/2}$ proton state in ^{55}Co. There is a great deal of selectivity and one can do a number of these analog type reactions. This of course is nothing different from light ion reactions except, perhaps surprisingly, one can get a very different population of states depending on the final states. I'll say something about this later concerning the selection rules for these reactions.

Figure 9 shows some two-nucleon transfer data on ^{208}Pb taken at Berkeley. The top is (^{12}C,^{14}C) and the bottom is (^{16}O,^{18}O). This shows another problem encountered in heavy-ion experiments: the excitation of the outgoing projectile. I refer you first to the bottom of Fig. 9 where we have ^{18}O coming out. ^{18}O has a low lying 2^+ state and then a number of levels above that. The two groups marked with arrows correspond very nicely to ^{18}O in its 2^+ state leaving ^{206}Pb

in its first two excited states. Although it is not completely apparent in this figure, these groups are Doppler-broadened due to the gamma decay of the excited ^{18}O. This is one way of detecting projectile excitation. However, if one observes a more appropriate outgoing projectile, for example in this case ^{14}C, the excited states don't start until ~ 6 MeV, which gives a fairly clean spectrum at least up to that excitation energy. Above ~ 6 MeV we have some groups that appear to be Doppler-broadened and don't appear as sharp states. Perhaps the interesting thing here is the lack of strength to states in ^{206}Pb other than the first few collective levels. The angular distributions, however, are featureless and somewhat discouraging. Figure 10 shows some other projectile excitation effects. This happens to be for ^{18}O induced reactions:[13] $(^{18}O,^{20}Ne)$ and $(^{18}O,^{19}F)$. A number of low-lying states in fluorine show up in the spectrum. Similarly, with $(^{18}O,^{20}Ne)$ many groups can be identified with states in ^{20}Ne, and are the strongest in the spectra.

Figure 11 shows some angular distribution for $(^{16}O,^{14}C)$. These data are from Argonne.[14] They show two angular momentum transfers (to the target) $\ell=0$ and $\ell=2$ to the ground state 0^+ and the first 2^+ excited states in the residual nuclei. These data are at 48 MeV for a number of f-p shell nuclei. If you compare $\ell=0$ and $\ell=2$ there is not much to distinguish between the two. This means, of course, that there are no signatures which one can use to assign the spin and parity of the final states. There are some systematics with regards to Q value and target Z. These, however, are not related to spectroscopy. Figure 12 shows the situation for the proton stripping reaction $(^{16}O,^{15}N)$, (again data from Argonne) as a function of bombarding energy and angular-momentum transfer. The ℓ is the angular-momentum transfer to the target, $\ell=3$ and $\ell=1$, i.e. $f_{7/2}$ and

$p_{3/2}$ final states. There are systematic shifts with bombarding energy, but again no discernable signatures. Figure 13 shows some data for $^{208}Pb + ^{16}O$ and ^{12}C to a number of single-particle states.[12] In this case we believe that most of these are good single-particle states. Again, we see the general characteristic of peaking at an angle, which corresponds to a grazing collision, and then a fall-off from that angle. Again, no discernable signatures. Figure 14 shows some data taken at Argonne for ^{18}O induced reactions.[15] In this case the outgoing projectile can be excited and one sees a difference in the angular distributions. In particular, for $(^{18}O,^{20}Ne)$ leaving ^{20}Ne in its 1.63 MeV state (2^+), the angular distribution is shifted forward in angle by $\sim 10°$. Similarly the $(^{18}O,^{19}F)$ reaction leaving fluorine in its excited state is also shifted forward. This may be explained, eventually, by a microscopic model. It is another way of telling if the projectile is excited. The shapes of $\sigma(\theta)$, however, do not depend strongly on ℓ-transfer.

This situation (lack of ℓ-signature) does not hold for inelastic scattering, however. Figure 15 shows data taken at Berkeley for $(^{16}O,^{16}O)$ on ^{208}Pb at 104 MeV.[16] The elastic data are also shown. I've shown the data unbiased by calculations. In this case we're exciting the 3^- octupole state, the 5^- state, and the 2^+ state. We see characteristic shapes which depend on ℓ-transfer (also Q value). There is an indication that the mechanism here is different or that some other feature, something about inelastic scattering, is unique. I will come back to this later.

GRIENER: What is the Coulomb barrier?

BECCHETTI: The barrier is about 75 MeV. All the data I am showing were taken above the Coulomb barrier.

Now if one looks at the magnitudes of transfer cross sections, there are a number of systematics. Figure 16 summarizes some data taken at the Niels Bohr Institute[7,13,17] for the one nucleon transfer reactions indicated: (^{16}O,^{17}O and ^{15}O), and (^{16}O,^{15}N), and (^{18}O,^{19}F). The proton transfers on the nickel and the zirconium isotopes show a very rapid change in the cross section with the target isotope. This cannot be explained by spectroscopy alone. For example, at the closed proton shells, we're adding just a proton. This leads one to a consideration of the kinematic effects since these, in many cases, determine whether or not one can do an experiment easily. The changes shown are roughly one to two orders of magnitude and can be correlated with the Q values. The Q values are only changing by a few MeVs and the cross sections, however, change rapidly over the limited range of Q value. This also applies to the multi-nucleon transfers, which are shown in Fig. 17. These are ground-state multi- for (^{16}O,^{14}C and ^{14}N) and (^{18}O,^{16}O and ^{20}Ne). If we look, for example, at the two-proton transfer on a closed proton shell nucleus, we see the same sort of behavior -- rapid variations of cross sections with the target. Again, these can be correlated with Q value.

Figure 18 summarizes some of the Saclay (^{16}O,^{12}C) data[9] in which a number of isolated levels are populated, in many cases very strongly and in other cases not so strongly. Because of the kinematics, however, one has to be very careful when interpreting the spectra. What I've shown in Fig. 19 are spectra as functions of Q value. This shows my own particular bias in looking at these spectra. This is for two-proton transfer (^{16}O,^{14}C) (again mostly data from Copenhagen) into the nuclei ^{60,62,64,66}Zn and into some heavier nuclei:

zirconium and molybdenum. If one looks at a particular type of state, for example the ground states or the 3^- states, there tends to be a preferential Q value. In this case it's $\sim$ -10 MeV for the two-proton transfer. If one now looks at the 4-nucleon transfer (^{16}O,^{12}C) to a specific type of state, say the collective states, again we see (Fig. 20) a preferred Q value. For example, the ground states which are well off the preferred Q value are populated weakly. An illustration of how this effects the comparison of spectra is shown in Fig. 21. The top is a comparison of (^{16}O,^{12}C) and (^{16}O,^{14}C) into ^{52}Cr, i.e. the same residual nucleus (data from Saclay). This shows the spectra as functions of excitation in ^{52}Cr. One sees a difference in the two spectra. If you then compare these spectra as functions of Q value, as shown below, you find that the strongest states in both spectra are at about the same Q value. Therefore, one has to be very careful in comparing spectra without consideration of the kinematic effects.

Now comes the painless theory, If one looks at kinematic parameters, one sees that they are completely different than those for light ion reactions. Figure 22 is a plot of the Coulomb parameter η versus the inverse wave number K. One can classify transfer reactions in terms of quantum-mechanical and semi-classical processes. The (d,n) and (^{3}He,d) reactions for example, are characterized by low values of K and η and are quantum-mechanical in nature. The typical L-transfers are comparable to the angular momentum being brought into the reaction and this leads to diffraction phenomena in the angular distributions. For heavy-ions, however, one has a situation where $\eta >> 1$, and the angular momentum transfer is typically less than the angular momentum brought in (in the reactions I have shown, typically 20 to 60 $\hbar$). The wavelength for these reactions above the Coulomb barrier is on the order of a few fermis.

If one calculates a mean free path, it is extremely small in nuclear matter i.e. much less than a nuclear radius. For projectiles where the motion of the wave-packet can be described semi-classically, one finds that the overlap between trajectories in either a semi-classical model or a distorted-wave model (a quantum-mechanical model) becomes extremely critical. This is shown very nicely in the work of Buttle and Goldfarb[18] using a quantum-mechanical treatment for sub-Coulomb reactions (CWBA). One finds that this same type of treatment should be applicable above the barrier. In fact, it may be even more applicable since the wavelengths become even smaller. In the case illustrated in Fig. 23 the overlap of some Coulomb-waves for a hypothetical reaction (L=0 neutron transfer) is shown.[18] The overlap is characterized by the parameter Δa, which is the difference in distance of closest approach in the incident and final channel. If the Q value is changed slightly, in this case 5 MeV (corresponding to a mismatch of 1.2 fermis, which is now on the order of the wave packet dimension) the overlap becomes very poor. A consequence of this is a strong Q-value dependence in the cross sections as shown in Fig. 24. The Q-value is shown at the bottom and overlap parameter Δa, in fermis, is on the top. One sees that for $\Delta a > \pm 1/2$ fm, the cross sections fall exponentially with Q value. Now above the barrier one can also use this type of approach if one introduces, instead of Δa, ΔD which is the difference in distances of closest approach for grazing collisions, that is, for the grazing angle [$D = \eta/k(1+\varepsilon)$; $\Delta D = D_f - D_i$; $\varepsilon \approx \csc^{\theta}/2$]. One can do better,[13] but for the purpose here I have used the semi-classical expression. Some one- and two-nucleon transfer data are shown in Fig. 25. Ground-state to ground-state and some ground-state to excited-state transitions are shown for a series of isotopes as a function of the parameter ΔD,

the overlap parameter, in fermis. For example, there is (^{16}O,^{14}C) on the nickel and iron isotopes. The data shown come from several sources.[7,9,13,14,19] There are also neutron transfer reactions. For example on the zirconium, molybdenum and nickel isotopes, neutron pick up and stripping are shown. One finds that above the barrier the criterion $\Delta D \sim 0$ appears to be applicable. The top of Fig. 25 shows some single-nucleon transfer data, again on series of isotopes, so the spectroscopy should not enter very strongly (of course, it does enter). Again, one finds the orbit mismatch limited to $\Delta D < \pm 1$ fermi, and beyond that the cross-sections drop rapidly.* Figure 26 shows some DWBA calculations using the Tobocman form factor with the DWBA program DWUCK (P.D. Kunz). The data are at 60 MeV, i.e. well above the barrier and, if you recall, the Buttle and Goldfarb calculations which were sub-Coulomb, showed exactly the same behavior. Shown are proton transfers on nickel plotted versus ΔD. I've shown two different L transfers (See Fig. 46). There is an effect due to L transfer.* This can be included, if you like, using some simple expressions.[13] We see the same general behavior: a Q value change of a few MeV can change the cross sections orders of magnitude.

Figure 27 shows the four-nucleon transfer (^{16}O,^{12}C), again on a series of isotopes, leading to the same type of final states. These are for the calcium and nickel isotopes. There are data from Saclay[9] (48 MeV) and some data from Copenhagen[13] (nickel $\longrightarrow$ zinc). Again we see the same sort of behavior with the overlap parameter ΔD. The calculation shown is a DWBA calculation due to Von Oertzen,[20] assuming a cluster-type transfer mechanism. Thus $\Delta D \sim 0$ holds for multi-nucleon transfer cross sections.

*The range of allowable mismatch, $\Delta D(L \neq 0) \propto (2L+1)\ \Delta D(L=0)$.

RASSMUSSEN: How is ΔD calculated above the barrier? As if Coulomb waves go on in?

BECCHETTI: Yes. So there is an approximation there. In the simple semi-classical picture ΔD appears as an exponential factor in the overlap integrals.* I refer you to a paper by Winther.[21] Also in the theory of Tautmann and Alder, the overlap appears as an exponential factor.[22] This has the consequence that the optimum Q-value can be written, at least in first order, as

$$Q/E \doteq Z_t/Z_i$$

where Z_t is the charge transfer to the projectile and Z_i is the projectile charge. This is the criterion given by Buttle and Goldfarb[18] and appears to be applicable above the barrier also.

The angular distributions can also be interpreted in terms of semi-classical theory. Figure 28 reviews the theory (most of the theory is due to Rutherford, or actually Kepler, or ?). That's about all one needs for a qualitative interpretation. Unfortunately, there's a quantum jump between obtaining qualitative results and the quantitative or quantum-mechanical results. But anyway, for elastic scattering we assume that we have well defined orbits given by the incident angular momentum, energy and charges. There is an impact parameter b, a distance of closest approach, D, and an eccentricity ε. For elastic scattering we have $\varepsilon = 1/\sin(\theta/2)$. We also have the relation that $D(\theta) = \eta/k(1+\varepsilon)$, which reduces to the expression shown. For transfer reactions, one must be careful

*The dependence of the cross sections with ΔD is $\exp - \frac{1}{2\alpha D} \left| \frac{\Delta D}{\pi} \right|^2$ where α is the bound state parameter. (see Ref. 21)

since the eccentricities are not simply related to the observation angle, θ, unless other approximations are made.[13] The angular momenta are related by the relation shown which involves D, K, and η. To describe the angular distributions it is useful to define the apsidal distance distribution $d\sigma/dD$ which is just a geometrical factor times the angular distribution ,$d\sigma/d\Omega$. One sees that for elastic scattering this transforms the angular distribution which is a function of θ into a linear distribution in D, where Θ = 180° to 0° and D = a/2 to infinity. For transfer reactions Breit and Ebel[23] among others, showed that in the semi-classical picture $d\sigma/dD$ has a very simple form given essentially by the expression shown in Fig. 28. The main dependence with angle is given by an exponential term ,$\exp(-2\alpha D)$, where α is the bound-state parameter of the transferred nucleon. To be symmetric, one takes averages for α, D, etc. One finds that log $(d\sigma/dD)$ is nearly linear, with slope related to the bound-state parameter of the transferred nucleon. One can make some hand waving arguments that the apsidal distance distribution is approximately equal to D^3 times the square of the form factor (as a function of D) times a quantity $(1-P_{abs})$ which I'll call the absorption factor (I'll show how one gets this quantity later). One sees that for Rutherford scattering or tranfer reactions (and also I'll show for inelastic scattering) one can make a relation between features in the angular distributions and features in the radial part of the form factor.

So that's the painless theory and now I have to convince you that it has some application. Figure 29 shows $d\sigma/dD$, the apsidal distance distribution, versus a quantity d_0, which is D, the average distance of closest approach, divided by $A_1^{1/3} + A_2^{1/3}$. This gives an idea of where the reactions are taking

place. We find (if D has any physical meaning, which is another problem) that $d_0 \approx 1.6$-1.8fm i.e. $\sim 60\%$ larger than the sum of half density radii and well outside the nuclear interiors. I've shown in Fig. 30 a number of different nucleon transfers as functions of energy and masses. We see at a certain radius that the angular distributions turn over and fall off. Figure 31 shows the same sort of thing for some multi-nucleon transfers. The angular distributions here are not so pronounced, as far as features, but again one can say that the maxima occur in the same interaction region, which is well outside the nuclear interiors. One would expect a simple behavior for $(d\sigma/dD)$ from tunneling.[23] The absorption factor $(1-P_{abs})$ which appeared (Fig. 28), can be determined by measuring the elastic scattering $(1-P_{abs} = \sigma/\sigma_R)$. This is shown in Fig. 32. I've plotted the elastic scattering, which was measured for a number of nuclei,[13,24] versus the d_0 parameter, $D(\theta)/A_1^{1/3} + A_2^{1/3}$. We see that the elastic scattering turns over at $d_0 \approx 1.6$fm, which was the same d_0 that the apsidal distance distributions turned over. One can represent the elastic scattering by a two parameter model.[13] Such a model comes out of a simple semi-classical picture where one takes Coulomb orbits and introduces absorption[13] (there will be a paper by Winther et al. on this subject). In this simple picture, then, we have an absorption factor, which we can now divide out and in principle get the tunnelling distributions. These are shown in Fig. 33. Taking out the absorption in this sort of a crude manner, one obtains $d\sigma/dD$ versus D. Determining the slope, gives a parameter here which I will call κ. In other words, $d\sigma/dD \alpha e^{-\kappa D}$. Above the barrier κ can be considered to be a phenomonlogical parameter. Essentially only one parameter, κ, is necessary to describe an angular distribution and κ should be related to the

form factor. This is shown in Figs. 33-34 for some one-, two-, and three-nucleon transfers.[13] This is all "super-Coulomb" and one finds the typical values of κ shown. We see as we go towards the barrier, this phenomenological parameter κ, converges toward the value expected in the simple tunnelling model, $\kappa \approx 2\alpha$. In this picture then, the angular distributions should have little L-signature. The angular distributions mostly reflect some geometrical properties of the form factor and do not depend on L-transfer, unless the form factor itself depends strongly on L transfer. For single nucleon transfer, we are looking at the asymptotic part of the form factor, since the strong absorption limits the transfer to large separations. This yields a simple, featureless angular distribution, as is observed.

An indication of L-signature comes from inelastic scattering,[16] as shown in Fig. 13. I will go into the details of the form factor later, but it may have a node at a (large) radius depending on the L-transfer. One can see that this produces oscillations in the angular distributions. By dividing out the absorption, σ/σ_R, one can see the correlation between the radial dependence of the form factor and angular distribution. Shown in Fig. 35 is a form factor[24] plotted versus $D(\theta)$. In principle the minimum in $d\sigma/d\Omega$ should occur at the same radius as the node in the form factor. In fact, we find that there is a shift. This may be attributed to distortion effects. The qualitative picture appears to be valid, however.

Figure 36 shows an excitation function. In the simple model $d\sigma/d\Omega \alpha d\sigma/dD \alpha f(D)$ and one can vary either the bombarding energy or the scattering angle to measure $d\sigma/dD$. The last figure showed an angular distribution[24], this

figure shows some data (taken at Copenhagen[25]) where the bombarding energy was varied. A minimum appears, in this case at $D(\theta) \sim 11.5$ fm, which is again near the node in the form factor.

Well all this may be very interesting to someone interested in semi-classical theory. What does it say about nuclear structure, however? This is more complicated since we usually have to do calculations. There are some things that we can learn by judiciously comparing spectra, for example. I will give some examples but will not say anything very quantitative. Figure 37 shows $(^{16}O,^{14}C)$ into ^{52}Cr. We compare, in this case, (p,t), (t,p), and two-proton transfer. What one does not see in $(^{16}O,^{14}C)$ is strong excitation of the second 0^+ and 2^+ states. What one does see is the ground state and a 3^- state; this, I believe, says something interesting about the states seen in (p,t) and (t,p). In Fig. 38 I have taken cross sections to some 2^+ and 3^- states seen in $(^{16}O,^{14}C)$ as ratios to the ground state cross section and plotted these versus residual nucleus. These ratios have been modified by a semi-empirical Q value dependence. What one sees is that these ratios are largest in the Ni and Zn region and then fall off as $A \longrightarrow 100$. I would say that this indicates that in regions where we have a neutron excess, we get a reduction in the cross section to the collective states for the two proton transfers, i.e. there appears to be a blocking effect (calculations will be needed to show if this is kinematics or spectroscopy). The next figure, Fig. 39 shows some p-n transfers obtained at Copenhagen[7,13] and Oxford.[26] One finds in the reactions $(^{16}O,^{14}N)$ and $(^{12}C,^{10}B)$ that the strong groups can be identified with high spin states of a particular configuration. In this case, $(^{16}O,^{14}N)$ to ^{56}Co populates a 5^+ state at 0.6 MeV which is considered to be a $f_{7/2}$ proton coupled to a $p_{3/2}$ neutron with their angular momenta aligned

to give $J^{\pi} = 5^{+}$. We see also a number of other cases, for example, $(g_{9/2}) \times (d_{5/2})$ coupled to 7^{+}. Cross sections here are typically 50 to 150 microbarns/sr. Similarly, for the reaction (^{12}C,^{10}B) to ^{42}Sc, the 7^{+} state at 600 keV is $(f_{7/2})^2$. One observes in the single nucleon transfer that $1f_{7/2}$, $2p_{3/2}$, $1g_{9/2}$ and $2d_{5/2}$ states are also populated strongly. One can say from this that the p-n transfers populate high-spin states (the so-called stretched states) where the angular momenta are aligned. This appears to be verified by microscopic DWBA calculations.[27]

Figure 40 shows some data taken at Orsay[28] at fairly high energy comparing two analog reactions, if you like, (^{16}O,^{14}C) and (^{16}O,^{14}N). Again these populate high spin, stretched states. The 4^{+} analog in ^{56}Ni has been aligned with the corresponding state in ^{56}Co. One can identify many of the states in ^{56}Co and perhaps make assignments then for the analog states in ^{56}Ni.

There is also the possibility now to obtain quantitative information using DWBA programs. Tobocman and co-workers, in particular, have a form factor program which can be used to do DWBA calculations. Also, Buttle and Goldfarb have shown[18] how one can include the finite-range effects in a very simple way which would also appear to be applicable to multi-nucleon transfers.[29] Figure 41 shows some DWBA calculations. These use the Tobocman form factor program with DWUCK. The only parameter adjusted is a normalization factor. One finds in many cases rather good fits, even as a function of bombarding energy (fixed normalization). So at least the kinematic features seem to be accounted for by DWBA. The spectroscopic factors are in most cases reasonable, and what one might expect from other light ion reactions, but there are some discrepancies for certain states[12,13] and also for the very negative Q value

reactions. The latter can be related to the overlap parameter ΔD, and suggests that for a poor overlap in the semi-classical picture, the DWBA also apparently does not work well. Figure 42 shows some work done at Argonne.[30] Again, these are DWBA calculations and one sees this mismatch with large negative Q values. The spectroscopic factors compared to (^{3}He,d) are reasonable, however.* The states analyzed are particular states, though, in that they are the states that have their spin and orbital angular momentum parallel ($j = \ell + 1/2$). One finds that in the other cases (where the spin and angular momentum are anti-parallel) the spectroscopic factors are not so reasonable.[12,13]

Well, why does DWBA work at all above the barrier? Many years ago, there were a number of doubts expressed that DWBA might fail. In Fig. 43 we have put a radial cut-off in the form factor (this is now the Tobocman form factor) at a large radius so we see just the asymptotic part of the form factor. Although this eliminates the nuclear interior, it really does not affect the calculations or the spectroscopic factors. This is illustrated in Fig. 44. We have shown semi-classically that the transfer occurs well outside the nuclei. This is confirmed by DWBA.** Again, we have the problem with the orbit mismatch. We could improve this fit by adjusting optical parameters (without changing the spectroscopic factor beyond reason, I would say), but there may be problems with the DWBA itself.

It thus appears then, that the tunnelling mechanism dominates even well above the barrier. This is very encouraging since it allows one to do a lot of the more complicated calculations e.g. multi-nucleon transfer, in particular,

*The DWBA calculations are renormalized, however.
**This result is valid for strongly absorbing optical potentials.

using the simple tunnelling mechanism. This has been explored by Broglia and Winther et al. at Copenhagen.[29] In fact they have now, at least conceptually, worked out the form factors one needs for multi-nucleon transfer.[29]

Figure 45 shows some calculations for four-nucleon transfer by Bonche, et al., at Saclay for $^{54}Fe(^{16}O,^{12}C)$ using a microscopic model[27]. For ^{58}Ni they use the configuration $(p_{3/2})^4(f_{7/2})^{-2}$. The number shown at the bottom is the ratio of their experimental cross sections to the DWBA calculations using this configuration. The results look very encouraging, both as to the fits of the angular distribution and to the magnitudes (at least the relative magnitudes). In these calculations they find, incidentally, that the so called stretched states are enhanced by factors of up to ten. This may explain the enhancement seen in $(^{16}O,^{14}N)$ and $(^{16}O,^{12}C)$ and gives some support to the quartet model.[31]

I would now like to talk about some features which I think may be unique to heavy ion reactions since up to now everything I've shown could have been done with light ions except perhaps the 2p2n transfers, or other multi-nucleon transfers. To start with the selection rules, for example, for single nucleon transfer are interesting. I refer you to articles by Buttle and Goldfarb, in particular.[18] The situation is illustrated in Fig. 46. The projectile consists of a core plus the transferred nucleon. In the projectile, the nucleon is in a state n'ℓ'j' whereas in the residual nucleus the nucleon has nℓj.

Now for light-ion reactions things are simple because the nucleon in the projectile has no orbital angular momentum (an s state) and this leads to the rule that the L-transferred is just equal to ℓ, the orbital angular momentum of the nucleon in the residual nucleus. For example, a transfer to an

$f_{7/2}$ or $f_{5/2}$ orbital proceeds by L=3 for both spin orbit partners, and $d\sigma/d\Omega$ may be relatively independent of j. A j-dependence can enter, usually relatively weakly, through spin-orbit effects. Polarization measurements are perhaps the only sure way one can distinguish between different j-values. These effects are small when one does proton transfers, let's say with ^{3}He or alphas, or uses very heavy target nuclei. In heavy-ion reactions, the above restriction (L=ℓ) does not apply. If we look at (^{16}O,^{15}N), the nucleon in the projectile has orbital angular momentum with a particular coupling to spin and in the no-recoil approximation one obtains the selection rules shown in Fig. 46. The angular-momentum transfer differs depending on whether j is $\ell \pm 1/2$. In particular for the case $j = \ell + 1/2$, for example $f_{7/2}$, the angular-momentum transfer $L = \ell + 1$, = 4, whereas for $f_{5/2}$, the angular-momentum transfer ($j = \ell - 1/2$) would be $L = \ell - 1$, or 2. The cross section, $\sigma_{\ell j}$, is then $\sigma_L = \sigma_{\ell \pm 1}$ for $j = \ell \pm 1/2$. Now if one uses another projectile, for example in (^{12}C,^{11}B) (and therefore the relative orientation of initial nucleon spin and orbital angular momentum) the allowed L's change. In particular, for the (^{12}C,^{11}B) reaction, the cross section is an incoherent sum of two angular-momentum transfers which will be the same for both spin-orbit partners (see Fig. 46). Typically we find in the DWBA calculations that the cross section for $L = \ell + 1$ dominates by factors 2-10, over $L=\ell-1$. Therefore, one expects a j-selectivity. This is shown in Fig. 47 for the two reactions:[12] (^{16}O,^{15}N) and (^{12}C,^{11}B). One finds enhancement in (^{12}C,^{11}B) because of the additional allowed angular momentum transfers. Another way of seeing this is shown in Fig. 49. This compares cross sections to spin-orbit pairs. This is for ^{55}Co, ^{63}Cu, ^{209}Bi (work done at Berkeley).[12] Comparing the spin-orbit pairs, the ratio of the

cross sections to states $j = \ell + 1/2$ and $j = \ell - 1/2$ (these are known states so there's no problem), we see a difference between $(^{16}O,^{15}N)$ and $(^{12}C,^{11}B)$. This is mostly due to the difference in allowed angular momentum transfers and the large difference in the cross section for a given L-transfer. Figure 50 shows the ratio of $(^{16}O,^{15}N)$ to $(^{12}C,^{11}B)$ versus ℓ. Normally we know these ℓ values from other sources and its a problem of just determining j-values. This shows one way to do this, i.e. by comparing these two reactions, since we get a difference in cross sections depending on whether $j = \ell \pm 1/2$. Typically, this difference is a factor of 2. For the $i_{13/2}$ its perhaps extrapolating a bit far, but we hope to improve the experimental situation by obtaining some more data. One finds similar curves for the other nuclei I've discussed. This, then, is a feature which is inherent to heavy-ion transfer reactions, that is, the selection rules will depend on the nucleon angular momentum in the projectile. This should apply to multi-nucleon transfer, as well. This is an important feature and can be very useful both as a spectroscopic aid or as a test of the selection rules for a particular reaction model.

Figure 51 shows some preliminary spectroscopic factors deduced from the data described above.[12] These are for ^{209}Bi. The L transfers allowed (Fig. 46) are also shown. These L-transfers are from the L selection rules using the no-recoil approximation. Again, I refer you to the Buttle-Goldfarb papers.[18] The spectroscopic factors for $(^{16}O,^{15}N)$ at 104 MeV are shown along with those for $(^{12}C,^{11}B)$ at 78 MeV. For the latter, two angular momentum transfers are allowed. The $(^{12}C,^{11}B)$ calculation has been normalized to the $2f_{7/2}$ state while the $(^{16}O,^{15}N)$ is normalized to the sub-Coulomb transfer at 69 MeV which has been measured by Barnett and Phillips.[32] The 104 MeV calculation uses the same form factor. The spectroscopic factors are shown with the normalizations as

indicated. The cross sections change by two orders of magnitude from E = 69 to 104 MeV, and we see that the DWBA reproduces this. There's still a problem in relative values of the spectroscopic factors and this may be associated with some of the selections rules*, which is another interesting problem.[12,23] But we see by comparing the ratio of spectroscopic factors at 104 and 69 MeV that the kinematic part is apparently accounted for in DWBA. There is perhaps one exception $3p_{1/2}$, but this is a very weak transition. Also shown is a calculation due to Buttle and Goldfarb. This is a sub-Coulomb DWBA calculation, i.e. a Coulomb-wave Born-approximation. They obtain the spectroscopic factors shown. We notice that in their calculation, which includes a recoil correction, there is a good correspondence with the spectroscopic factors obtained super-Coulomb. So any problems with the DWBA do not appear to be associated with the fact that one is above or below the Coulomb barrier. There still may be intrinsic problems.[33] Figure 52 shows some data from ORIC[34] (Oak Ridge), for (^{12}C,^{11}B) again at a high energy (116 MeV), about twice the Coulomb barrier. The curves shown are calculations based on the 78 MeV LBL data i.e. the same optical parameters and form factor are used. The spectroscopic factors shown are similar to those obtained at the lower energy (Fig. 51). There is one interesting feature which these data show. I mentioned the cross section should be an incoherent sum of the two allowed angular-momentum transfers. Now the calculation doesn't predict this to produce a visable effect. The two L values are predicted to have the same shape and hence add tc give the same angular distribution. But in fact if you look carefully at this data, and also other data, there may be features which indicate the presence of two L-contributions. This effect should show up in some cases.

*Recoil will allow L-transfers in addition to those given in Fig. 46. In particular, L=ℓ will be allowed for (^{16}O,^{15}N) and (^{12}C,^{11}B) (Ref. 33).

Now I would like to talk a little bit about inelastic scattering. This is another interesting topic. As I mentioned earlier, the inelastic scattering shows structure. In the simple picture (shown in Fig. 53) we use the collective model to give a Coulomb excitation and a nuclear excitation form factor. In a light-ion reaction above the barrier, nuclear excitation dominates. When one uses heavy-ions, one finds that both must be included at all energies. The heavy-ion form factor has the interesting property that the Coulomb and nuclear excitation parts have opposite signs and can cancel near the nuclear surface. This leads to a marked interference effect. One problem in heavy-ion reactions is the definition of the deformation parameters. In the simple collective model β is the potential deformation and includes the finite size of the projectile. It should be smaller than the mass deformation of the target. One way to obtain the corresponding mass deformation from β is to compare the deformation lengths as shown here, although there are better prescriptions. Figure 53 shows the form factor: the nuclear part, which is a derivative of the optical potential, and the Coulomb part. These add to give a form factor, F_L, with F_L^2 having an L-dependent node outside the nuclear radius. Satchler has pointed out that one can add a phase factor and determine explicitly the phase between the nuclear and Coulomb interactions from the interference effect.[35] Figure 54 shows a DWBA calculation for some data taken at Berkeley[16] which I showed earlier (not all the data are shown on this slide). This shows the two effects. Coulomb excitation (with DWBA) is shown as the dashed line. It includes distorted waves, but not the nuclear interactions in the form factor. The dotted-solid line shows the effect of just the nuclear part of the interaction. The solid curve shows the combined effects of the two excitation processes. The latter depends on

the L transfer mainly since the Coulomb excitation depends sensitively on the L transfer. The potential deformations, β_L^N, are indicated in Fig. 54. These are smaller than the corresponding mass deformations (from α,α' e.g.). Figure 55 shows the same effect (data from Copenhagen[24]). The data are primarily for the 3^- state in ^{96}Zr, although the 2^+ and 3^- states are not resolved completely. Again we show Coulomb excitation (with DWBA), nuclear excitation, and Coulomb plus nuclear excitation, where we adjust the deformation parameter of the potential to fit the data. The deformation parameter, incidently, changes both the shape and the magnitude of the cross section. This is different from light-ion reactions where the deformation parameter just scales the DWBA calculation, and requires that one fit simultaneously the magnitude and shape of $d\sigma/d\Omega$. The calculations also depend on the phase of the form factor. In this case we've taken the phase to be the one obtained from the collective model ($\alpha \doteq 20°$). That is a real, attractive plus a smaller, absorptive (imaginary) nuclear interaction with the ratio given by the optical potentials for the elastic scattering. Figure 56 shows some other transitions, but the data are not so complete.[24] Again, we don't have too much degree of freedom over the calculated shapes for $d\sigma/d\Omega$, but we can deduce β_L^N rather unambigiously. Figure 57 compares some different results. The B(EL)'s are fixed from Coulomb excitation, and we extract the deformation (which is the potential deformation) and then equate potential and mass deformation lengths to obtain a mass deformation. At least this is a first approximation to the corresponding mass deformation of the target, and can be compared with other measurements: (α,α'), (d,d'), (p,p'), etc. In general, the correspondence is good, particularly for low-lying transitions for which we believe the collective model should work.

Figure 58 shows another interesting feature of the inelastic scattering. If we fit just the elastic scattering, we find that we obtain a wide range of potentials which, in fact, differ substantially in the interior. I've shown three different optical potentials which fit the elastic data.[24] The solid line is for two that have the same diffuseness (a = 0.5fm). We find that everything is dominated at the exterior where these potentials are similiar. However, if we look at the nuclear excitation (which is determined by a derivative of the potentials) we find that there is a distinction. The problem with the elastic scattering is that we have the dominant Coulomb amplitude which hides many details of the nuclear potential. This is removed when we look at the inelastic scattering. Figure 59 shows calculations for different optical model sets. In particular, the solid curve is with a diffuseness of 0.5fm, while the dashed curve is with a diffuseness of 1.0fm. Again, the shapes also depend on the β parameters. This, then, is one way of determining optical parameters. We find that in fitting the data on ^{208}Pb, e.g., and some other cases, that the optical potential diffuseness must be about 0.5fm to fit the interference pattern in the inelastic data. Figure 60 shows the calculated interference effect as a function of L-transfer and Q-value. We see that for the low-lying states, which are dominated by Coulomb excitation, the effect is less pronounced than for higher excitations, which are dominated by the nuclear excitation. In between there is a region where the effect is very much L dependent and can probably be used to assign L-values.

In conclusion, although kinematic effects and the lack of L-signatures (for the nucleon transfers) are limitations, the selection rules and the strong Coulomb and nuclear interactions for heavy-ions produce many interesting effects which can be useful in spectroscopy and the study of nuclear interactions.

DISCUSSION

GOLDFARB:

I think there is a danger of over complacency. You have a very happy picture from many of the curves you show from DWBA calculations and I think this must have to do a little bit with the simplicity of the curves. That is there is not much structure and the numbers that you get out of the curves involve many, many parameters that go into the calculations, certainly with the high energy work, and I think the same remarks apply at low energy in the sub-Coulomb region, particularly with semi-classical treatments. In the sub-Coulomb region you have a tremendous change in the cross section with very small changes in parameters and this, I think, can lead to wrong information about nuclear structure.

BECCHETTI:

Yes, I'm not really happy with DWBA for a number of reasons. For example, apparently it works only when you have the so-called quasi-elastic case i.e. where the orbits are very similar ($\Delta D \sim 0$). DWBA does not work very well when the orbits are mismatched, which is the case where you need it to work. But I would say, as you mentioned, that sub-Coulomb everything is very sensitive to parameters. Above the barrier the calculations may be less sensitive to parameters in that things aren't changing rapidly with bombarding energy, etc. I think perhaps super-Coulomb may be a little safer than sub-Coulomb, or at least I think there are no inherent problems in going above the barrier.

GOLDFARB:

Could I ask you something about what you said about the Saclay experiment?

You said that in this plateau region, the negative Q-value region, that this had something to do with the break up of ^{16}O into ^{12}C. Do you mean that's different from the Q-dependence that you've been talking about?

BECCHETTI:

Yes. That's apparently another process, projectile break up, which can obscure direct reactions. There is apparently a mechanism which leads to the break up: $^{16}O \longrightarrow {}^{12}C+\alpha$

GOLDFARB:

But isn't it true that the Q-dependence does point out that the peak should be just where you would expect it to be.

BECCHETTI:

Well, for $^{16}O \longrightarrow {}^{12}C+\alpha$, the Q for the break up is -8 MeV which happens to be near the optimum Q-value for the 2p2n transfer (^{16}O,^{12}C), so this will always be true. But if you look at other reactions where the break-up Q-value is a little different then you find break up occuring at non-optimum Q-values. There are data, for example, for neon and other projectiles which break up into certain other channels and you see essentially the same phenomena.

ALDER:

I would like to make a comment on the distorted-wave Born-approximation versus the classical approximation. I think it has been pointed out by Winther that for such transfer reaction where the parameter η is so large, the classical picture is a very natural picture and one should usually use it, but on the other hand there is a very close correspondence between DWBA and the classical picture. The classical picture, at least in first order, is completely equivalent to the distorted-wave Born approximation. In the distorted-wave Born approximation

sometimes one neglects certain interactions. The same neglection occurs in semi-classical theory. Sometimes the form factor is included or not included. The same you can do also in the semi-classical theory. In this way the two pictures are completely equivalent and the only thing is that the semi-classical picture probably is a much more natural picture; it is simpler; it is very easy to understand, and it can very easily be parameterized.

BECCHETT:

Also I think the semi-classical picture will be necessary to do a coupled channels calculation.

ALDER:

Yes, that is just a remark I would like to make. Of course, in such collisions always Coulomb excitation occurs, it might even sometimes be multiple Coulomb excitation. And, if these effects play a rule, then I think the distorted-wave Born-approximation cannot be applied. But, the semi-classical picture can be generalized, even to such pictures as inclusion of multiple excitation, and so on. I think really one should use in the future the semi-classical theory of these ideas to analyze the data.

BECCHETTI:

I think what one would hope for is a transfer code equivalent to the Winther-deBoer code for Coulomb excitation.

ALDER:

Such a code is now being developed by different people. It is underway. And I would like to ask a question. I have seen this slide where you have ^{208}Pb, and there was a curve for Coulomb excitation and the nuclear interaction. This curve for Coulomb excitation had some wiggles in it, and I am wondering very much if these wiggles are not due to too little angular momentum being taken into account.

BECCHETTI:

Partially, the calculations only went up to 140 partial waves, which is not enough to do accurately Coulomb excitation for small angles.

ALDER:

Finally, I would like to mention that you mention a forthcoming paper by Winther about inelastic scattering. I have this paper here. I got it just two days before I left, and anyone who is interested can have a look at it.

BECCHETTI:

I believe he now uses the semi-classical treatment for the inelastic scattering.

ALDER:

Elastic and inelastic scattering, yes.

HOREN:

Of all the data that you have shown I would like to ask, how much nuclear structure do you feel that you could have extracted if you did not have the light ion work upon which to base the analysis?

BECCHETTI:

Well, I think for the single nucleon transfer it is really essential that you have the light ion data to compare with to give you the ℓ-values, for example. I think the most useful thing one can do is to compare different heavy ion reactions, as opposed to measuring angular distributions. So, I guess it is up to the theoreticians to decide how much information is going to come out. There are a number of reactions, for example the multi-proton transfers and the four nucleon transfers, which at the moment we can only do well with heavy ions. I think there are a number of cases, e.g. if the theoreticians can show that we

should populate stretched states via (^{16}O,^{14}N), where one could learn something about nuclear structure without necessarily having information from light ion reactions. But it may take a lot of faith in calculations.

REFERENCES

1. Nuclear Reactions Induced by Heavy Ions, ed. by R. Bock and W. Hering (North-Holland, Amsterdam, 1970)
2. Proceedings of the International Conference on Heavy Ion Physics (Dubna, 1971)
3. J. Phys. (Paris) Suppl. 11-12, Tome 32 (1971)
4. Proceedings of the European Conference on Nuclear Physics(Aix-en-Provence, France, 1972)
5. B. A. Watson, et al., preprint.
6. O. G. Artukh, et al., ref. 3, P. C6-129
7. V. I. Manko, et al., ref. 3, p. C6-225
8. J. C. Faivre, et al., Phys. Rev. Lett. 24, 1188 (1970)
9. H. Faraggi, ref. 3, p. C6-25 and references cited there.
10. H. Faraggi (private communication)
11. B. G. Harvey, et al., to be published in Nucl. Instr. Methods
12. D. Kovar, et al., submitted to Phys. Rev. Lett.
13. P. R. Christensen, V. I. Manko, F. D. Becchetti, and R. J. Nickles, submitted to Nucl. Phys.
14. G. C. Morrison, ref. 3, p. C6-69
15. R. H. Siemssen, C. L. Fink, L. R. Greenwood, and H. J. Körner, Phys. Rev. Lett. 28; 626 (1972)
16. F. D. Becchetti, et al., submitted to Phys. Rev. Lett.
17. P. R. Christensen, et al., ref. 2, p. 235; op cit, p. 361
18. P. J. A. Buttle and L. J. B. Goldfarb, Nucl. Phys. A176, 299 (1971) and references cited there.

19. C. Chasman, S. Cochovi, M. J. LeVine and A. Z. Schwarzschild, Phys. Rev. Lett. 28, 843 (1972)

20. W. von Oertzen, ref. 3, p. C6-233

21. A. Winther, ref. 3, p. C6-83.

22. D. Trautmann and K. Alder, Helv. Phys. Acta. 43, 363 (1970)

23. G. Breit and M. Ebel, Phys. Rev. 103, 679 (1956)

24. F. D. Becchetti, et al., submitted to Nucl. Phys.

25. F. Videbaek, I. Chernov, P. R. Christensen, and E. E. Gross, Phys. Rev. Lett. 28, 1072 (1972)

26. D. K. Scott, et al., Phys. Rev. Lett. 28, 1659 (1972)

27. P. Bonche, et al., submitted to Phys. Rev.

28. F. Pougheon, et al., ref. 3, p. C6-249;

29. R. Broglia, et al., ref. 3, p. C6-151

30. G. C. Morrison, H. J. Körner, L. R. Greenwood, and R. H. Siemssen, Phys. Rev. Lett. 28, 1662 (1972)

31. V. Gillet, ref. 3, p. C6-17

32. A. R. Barnett, P. J. A. Buttle, L. J. B. Goldfarb, and W. R. Phillips, Nucl. Phys. A176, 321 (1971)

33. M. Nagarajan, submitted to Nucl. Phys.

34. J. Larsen, J. Ball, and P. Ford (private communication)

35. G. R. Satchler, Phys. Lett. 33B, 385 (1970)

FIGURE CAPTIONS

Fig. 1. Reaction products from $^{16}O + ^{40}Ca$ (Ref. 5).

Fig. 2. Reaction products from $^{40}Ar + ^{232}Th$. A spectrometer with a ΔE-E counter telescope was used (ref. 6).

Fig. 3. ^{15}N and ^{14}N spectra from $^{16}O + ^{54}Fe$ (Refs. 7,13). Levels and transition strengths observed in (^{3}He,d) and (^{3}He,p) are indicated.

Fig. 4. ^{14}C and ^{12}C spectra from $^{16}O + ^{54}Fe$ (Refs. 7,13). Levels and transition strengths observed in (^{3}He,n) are indicated.

Fig. 5. ^{12}C spectra from $^{16}O + ^{54}Fe$ as functions of bombarding energy (Refs. 8,9).

Fig. 6. $^{54}Fe(^{16}O,^{12}C)$ spectrum, E_L = 80 MeV (Ref. 28).

Fig. 7. Levels in ^{58}Ni observed in $(^{14}N,^{10}B)$ and $(^{18}O,^{14}C)$ reactions (Ref. 10). Compare with Figs. 4-6.

Fig. 8. Spectra for $^{54}Fe(^{12}C,^{11}B)^{55}Co$, $^{54}Fe(^{16}O,^{15}N)^{55}Co$, and $^{54}Fe(^{16}O,^{15}O)^{55}Fe$ (Ref. 12, and unpublished data). The energy scale refers to states in ^{55}Co.

Fig. 9. Spectra for $^{208}Pb(^{12}C,^{14}C)^{206}Pb$ and $^{208}Pb(^{16}O,^{18}O)^{206}Pb$ (Ref. 12, and unpublished data).

Fig. 10. Spectra for some ^{18}O induced reactions. Positions of groups from target or projectile excitation are indicated (Ref. 13).

Fig. 11. $d\sigma/d\Omega$ for $(^{16}O,^{14}C)$ on some 1f-2p shell nuclei (Ref. 14).

Fig. 12. $d\sigma/d\Omega$ for $(^{16}O,^{15}N)$ on ^{48}Ca (Ref. 14). Transitions to ℓ=3 ($1f_{7/2}$) and ℓ=1 ($2p_{3/2}$) final states are indicated (Ref. 14).

Fig. 13. $d\sigma/d\Omega$ for $^{208}Pb(^{16}O,^{15}N)^{209}Bi$. The known spins of the final states are indicated with excitation energies given in parentheses (Ref. 12, and unpublished data). The allowed orbital angular momentum transfers (no recoil, Ref. 18) are shown.

Fig. 14. $d\sigma/d\Omega$ for some ^{18}O induced reactions (Ref. 15).

Fig. 15. $d\sigma/d\Omega$ for inelastic scattering of ^{16}O from ^{208}Pb (Ref. 16). Known spins and excitation energies are indicated.

Fig. 16. Systematics of peak cross sections for some one nucleon transfers: (^{16}O,^{15}O), (^{16}O,^{17}O), (^{16}O,^{15}N), and (^{18}O,^{19}F) for $E_L \sim 60$ MeV (Ref. 13).

Fig. 17. Systematics of peak cross sections for some two nucleon transfer reactions: (^{16}O,^{14}C), (^{16}O,^{14}N), (^{18}O,^{16}O), and (^{18}O,^{20}Ne) for $E_L \sim 60$ MeV (Ref. 13).

Fig. 18. Levels and relative cross sections observed in (^{16}O,^{12}C) (Ref. 9).

Fig. 19. Levels and peak cross sections observed in the two proton transfer (^{16}O,^{14}C) at $E_L \sim 60$ MeV (Ref. 13). Known spins of levels in the residual nuclei indicated are labelled.

Fig. 20. Levels and peak cross sections observed in the 2p2n transfer (^{16}O,^{12}C) (Refs. 9,13). Known spins of levels in the residual nuclei indicated are labelled. E_b is the ^{12}C Coulomb barrier.

Fig. 21. A comparison of (^{16}O,^{12}C) and (^{16}O,^{14}C) spectra for ^{52}Cr versus excitation energy (top) and Q value (bottom). Data are from Ref. 31.

Fig. 22. η vs. K for different reactions (shaded regions).

Fig. 23. Overlap of Coulomb waves for Q=0 and 5 MeV, for L=0 neutron transfer (from Ref. 18).

Fig. 24. Variation of 180° cross section vs. Q value for neutron transfer (Ref. 18): a_i is the apsidal distance in the initial channel, and $\Delta = a_f - a_i$ [$=\Delta D(180°)$]

Fig. 25. Peak cross sections vs. ΔD for one and two nucleon transfer on different sequences of isotopes (data from Refs. 9,13,14,19). Transitions are 0^+(g.s.) $\longrightarrow$ 0^+(g.s.) unless otherwise noted. The data for neutron transfer have been divided by shell model spectroscopic factors.

Fig. 26. DWBA calculations and data vs. ΔD for $^{58,60,62,64}Ni(^{16}O,^{15}N)$, E_L = 60 MeV (Ref. 13).

Fig. 27. Peak cross sections for $(^{16}O,^{12}C)$ vs. ΔD (Refs. 9,13). The DWBA calculation is due to Von Oertzen (Ref. 20).

Fig. 28. Formulae for semi-classical interpretation of heavy ion reactions.

Fig. 29. $d\sigma/dD$ vs. $d_0 \equiv D/(A_1^{1/3} + A_2^{1/3})$ for some single neutron transfer data (Ref. 13).

Fig. 30. $d\sigma/dD$ vs. d_0 for some single proton transfers (Ref. 13).

Fig. 31. $d\sigma/dD$ vs. d_0 for some multi-nucleon transfers (Ref. 13).

Fig. 32. Elastic scattering (ratio to Rutherford) vs. d (Ref. 13,24).

Fig. 33. $d\sigma/dD$ vs. $D(\theta)$ where $d\sigma/dD$ has been obtained by dividing the data shown in Figs. 29,30 by $1-P_{abs}(\equiv \sigma/\sigma_R$ (D), Fig. 32). Data from Ref. 13. $\overline{\alpha}$ is the average bound state parameter (see Fig. 28).

Fig. 34. Same as Fig. 33 with data from Figs. 30,31 (Ref. 13).

Fig. 35. The inelastic scattering probability of ^{16}O and ^{12}C from ^{96}Zr vs. $D(\theta)$ compared with a DWBA calculation. The square of the form factor vs. separation is shown below (Ref. 24).

Fig. 36. Data for elastic and inelastic scattering of ^{16}O from ^{58}Ni vs. E_{LAB} (bottom) and $D(\theta)$ (top). Data from Ref. 25.

Fig. 37. Levels seen in two proton and two neutron transfers into ^{52}Cr (Ref. 13).

Fig. 38. Ratio of peak cross sections 2^+/g.s., 3^-/g.s. (corrected by a semi-empirical Q-dependence) for the $(^{16}O,^{14}C)$ reaction (E_L ~ 60 MeV) leading to the residual nuclei indicated (Ref. 13).

Fig. 39. Strong pn transfers, $(^{16}O,^{14}N)$ and $(^{12}C,^{10}B)$, populating known stretched states (Refs. 13,26)

Fig. 40. Comparison of 2p and pn transfer (Ref. 28).

Fig. 41. Comparison of $d\sigma/d\Omega$ for (^{16}O,^{15}N) with finite range DWBA calculations (Ref. 13). The allowed L-transfers are indicated (see Fig. 46).

Fig. 42. DWBA fits and spectroscopic factors for (^{16}O,^{15}N) populating 1f and 2p states (Refs. 14,30).

Fig. 43. The finite range form factor for $^{58}Ni(^{16}O,^{15}N)^{59}Cu(2p_{3/2})$. Data from Ref. 13.

Fig. 44. DWBA fits for $^{58,64}Ni(^{16}O,^{15}N)$ including a calculation with a radial cut off at 8.5fm (see Fig. 43). Data from Ref. 13.

Fig. 45. DWBA fits to $^{54}Fe(^{16}O,^{12}C)^{58}Ni$ assuming $(p_{3/2})^4$ $(f_{7/2})^{-2}$ configurations. The ratios of experimental to DWBA cross sections are shown at the bottom (Ref. 27).

Fig. 46. Selection rules for single nucleon transfer, neglecting recoil (Ref. 18): $|\ell'-\ell| \leq L \leq \ell' + \ell$; $|j'-j| \leq L \leq j' + j$; $\ell' + \ell + L$ = even.

Fig. 47. Spectra for (^{12}C,^{11}B) and (^{16}O,^{15}N) on ^{208}Pb. Known proton single particle states are indicated (Refs. 11,12).

Fig. 48. Spectra for (^{12}C,^{11}B) and (^{16}O,^{15}N) on ^{62}Ni (Ref. 12). Known single particle states are indicated.

Fig. 49. Ratio of peak cross sections for (^{16}O,^{15}N) and (^{12}C,^{11}B) for spin orbit partners in the residual nuclei indicated (Ref. 12).

Fig. 50. Ratio of peak cross sections to states $j = \ell \pm 1/2$ for (^{16}O,^{15}N) and (^{12}C,^{11}B) on ^{208}Pb leading to ^{209}Bi (Ref. 12).

Fig. 51. Spectroscopic factors for proton single particle states in ^{209}Bi deduced from the reactions indicated using DWBA. The DWBA used in the LBL calculation was normalized to the underlined values. The indicated L's are the values allowed neglecting recoil (Ref. 18). See Fig. 46.

Fig. 52. DWBA fits to (^{12}C,^{11}B) (see Fig. 51). Data from Ref. 34.

Fig. 53. The collective model form factor for inelastic scattering.

Fig. 54. DWBA fits to inelastic scattering of ^{16}O from ^{208}Pb. The potential deformations are indicated (Ref. 16).

Fig. 55. DWBA calculations for Coulomb, nuclear, and Coulomb plus nuclear excitation in $^{96}Zr(^{12}C,^{12}C')$. (Refs. 13,24).

Fig. 56. DWBA fits to inelastic scattering of ^{16}O from some 1f-2p shell nuclei (Refs. 13,24).

Fig. 57. Potential (β) and mass (β_m) deformation parameters deduced from ^{16}O inelastic scattering (Refs. 13,24).

Fig. 58. Elastic scattering of ^{16}O (top) and optical potentials (bottom) which yield fits to the data as shown (Ref. 24).

Fig. 59. DWBA calculations for inelastic scattering of ^{16}O using a collective model form factor and different optical potentials (see Fig. 58) (from Ref. 24).

Fig. 60. DWBA calculations for inelastic scattering of ^{16}O from ^{96}Zr as a function of ℓ-transfer and Q value.

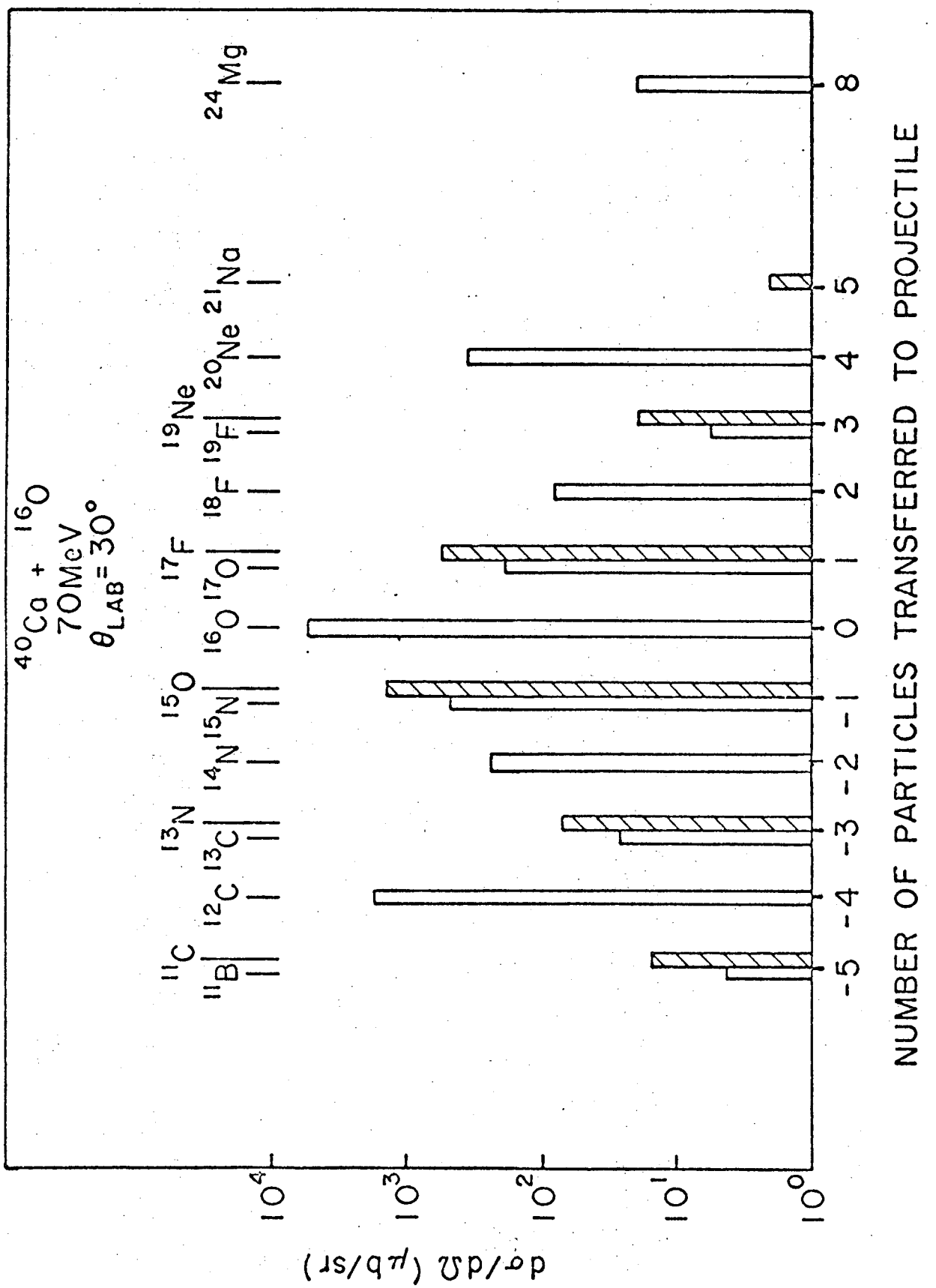
$^{40}Ca + {}^{16}O$
70MeV
$\theta_{LAB} = 30°$
^{11}B ^{11}C ^{12}C ^{13}C ^{13}N ^{14}N ^{15}N ^{15}O ^{16}O ^{17}O ^{17}F ^{18}F ^{19}F ^{19}Ne ^{20}Ne ^{21}Na ^{24}Mg
$d\sigma/d\Omega$ (μb/sr)
10^0 10^1 10^2 10^3 10^4
-5 -4 -3 -2 -1 0 1 2 3 4 5 8
NUMBER OF PARTICLES TRANSFERRED TO PROJECTILE

Fig. 1

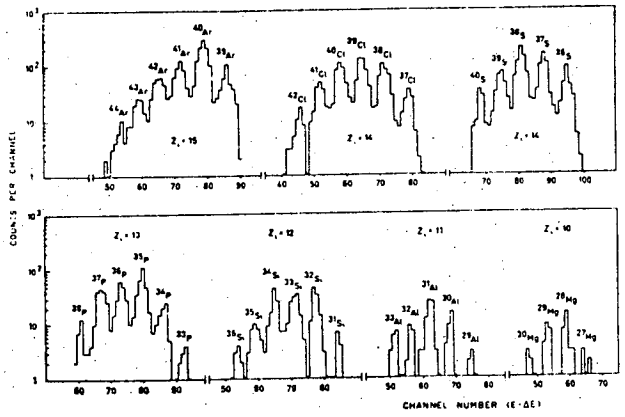

Yields of different ions of Mg, Al, Si, P, S, Cl and Ar produced in the $^{232}Th + ^{40}Ar$ reaction at $E(^{40}Ar) = 290$ MeV and $\theta = 40°$. The yields were measured for the discrete energies of the reaction products : $E(\text{MeV}) = 41.75\ Z_i^2/A$.

Fig. 2

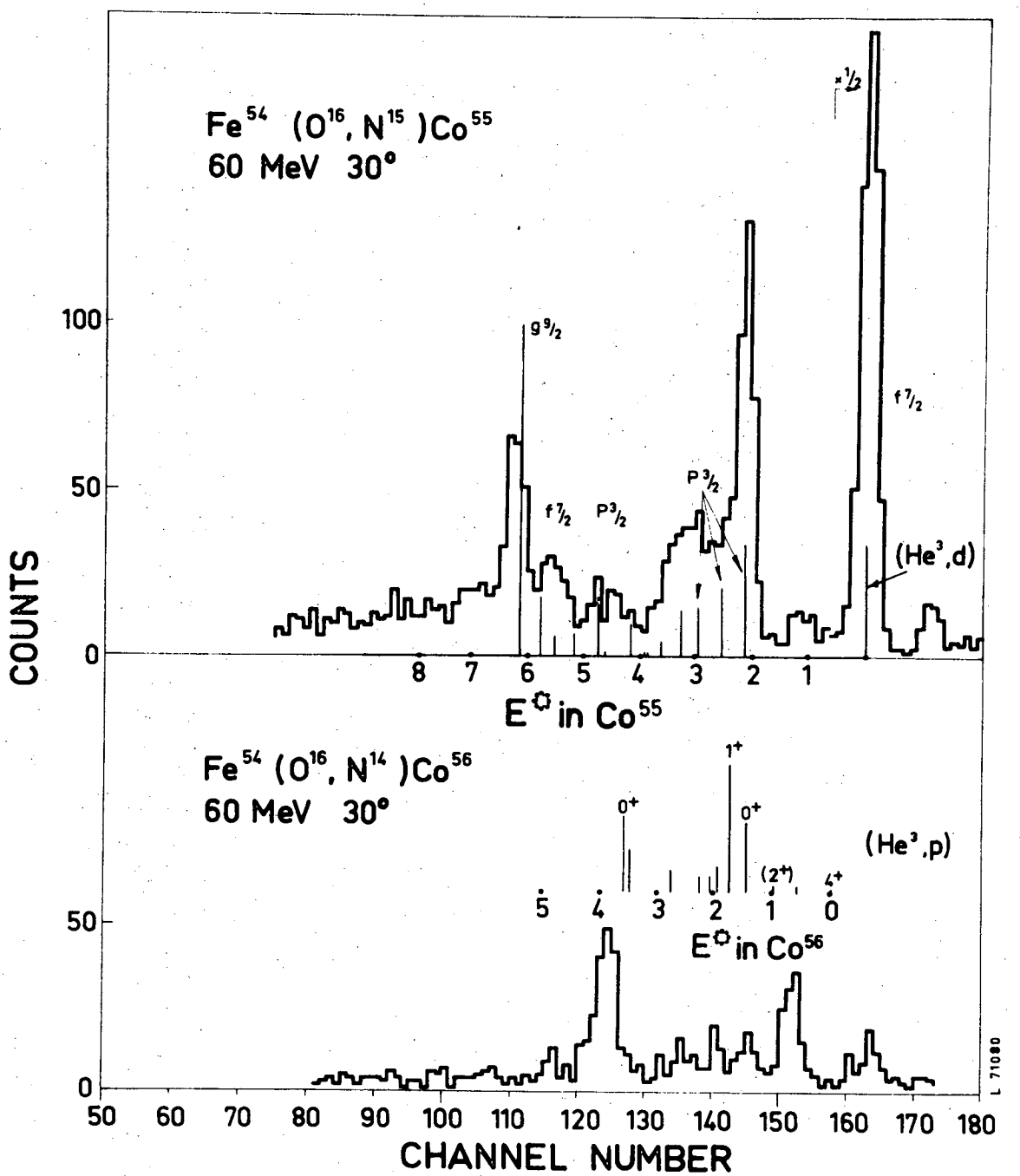
Fe54 (O16, N15)Co55
60 MeV 30°
g9/2
f7/2
P3/2
f7/2
P3/2
(He3,d)
8 7 6 5 4 3 2 1
E* in Co55
Fe54 (O16, N14)Co56
60 MeV 30°
0+
1+
0+
(2+)
4+
(He3,p)
5 4 3 2 1 0
E* in Co56
COUNTS
100
50
0
50
0
50 60 70 80 90 100 110 120 130 140 150 160 170 180
CHANNEL NUMBER
L 71080

Fig. 3

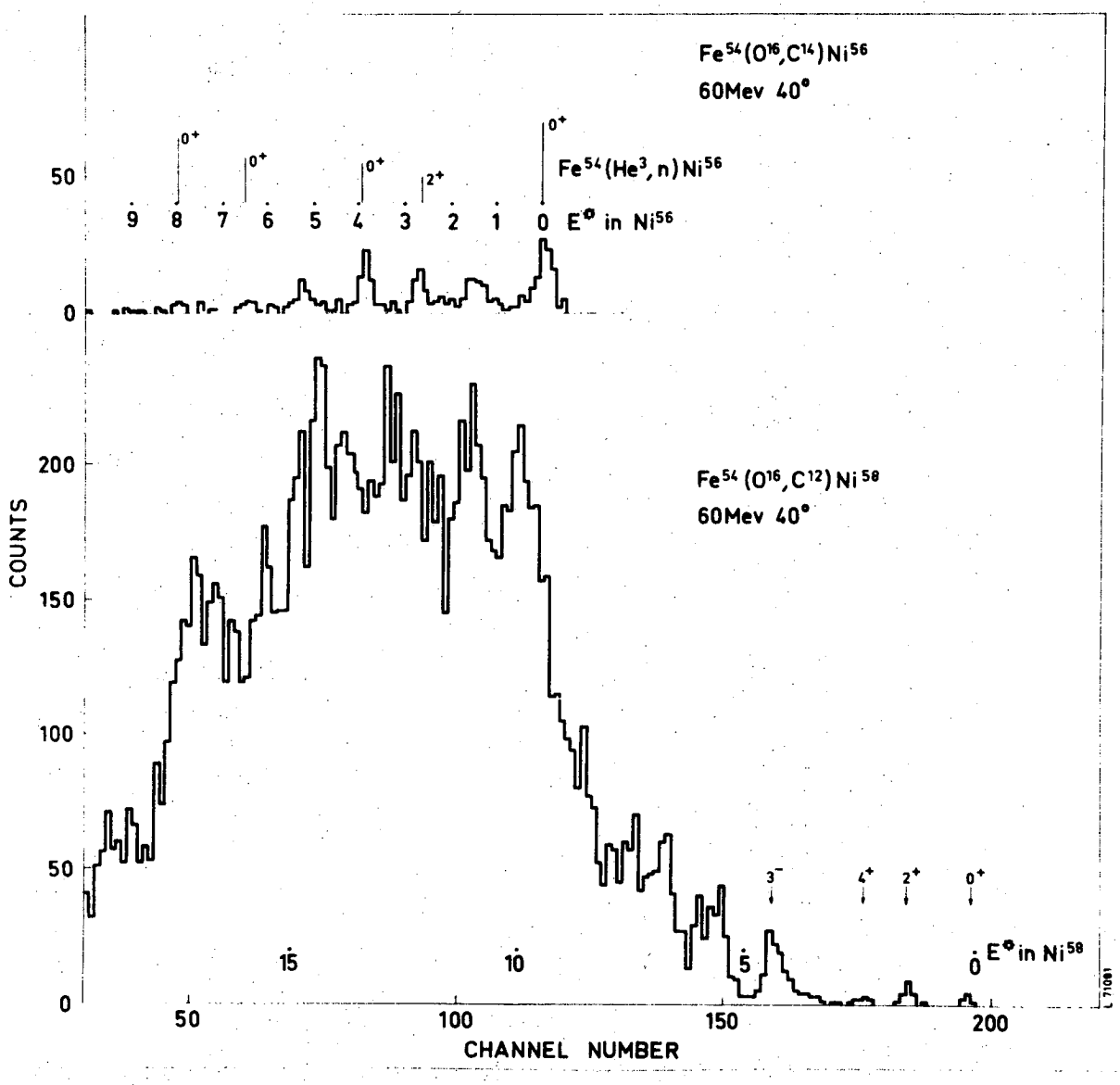
Fe54(O16,C14)Ni56
60Mev 40°
Fe54(He3,n)Ni56
E* in Ni56
Fe54(O16,C12)Ni58
60Mev 40°
E* in Ni58
COUNTS
CHANNEL NUMBER

Fig. 4

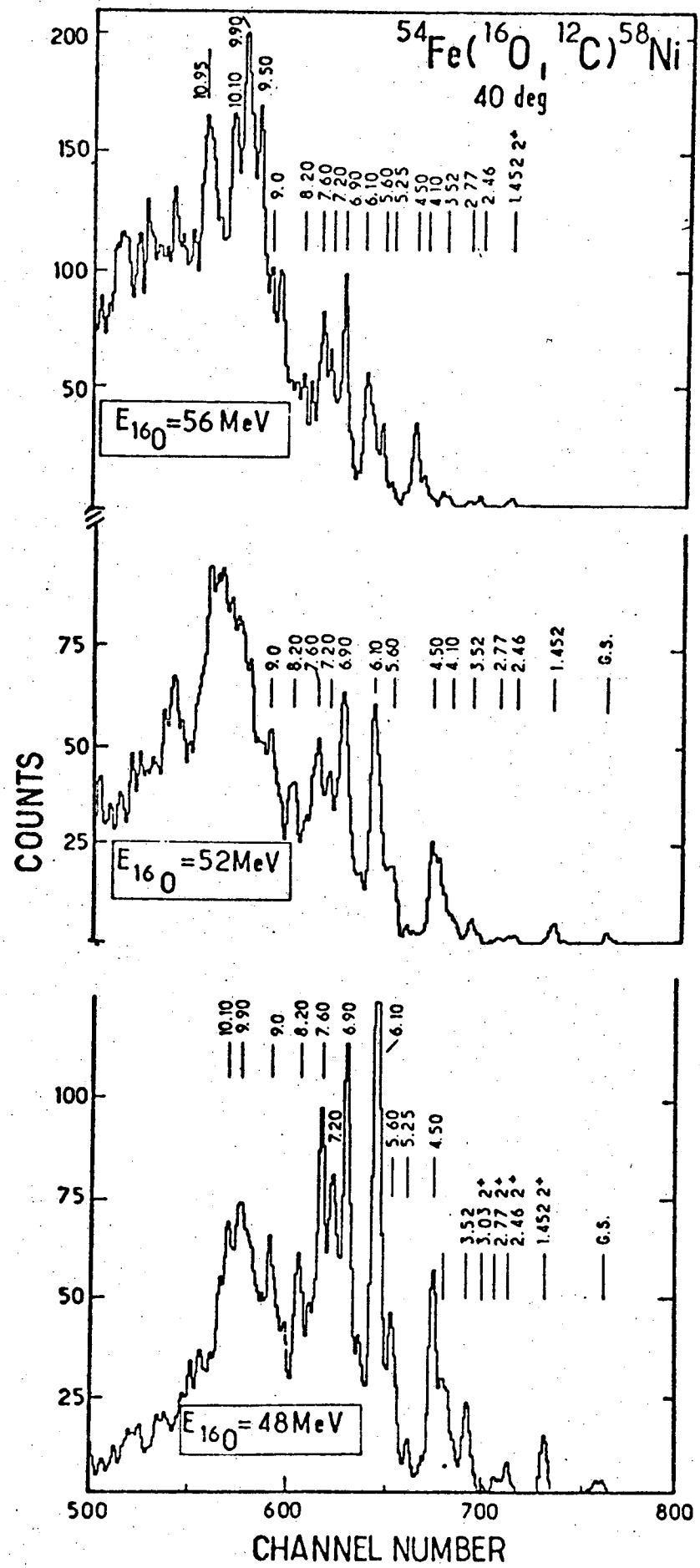
$^{54}Fe(^{16}O, ^{12}C)^{58}Ni$
40 deg
E_{16_O}=56 MeV
E_{16_O}=52MeV
E_{16_O}=48MeV
COUNTS
CHANNEL NUMBER
10.95
10.10
9.99
9.50
9.0
8.20
7.60
7.20
6.90
6.10
5.60
5.25
4.50
4.10
3.52
3.03 2+
2.77
2.46
1.452 2+
G.S.

Fig. 5

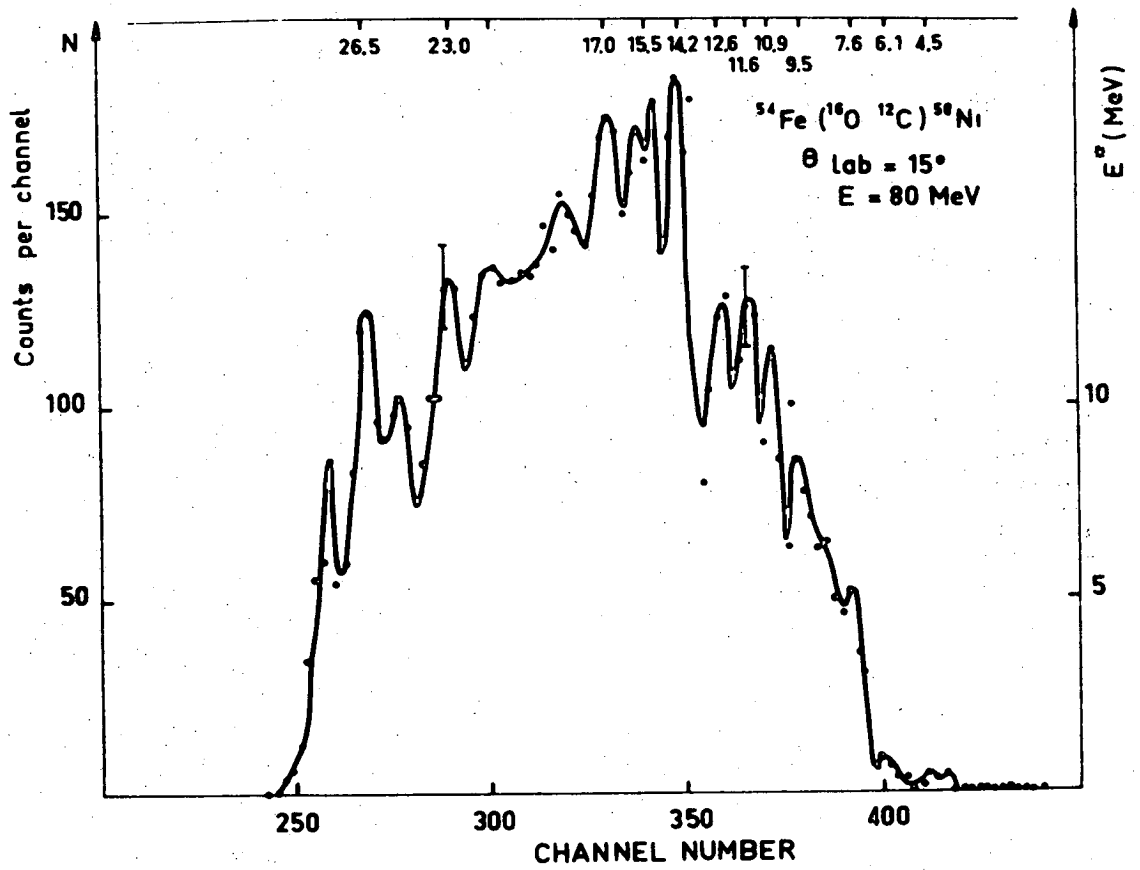
N
Counts per channel
150
100
50
26.5
23.0
17.0
15.5
14.2
12.6
11.6
10.9
9.5
7.6
6.1
4.5
^{54}Fe (^{16}O ^{12}C) ^{58}Ni
θ lab = 15°
E = 80 MeV
E* (MeV)
10
5
250
300
350
400
CHANNEL NUMBER

Fig. 6

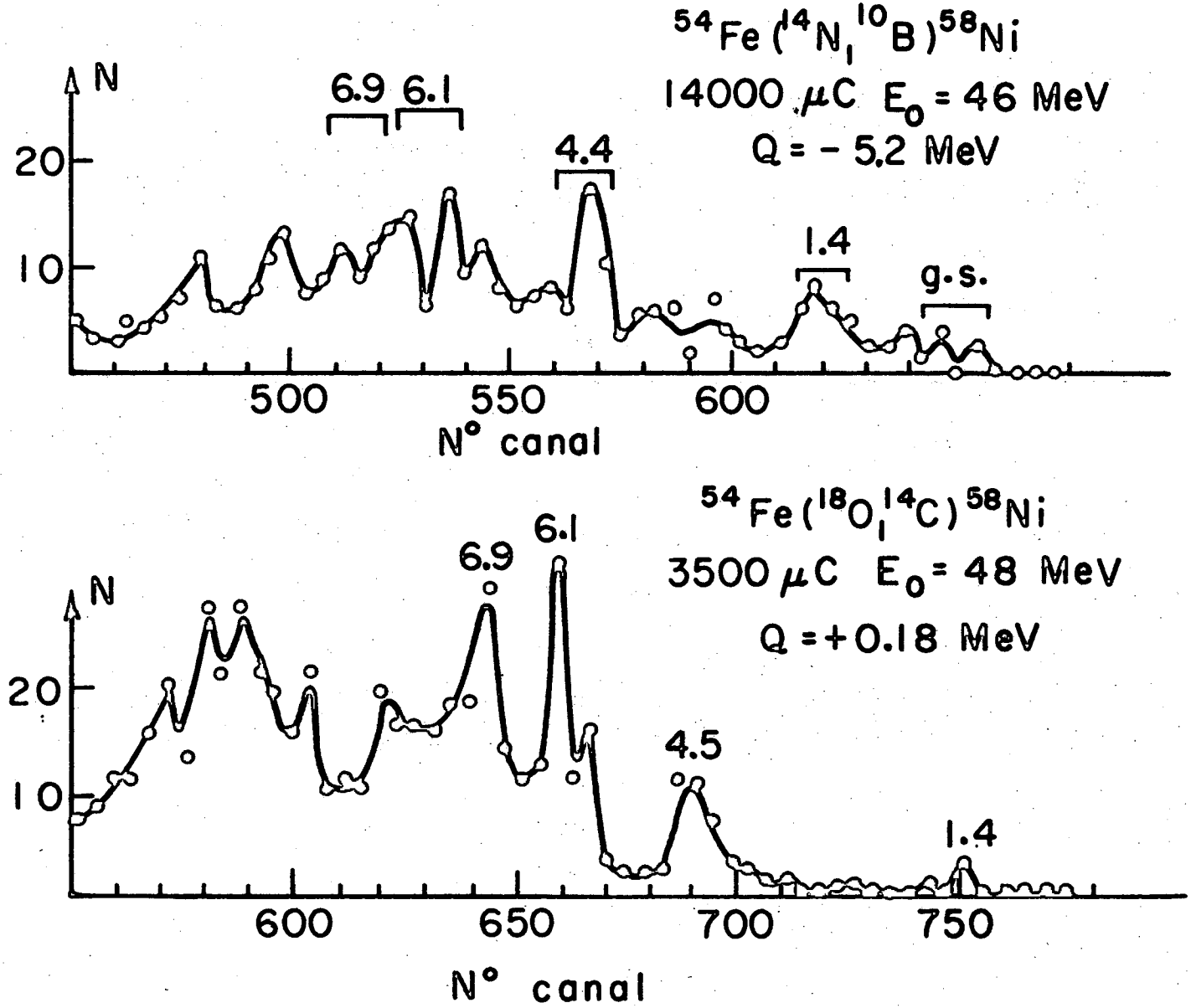

Fig. 7

XBL729-3967

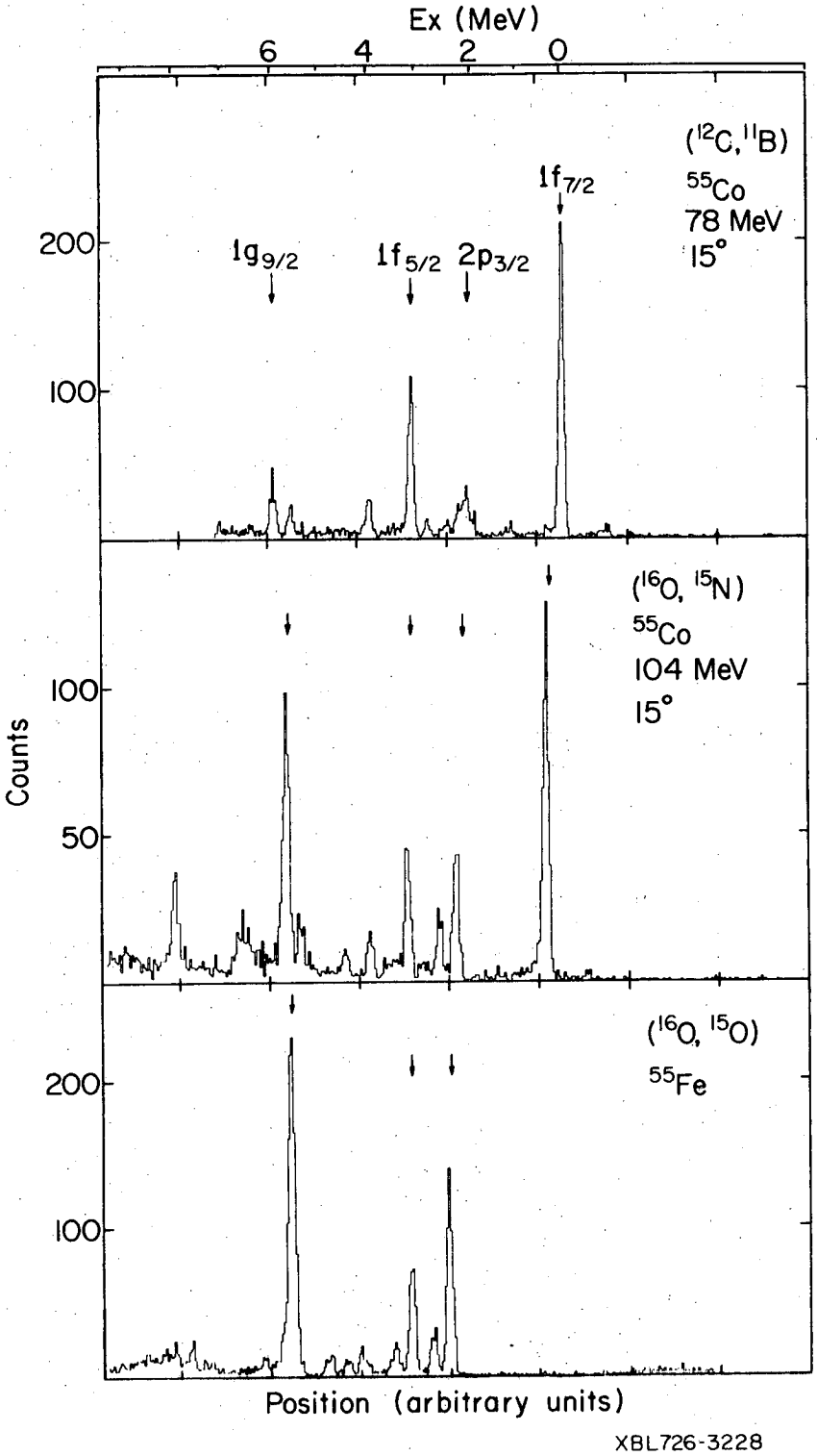
Ex (MeV)
6
4
2
0
(^{12}C, ^{11}B)
^{55}Co
78 MeV
15°
1f$_{7/2}$
1g$_{9/2}$
1f$_{5/2}$
2p$_{3/2}$
200
100
(^{16}O, ^{15}N)
^{55}Co
104 MeV
15°
100
50
Counts
(^{16}O, ^{15}O)
^{55}Fe
200
100
Position (arbitrary units)
XBL726-3228

Fig. 8

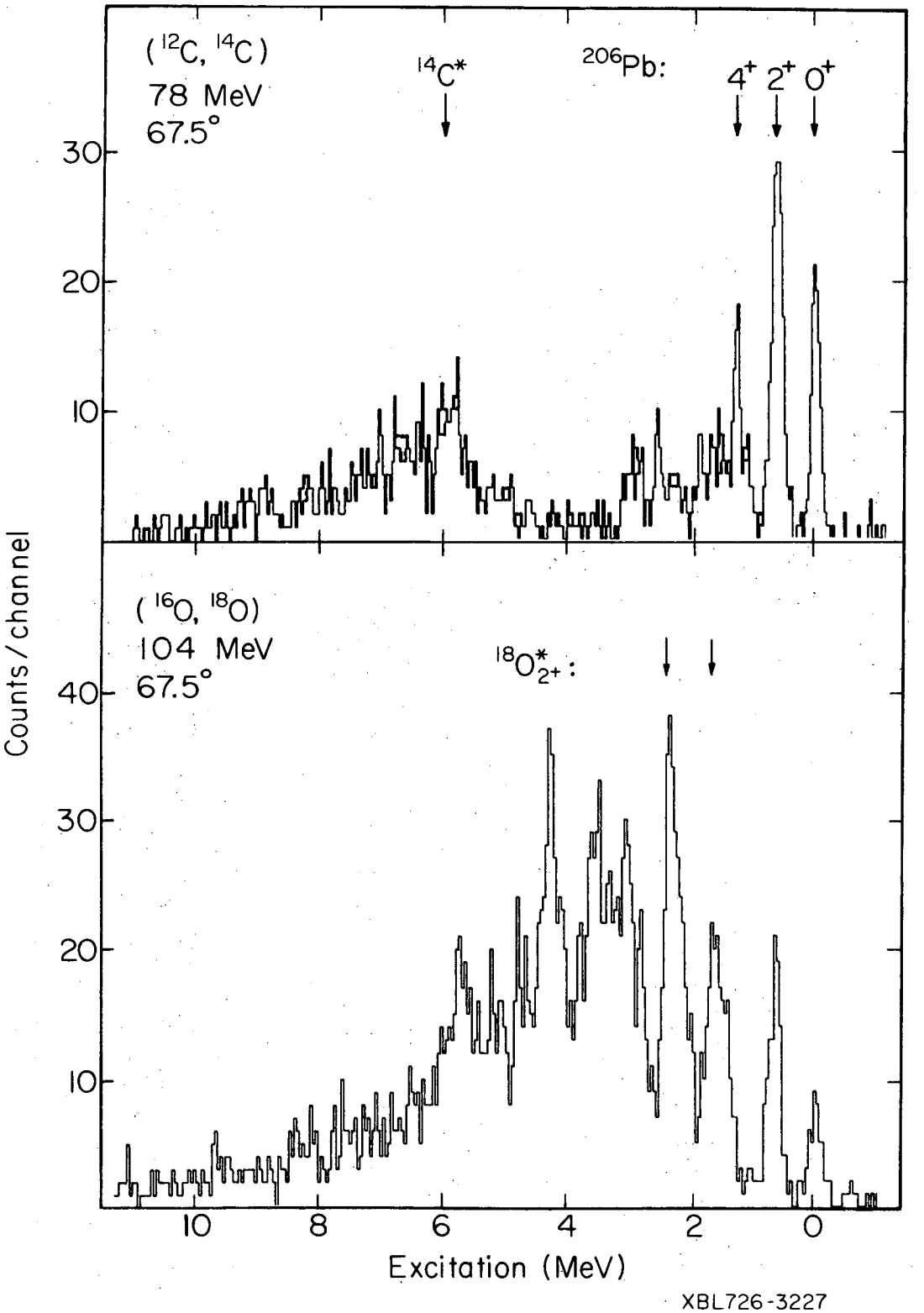
(^{12}C, ^{14}C)
78 MeV
67.5°
^{14}C*
^{206}Pb:
4$^+$ 2$^+$ 0$^+$
(^{16}O, ^{18}O)
104 MeV
67.5°
^{18}O$^*_{2^+}$:
Counts / channel
Excitation (MeV)
XBL726-3227

Fig. 9

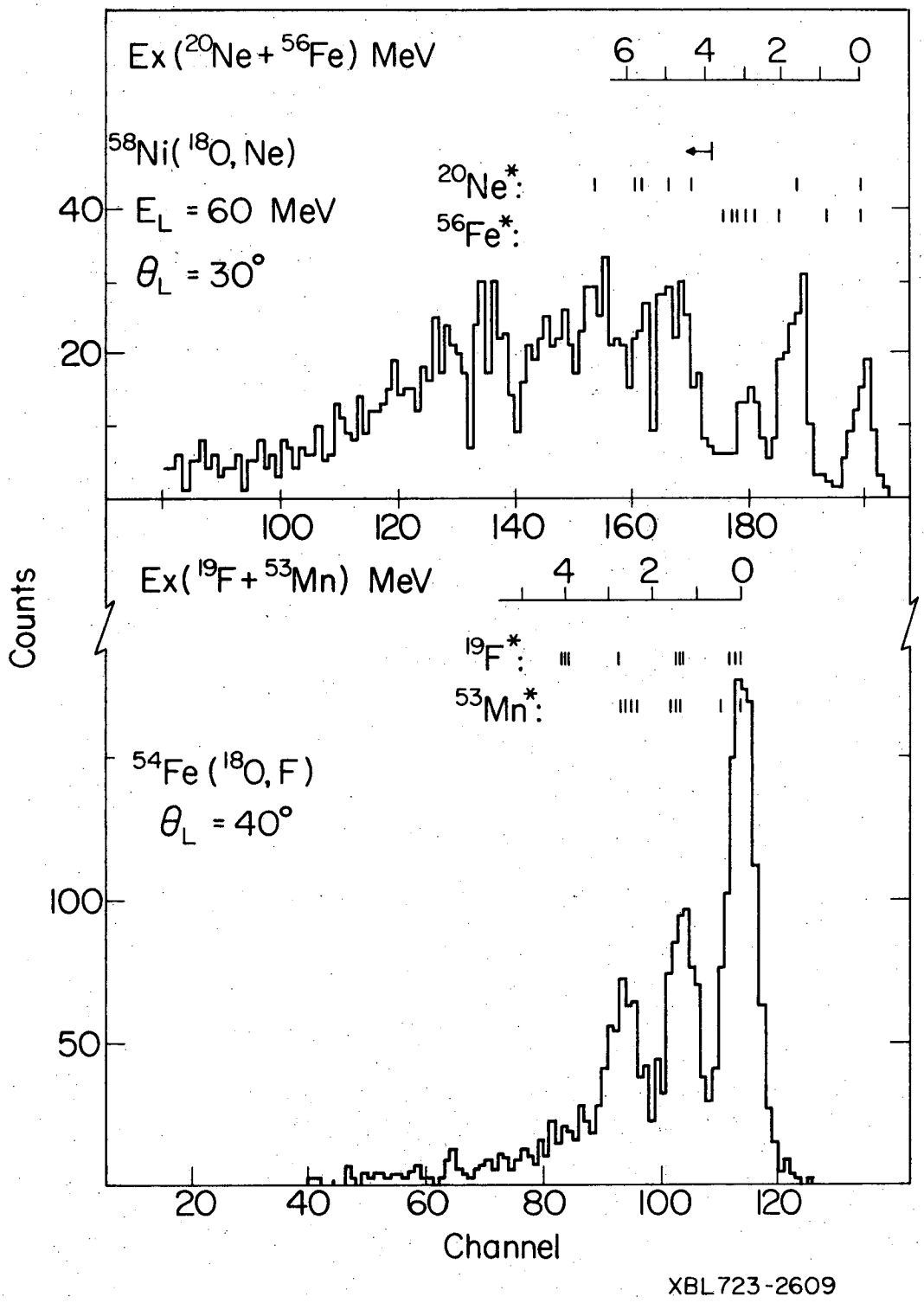
Ex(^{20}Ne+^{56}Fe) MeV
6 4 2 0
^{58}Ni(^{18}O, Ne)
E_L = 60 MeV
θ_L = 30°
^{20}Ne*:
^{56}Fe*:
40
20
100 120 140 160 180
Ex(^{19}F+^{53}Mn) MeV
4 2 0
^{19}F*:
^{53}Mn*:
^{54}Fe (^{18}O, F)
θ_L = 40°
100
50
20 40 60 80 100 120
Counts
Channel
XBL723-2609

Fig. 10

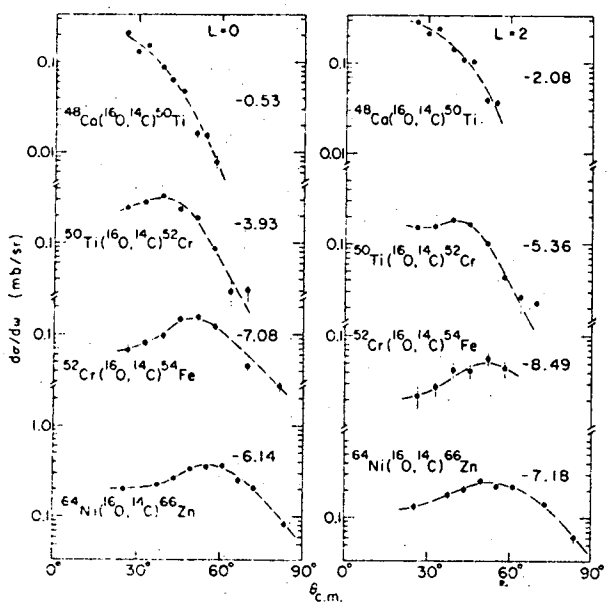

Angular distributions of various (^{16}O, ^{14}C) reactions for ground state ($L = 0$) and first excited state ($L = 2$) transitions; $E(^{16}O) = 48$ MeV.

Fig. 11

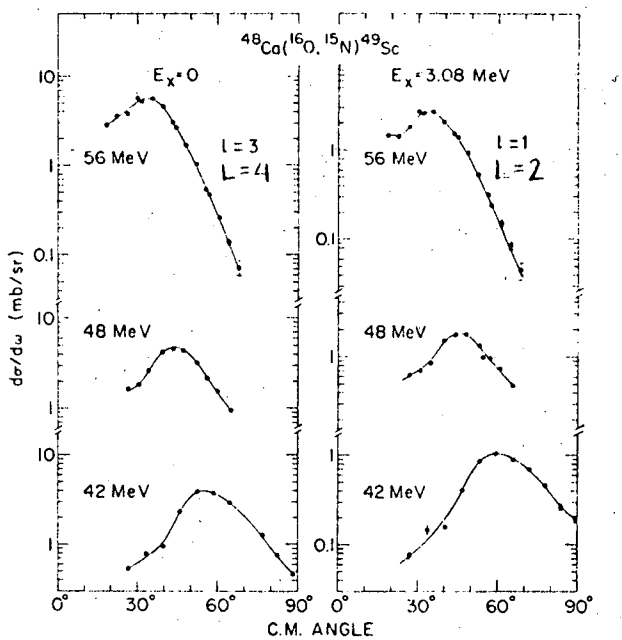

Angular distributions of the $^{48}Ca(^{16}O, ^{15}N)^{49}Sc$ reaction to the final states shown for $E(^{16}O) = 42, 48$ and 56 MeV.

Fig. 12

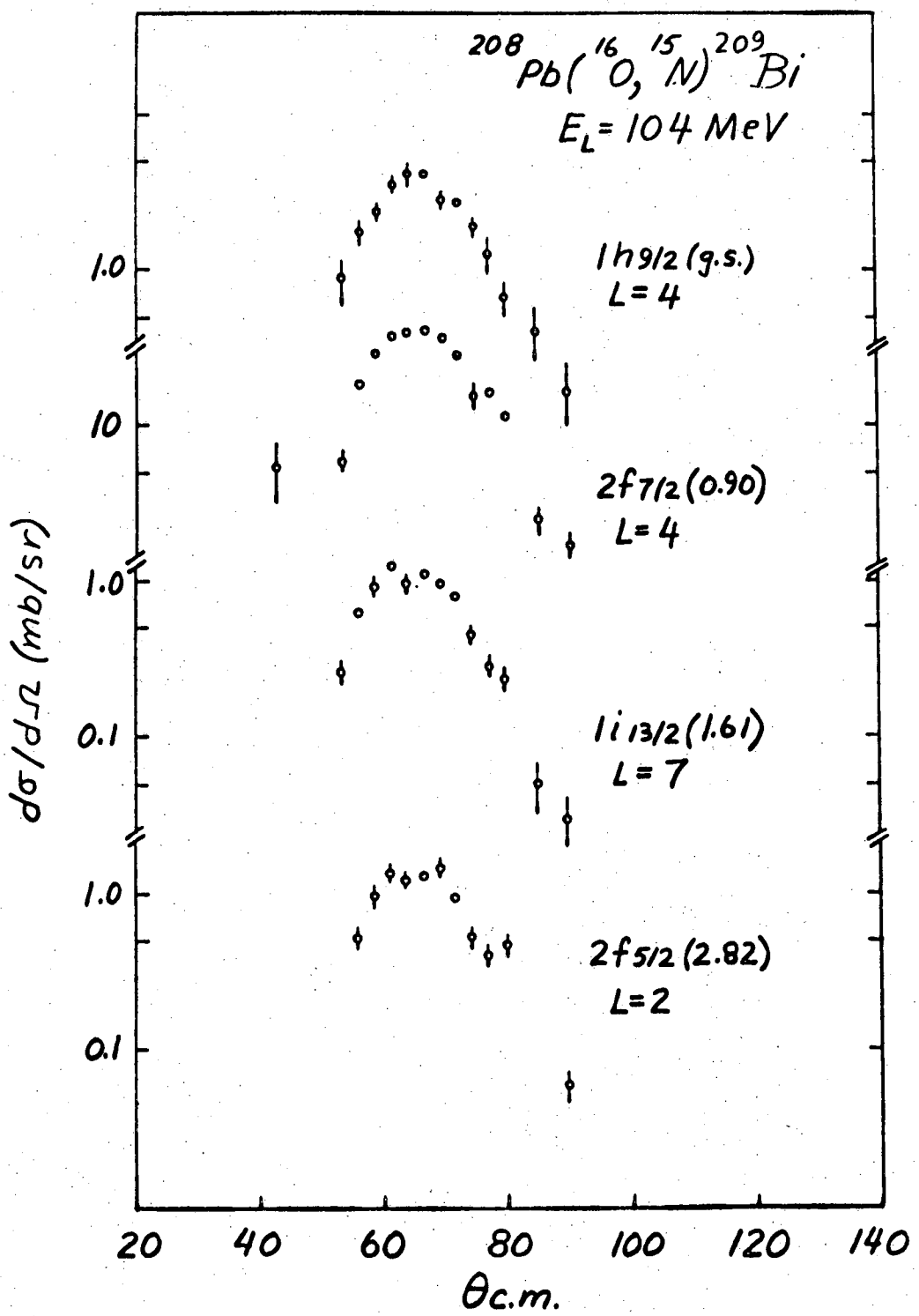
$^{208}Pb(^{16}O, ^{15}N)^{209}Bi$
$E_L = 104$ MeV
1h9/2 (g.s.)
L = 4
2f7/2 (0.90)
L = 4
1i13/2 (1.61)
L = 7
2f5/2 (2.82)
L = 2
1.0
10
1.0
0.1
1.0
0.1
dσ/dΩ (mb/sr)
20
40
60
80
100
120
140
θc.m.

Fig. 13

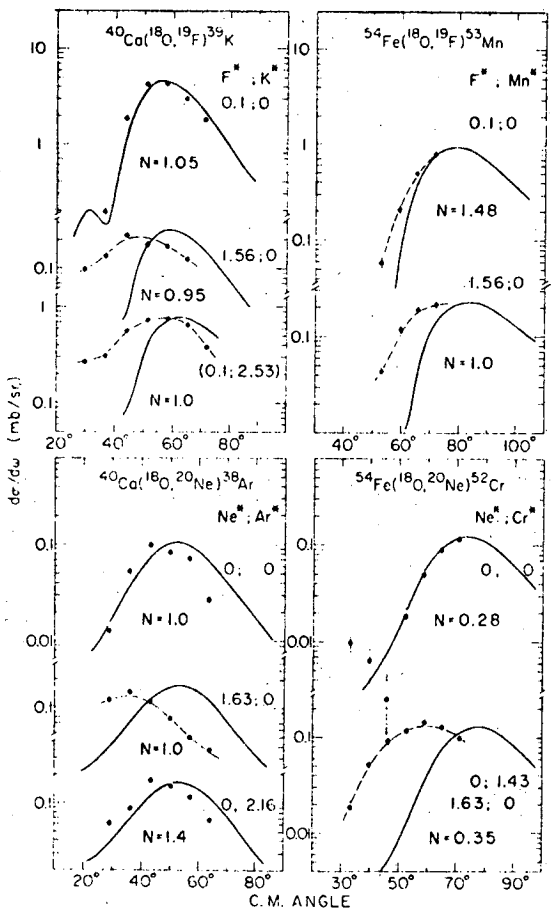

Angular distributions from the (^{18}O, ^{19}F) and (^{18}O, ^{20}Ne) reactions. Each is labeled with the excitation energies (MeV) in the outgoing particle and the residual nucleus. We use 0.1 to denote the g.s. triplet in ^{19}F. The solid curves are the results of DWBA calculations; the dashed ones are merely guides to the eye.

Fig. 14

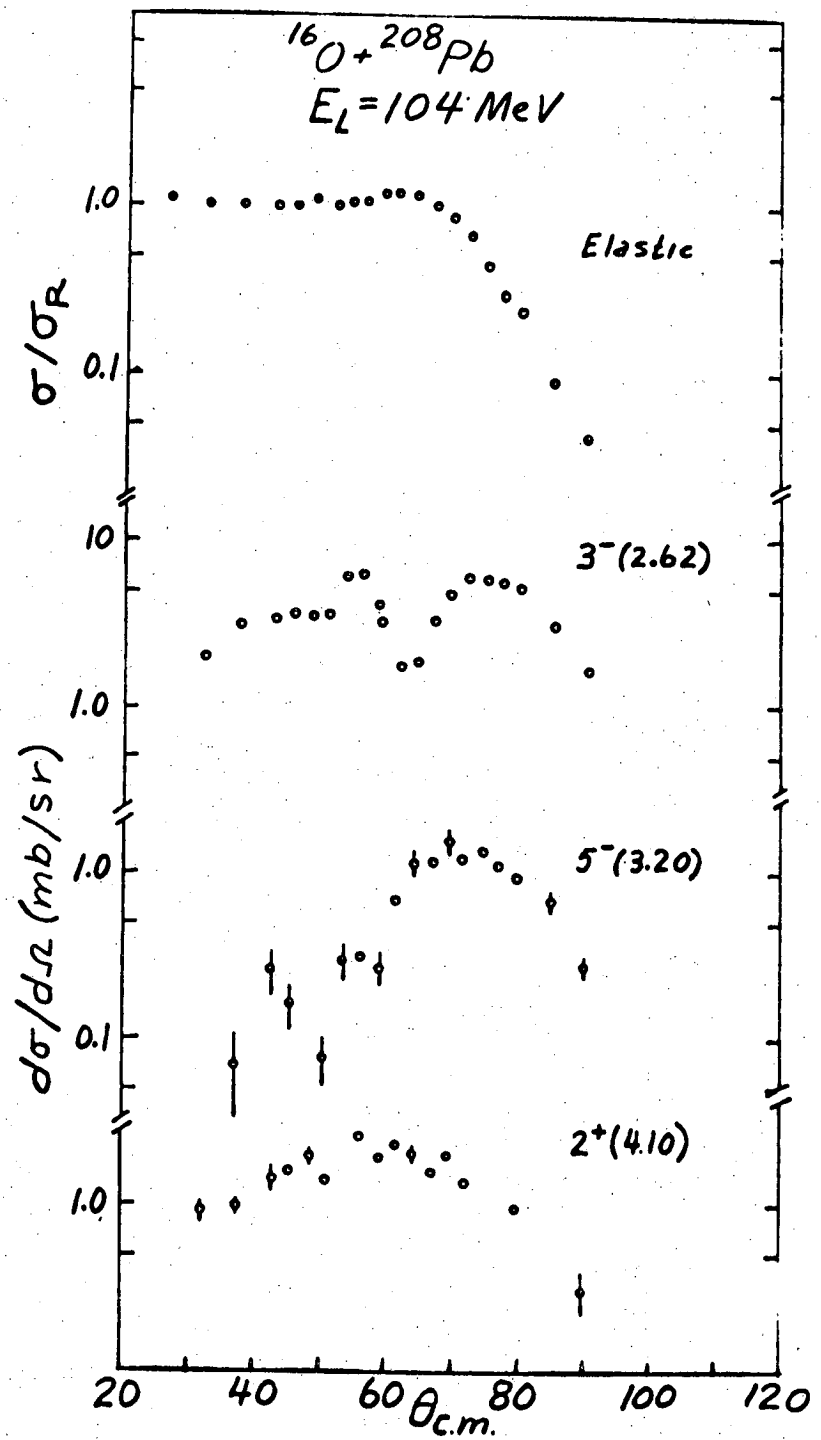
$^{16}O + ^{208}Pb$
$E_L = 104$ MeV
Elastic
$3^-(2.62)$
$5^-(3.20)$
$2^+(4.10)$
σ/σ_R
$d\sigma/d\Omega$ (mb/sr)
1.0
0.1
10
1.0
1.0
0.1
1.0
20
40
60
80
100
120
$\theta_{c.m.}$

Fig. 15

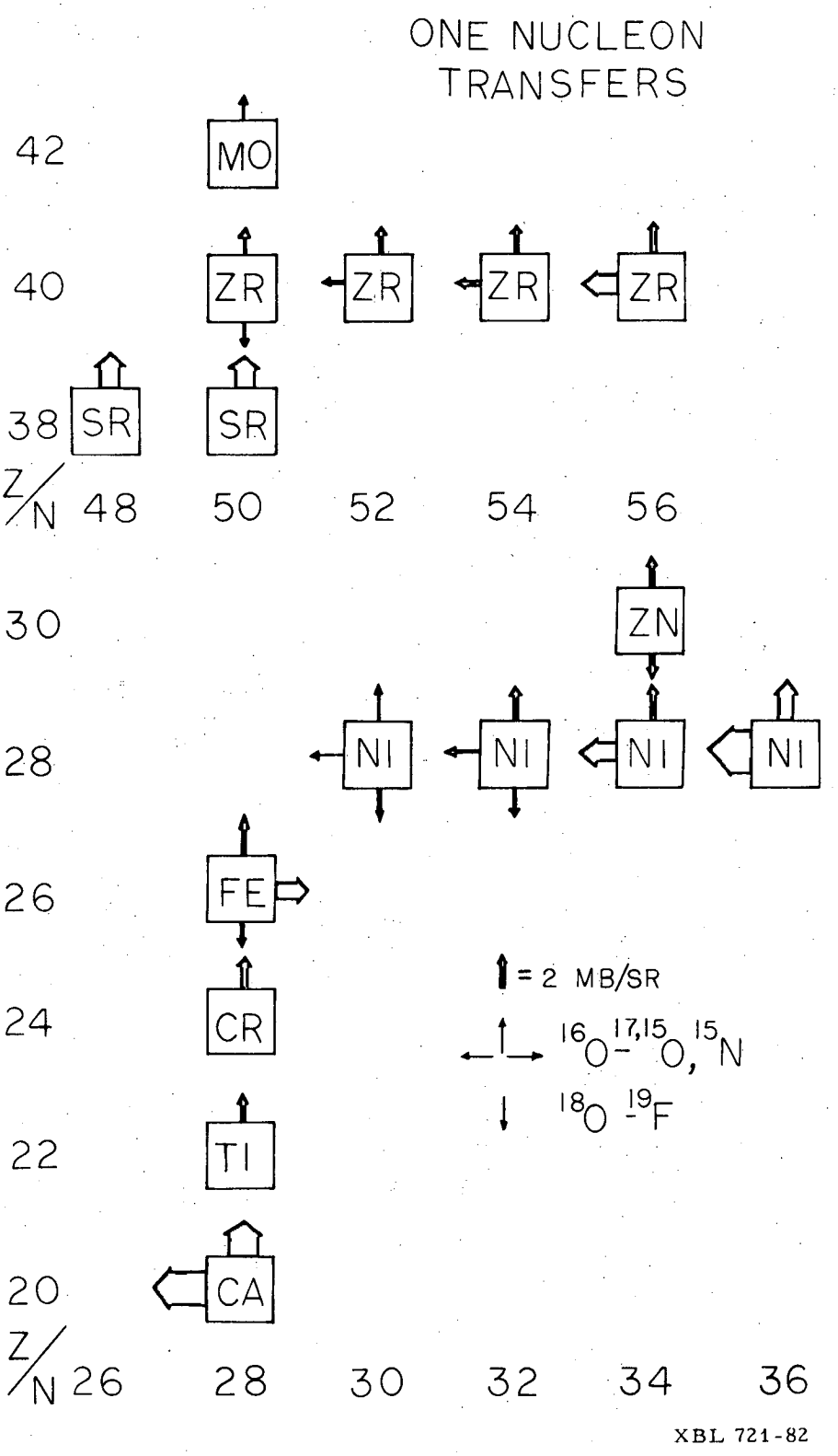
ONE NUCLEON
TRANSFERS
42
40
38
Z/N
48
50
52
54
56
MO
ZR
ZR
ZR
ZR
SR
SR
30
28
26
24
22
20
Z/N
26
28
30
32
34
36
ZN
NI
NI
NI
NI
FE
CR
TI
CA
= 2 MB/SR
16O-17,15O, 15N
18O 19F
XBL 721-82

Fig. 16

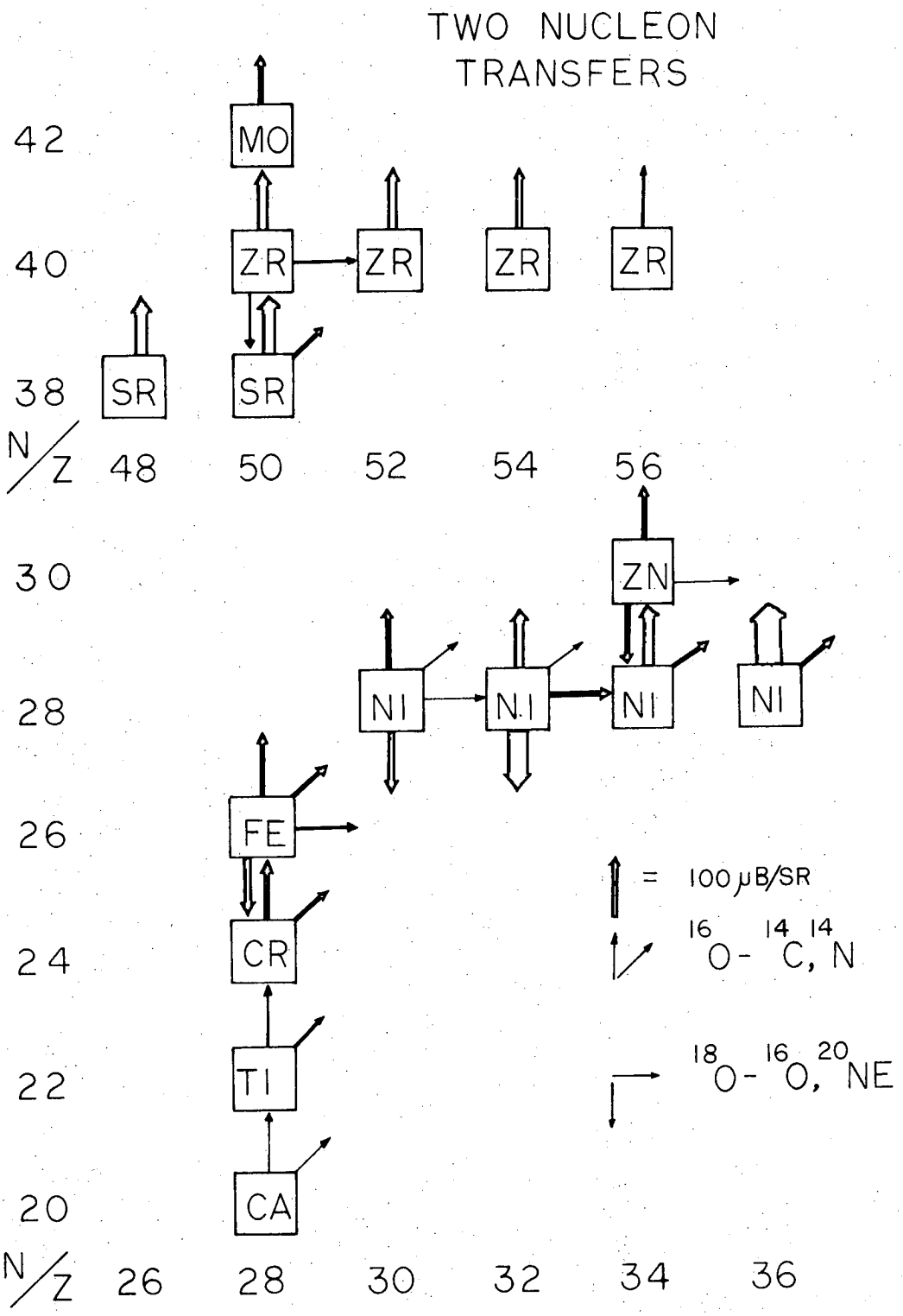
TWO NUCLEON
TRANSFERS
42
40
38
N/Z
48
50
52
54
56
MO
ZR
ZR
ZR
ZR
SR
SR
30
28
26
24
22
20
N/Z
26
28
30
32
34
36
ZN
NI
NI
NI
NI
FE
CR
TI
CA
= 100 μB/SR
16O - 14C, 14N
18O - 16O, 20NE

Fig. 17

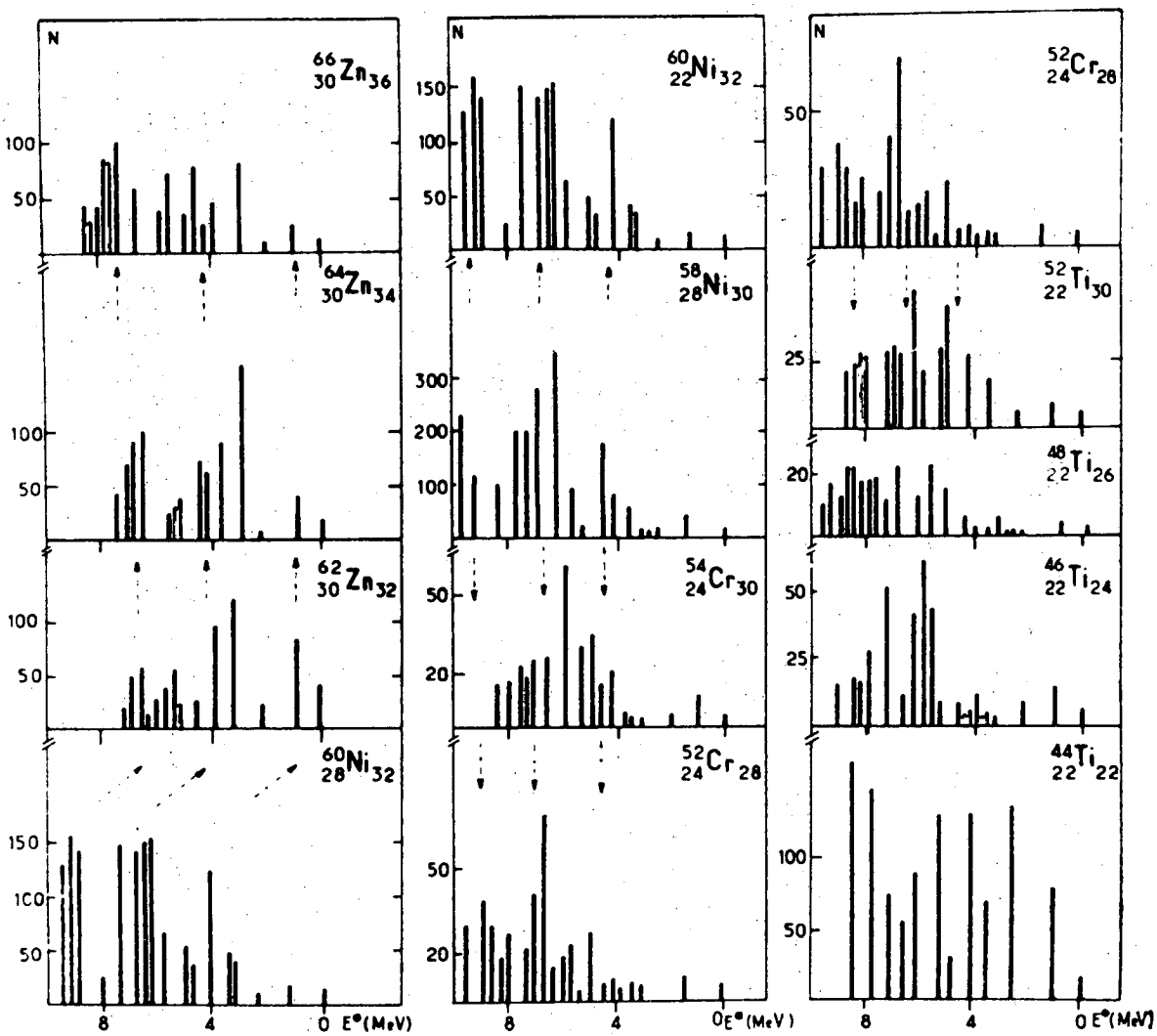
N
$^{66}_{30}Zn_{36}$
$^{64}_{30}Zn_{34}$
$^{62}_{30}Zn_{32}$
$^{60}_{28}Ni_{32}$
$^{60}_{22}Ni_{32}$
$^{58}_{28}Ni_{30}$
$^{54}_{24}Cr_{30}$
$^{52}_{24}Cr_{28}$
$^{52}_{24}Cr_{28}$
$^{52}_{22}Ti_{30}$
$^{48}_{22}Ti_{26}$
$^{46}_{22}Ti_{24}$
$^{44}_{22}Ti_{22}$
E*(MeV)

Fig. 18

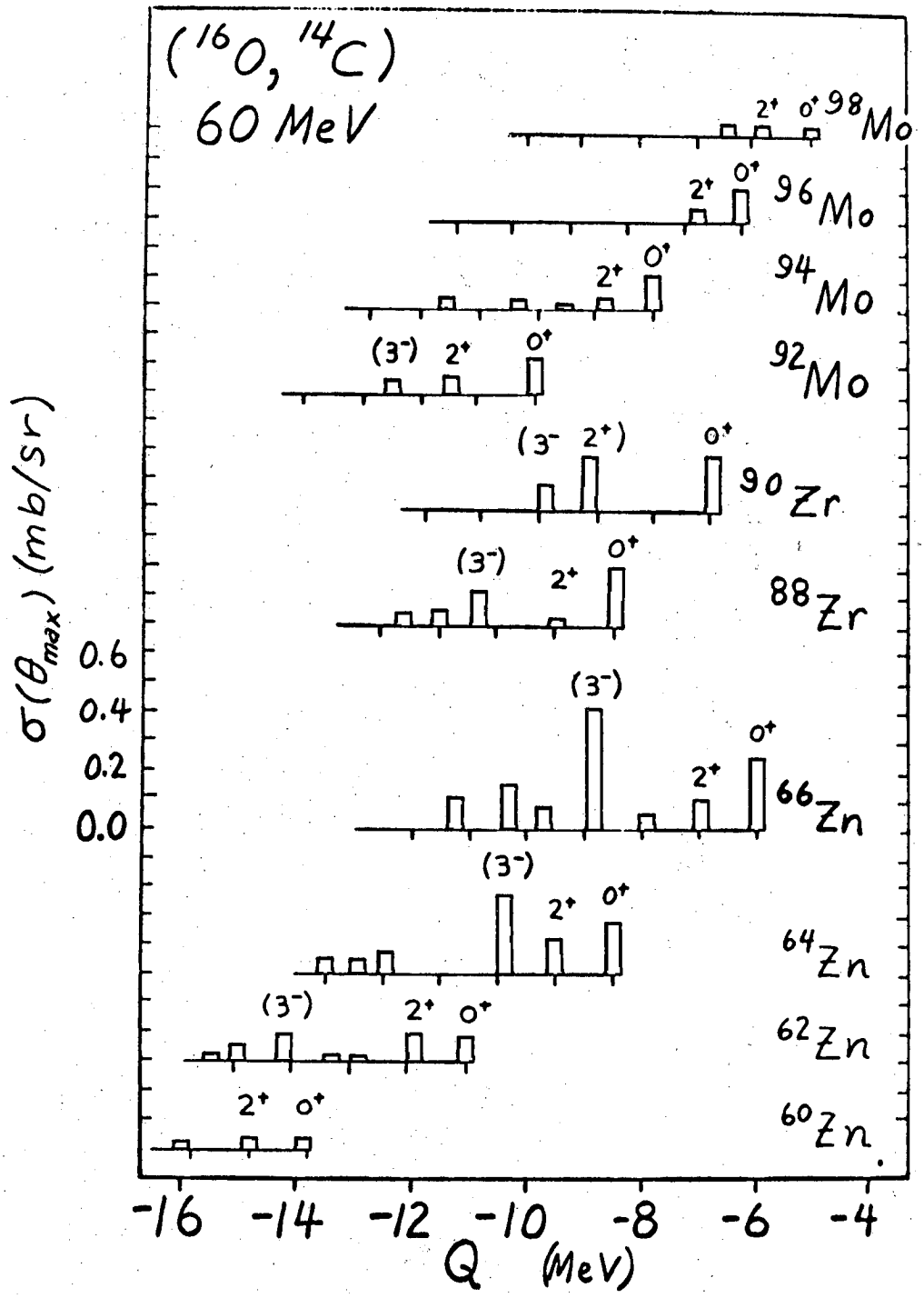
(16O, 14C)
60 MeV
2+ 0+ 98Mo
2+ 0+ 96Mo
2+ 0+ 94Mo
(3-) 2+ 0+ 92Mo
(3-) 2+ 0+ 90Zr
(3-) 2+ 0+ 88Zr
(3-) 2+ 0+ 66Zn
(3-) 2+ 0+ 64Zn
(3-) 2+ 0+ 62Zn
2+ 0+ 60Zn
σ(θmax) (mb/sr)
0.6
0.4
0.2
0.0
-16 -14 -12 -10 -8 -6 -4
Q (MeV)

Fig. 19

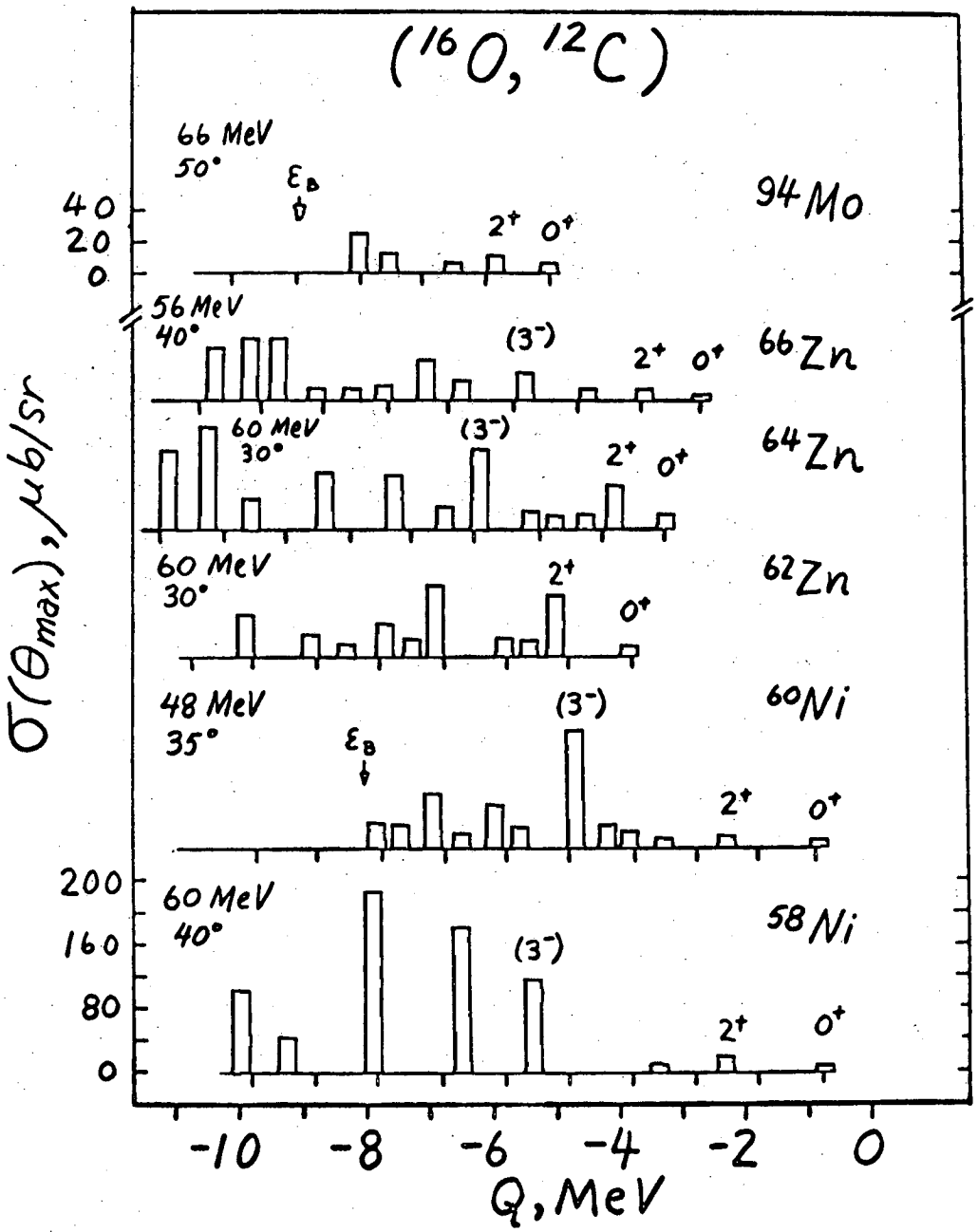
(16O, 12C)
66 MeV
50°
εB
2+ 0+
94Mo
40
20
0
56 MeV
40°
(3-)
2+ 0+
66Zn
60 MeV
30°
(3-)
2+ 0+
64Zn
60 MeV
30°
2+
0+
62Zn
48 MeV
35°
εB
(3-)
2+ 0+
60Ni
200
160
80
0
60 MeV
40°
(3-)
2+ 0+
58Ni
-10 -8 -6 -4 -2 0
Q, MeV
σ(θmax), μb/sr

Fig. 20

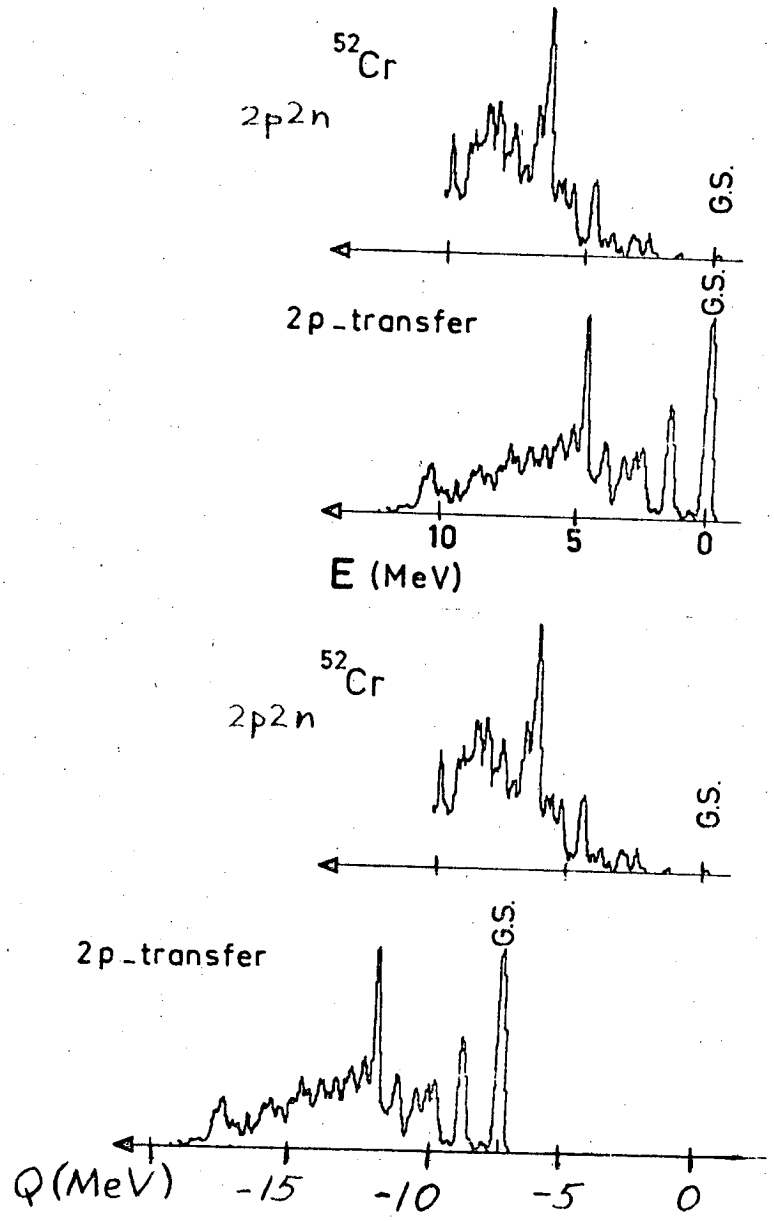
52Cr
2p2n
G.S.
2p_transfer
G.S.
10
5
0
E (MeV)
52Cr
2p2n
G.S.
2p_transfer
G.S.
Q(MeV)
-15
-10
-5
0

Fig. 21

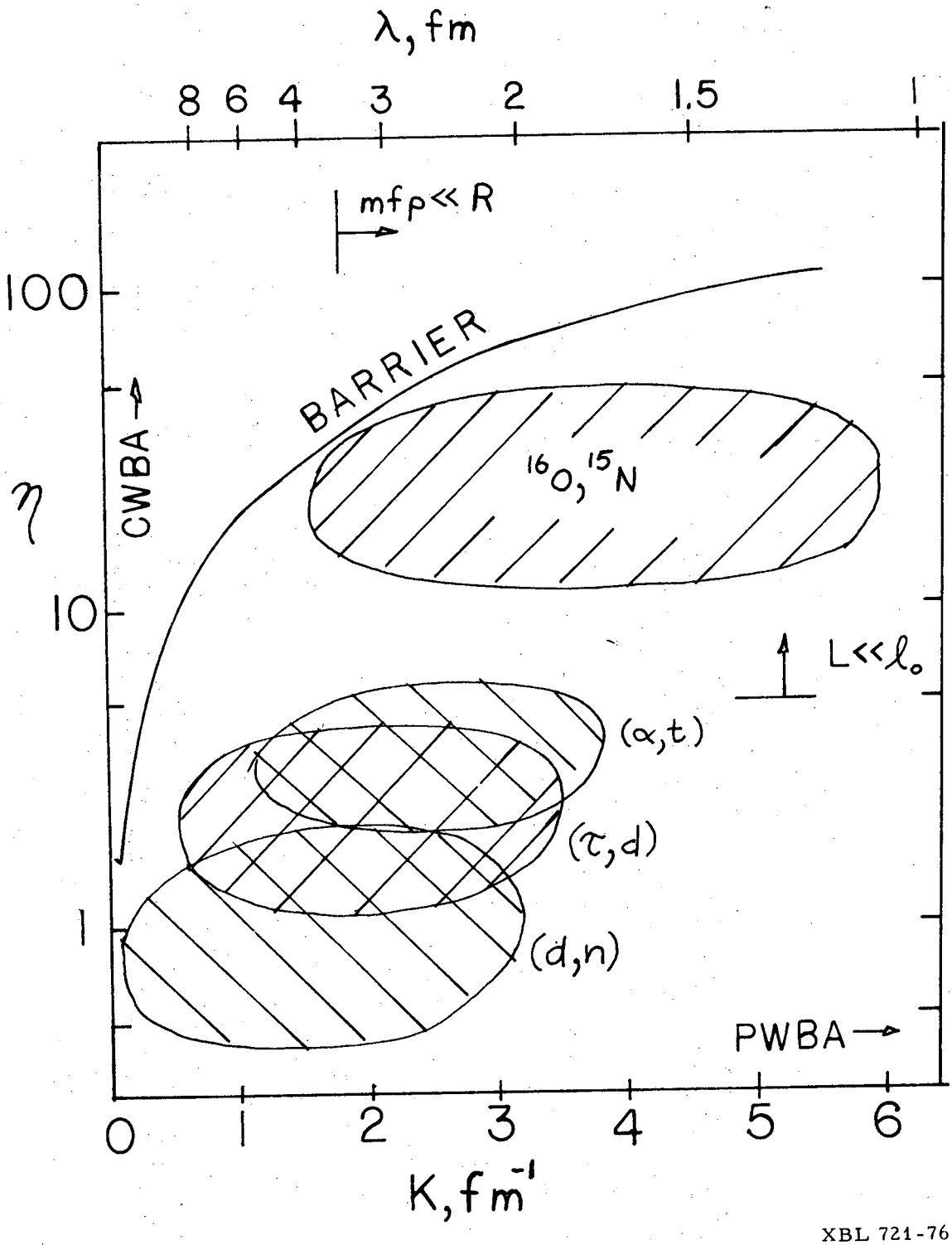
λ, fm
8 6 4 3 2 1.5 1
mfp≪R
100
BARRIER
CWBA
η
$^{16}O, ^{15}N$
10
L≪ℓ₀
(α,t)
(τ,d)
1
(d,n)
PWBA
0 1 2 3 4 5 6
K, fm⁻¹
XBL 721-76

Fig. 22

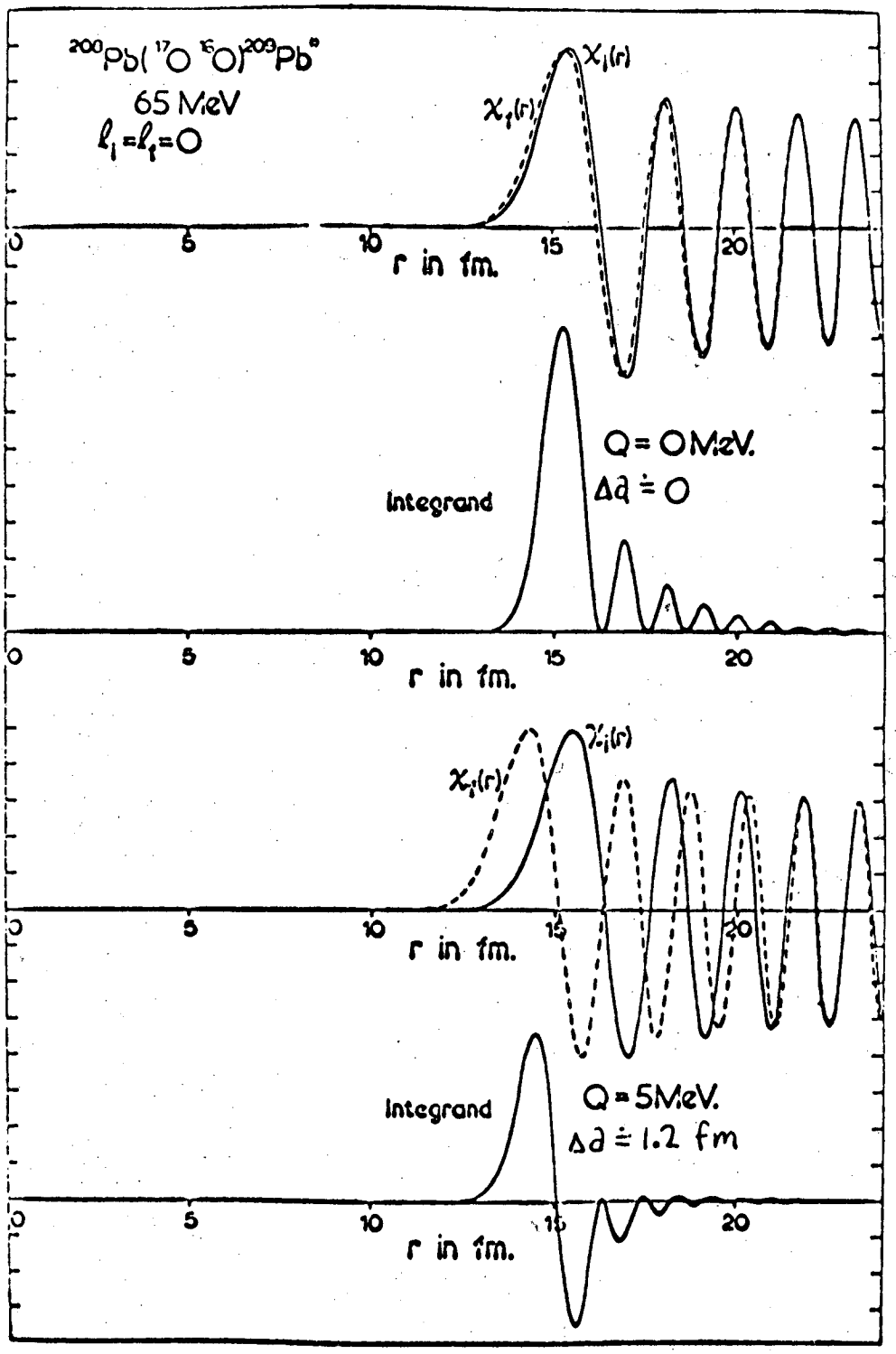
$^{200}Pb(^{17}O\ ^{16}O)^{209}Pb^{*}$
65 MeV
$l_i = l_f = 0$
$\chi_i(r)$
$\chi_f(r)$
r in fm.
Integrand
Q = 0 MeV.
$\Delta a \doteq 0$
r in fm.
$\chi_f(r)$
$\chi_i(r)$
r in fm.
Integrand
Q = 5 MeV.
$\Delta a \doteq 1.2$ fm
r in fm.

Fig. 23

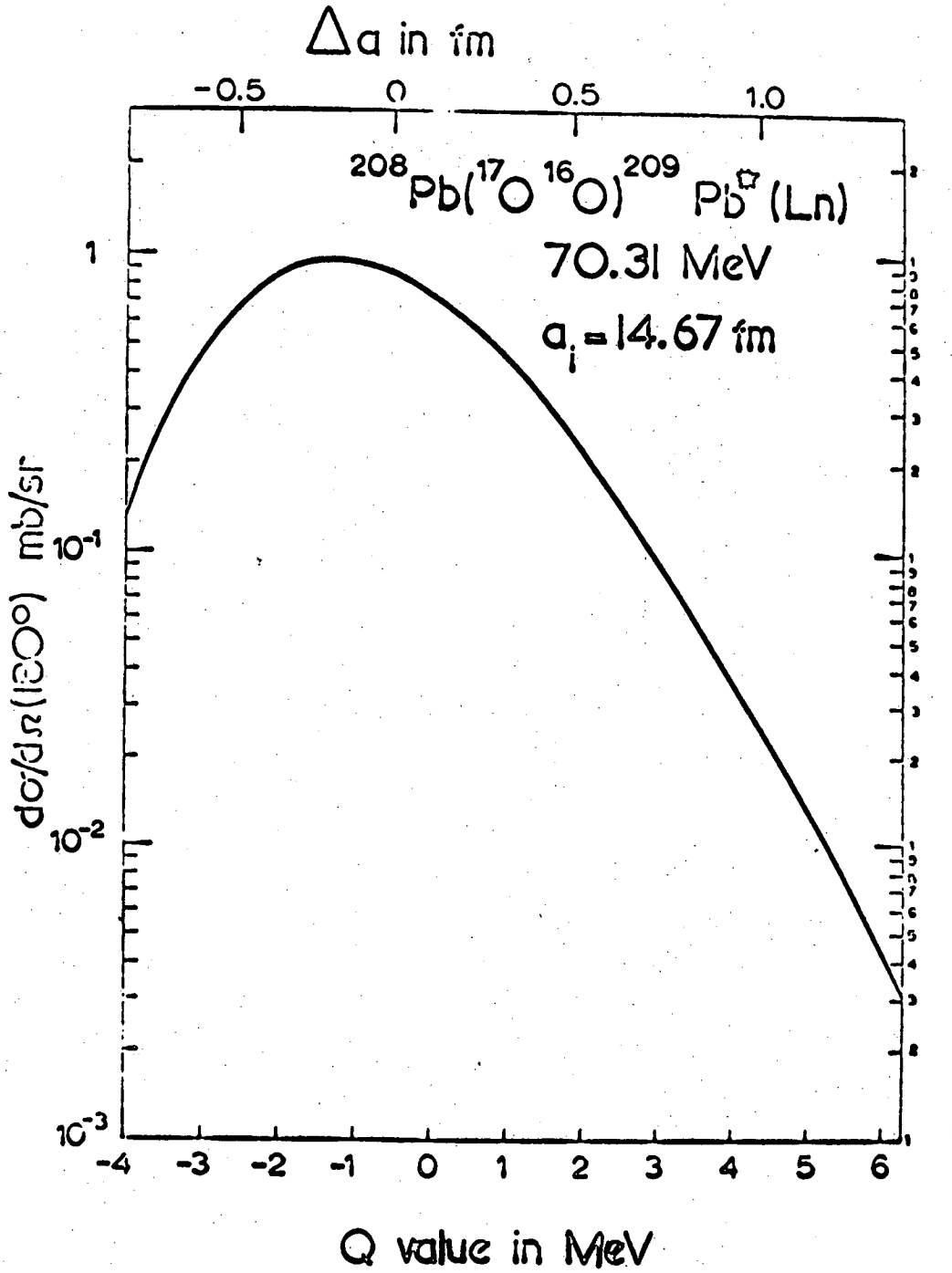
Δa in fm
-0.5
0
0.5
1.0
208Pb(17O 16O)209 Pb☆ (Ln)
70.31 MeV
a_i = 14.67 fm
dσ/dΩ(180°) mb/sr
1
10-1
10-2
10-3
-4
-3
-2
-1
0
1
2
3
4
5
6
Q value in MeV

Fig. 24

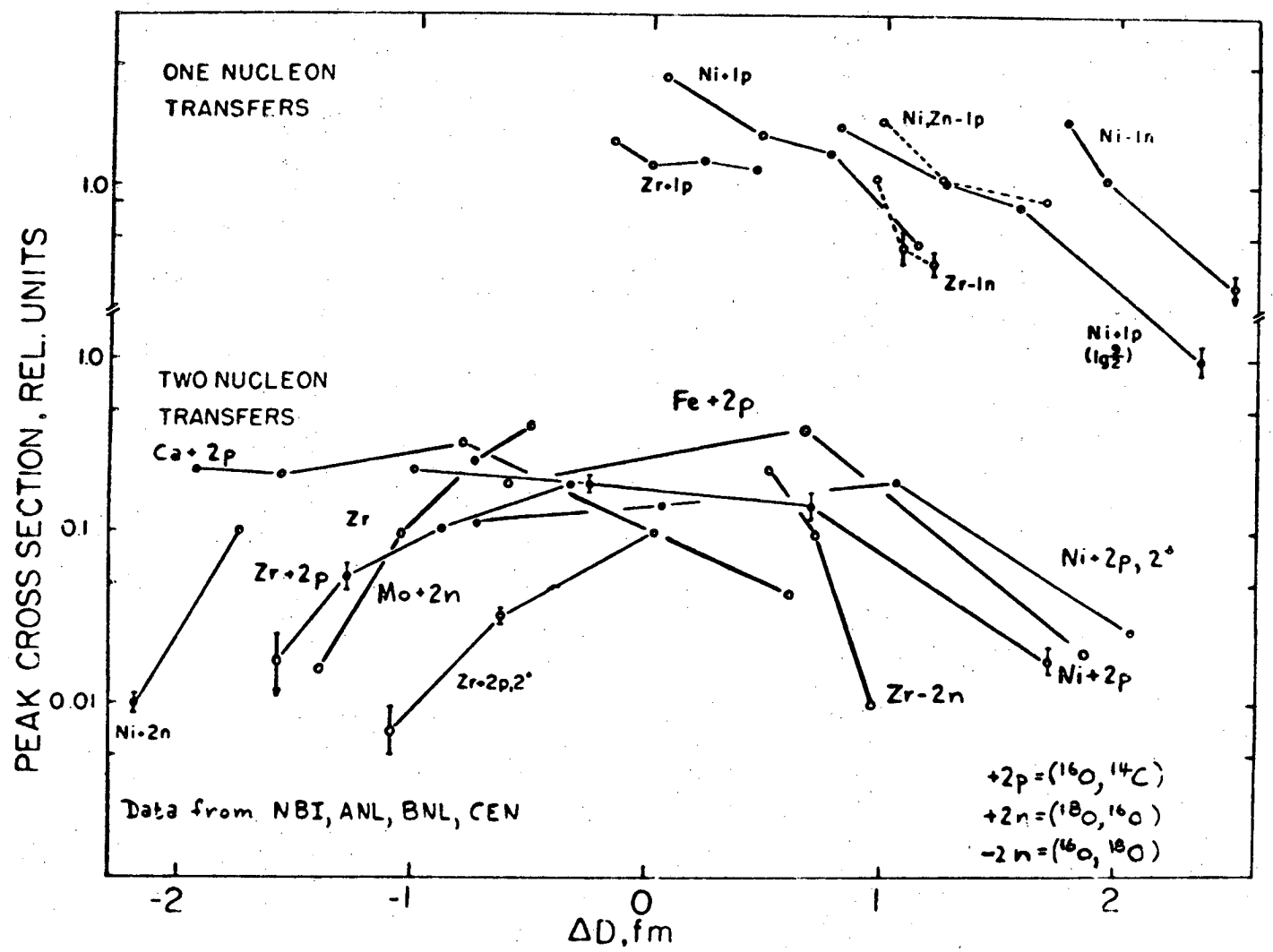
ONE NUCLEON
TRANSFERS
Ni+1p
Ni,Zn-1p
Ni-1n
Zr+1p
Zr-1n
Ni+1p
(lg9/2)
TWO NUCLEON
TRANSFERS
Fe+2p
Ca+2p
Zr
Zr+2p
Mo+2n
Ni+2p, 2+
Zr-2p,2+
Zr-2n
Ni+2p
Ni+2n
Data from NBI, ANL, BNL, CEN
+2p=(16O, 14C)
+2n=(18O, 16O)
-2n=(16O, 18O)
PEAK CROSS SECTION, REL. UNITS
1.0
1.0
0.1
0.01
-2
-1
0
1
2
ΔD, fm

Fig. 25

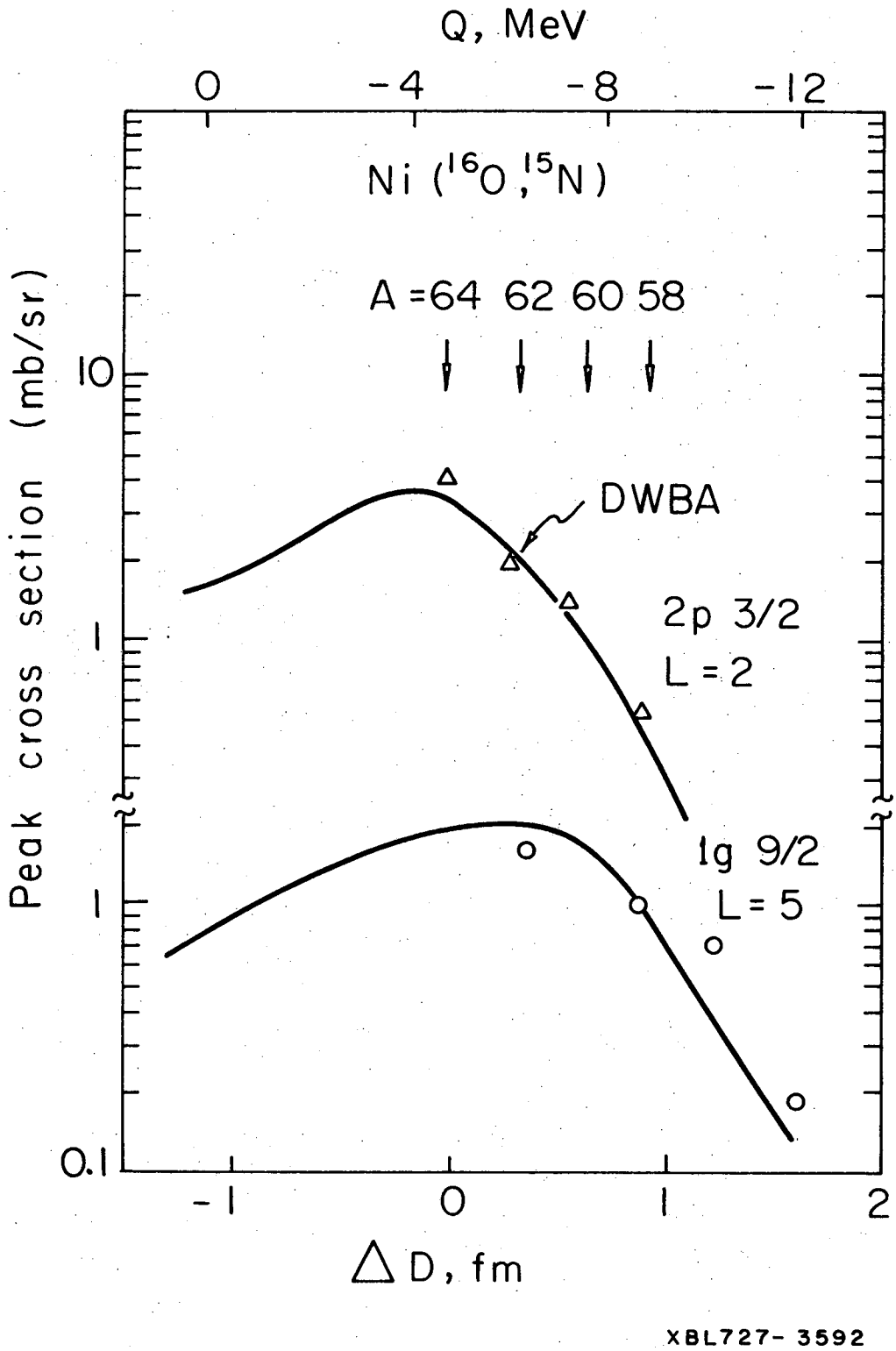
Q, MeV
0
-4
-8
-12
Ni (^{16}O, ^{15}N)
A =64 62 60 58
Peak cross section (mb/sr)
10
1
1
0.1
DWBA
2p 3/2
L = 2
1g 9/2
L = 5
-1
0
1
2
Δ D, fm
XBL727-3592

Fig. 26

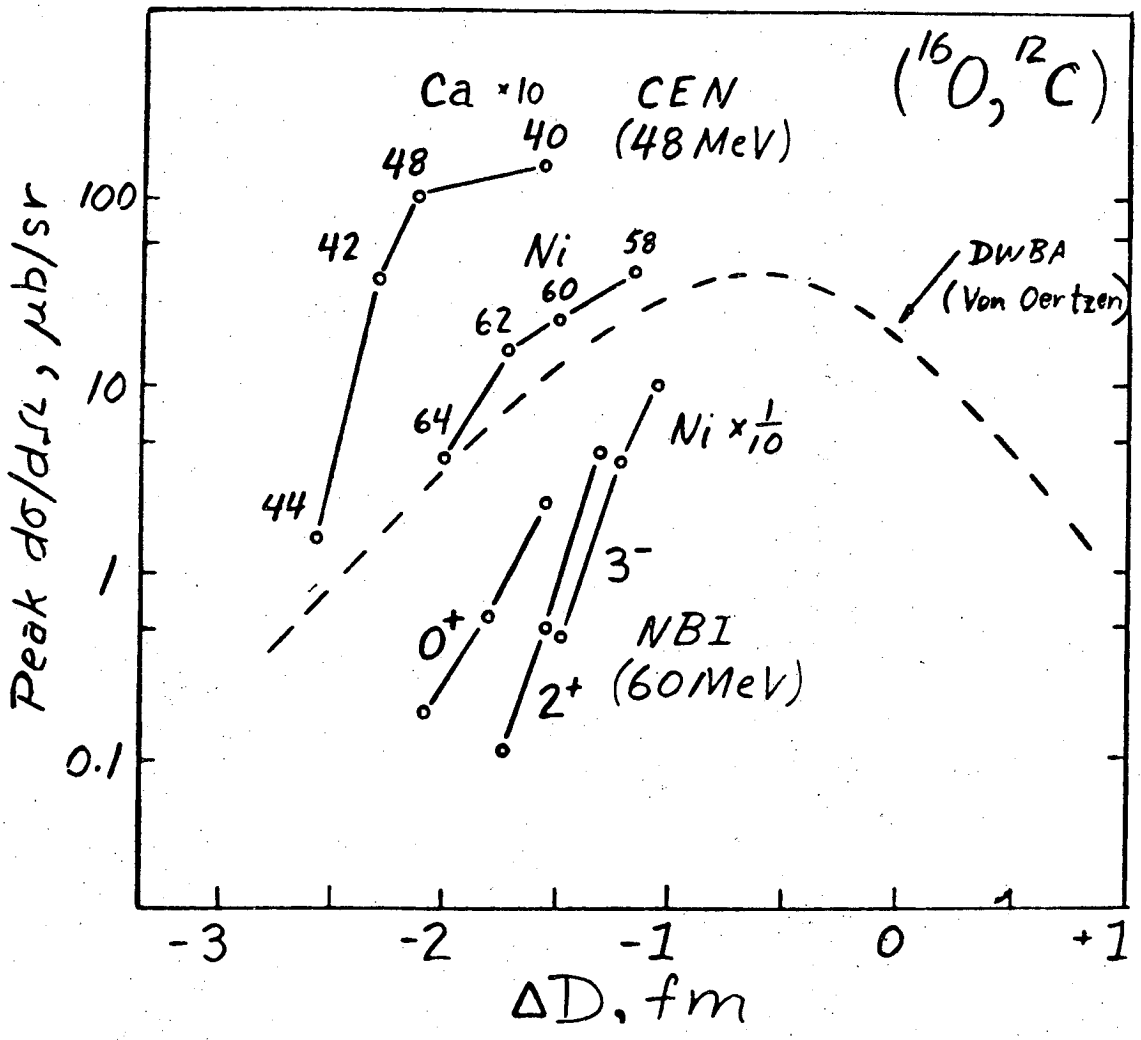
Ca ×10
CEN
(48 MeV)
(^{16}O, ^{12}C)
40
48
42
44
Ni
58
60
62
64
DWBA
(Von Oertzen)
Ni ×1/10
3⁻
0⁺
2⁺
NBI
(60 MeV)
Peak dσ/dΩ, μb/sr
100
10
1
0.1
-3
-2
-1
0
+1
ΔD, fm

Fig. 27

Semi-classical Orbits ($V \propto \frac{1}{r}$)

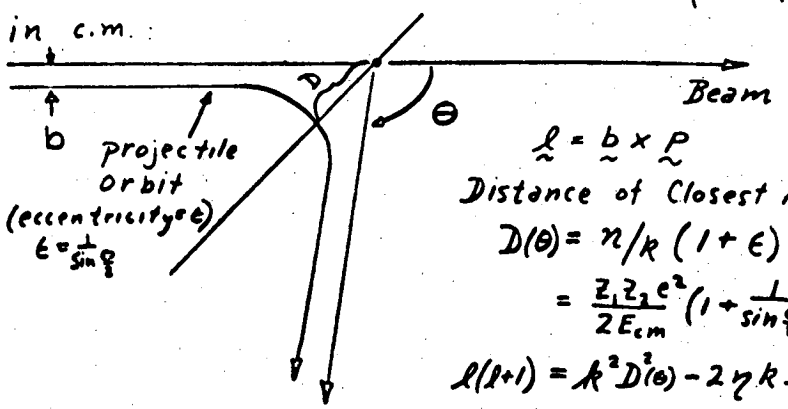

$$\underset{\sim}{\ell} = \underset{\sim}{b} \times \underset{\sim}{p}$$

Distance of Closest Approach:

$$D(\theta) = \eta/k\,(1+\epsilon)$$

$$= \frac{Z_1 Z_2 e^2}{2E_{cm}}\left(1+\frac{1}{\sin\frac{\theta}{2}}\right)$$

$$\ell(\ell+1) = k^2 D^2(\theta) - 2\eta k D(\theta)$$

Define:

$$\frac{d\sigma}{dD} = \frac{8\pi k}{\eta}\sin^3\frac{\theta}{2}\,\frac{d\sigma}{d\Omega}(\theta)$$

Rutherford Scattering:

$$\frac{d\sigma}{d\Omega}(\theta) = \frac{1}{4}\frac{\eta^2}{k^2}\frac{1}{\sin^4\frac{\theta}{2}}$$

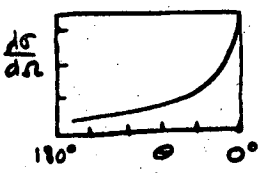

$$\frac{d\sigma}{dD} = 2\pi\left(D(\theta) - a/2\right)$$

where $a = D(180°)$

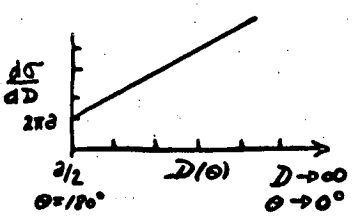

Transfer Reaction: ($E < E_B$)

$$\frac{d\sigma}{dD} \propto D\exp\left[-2\alpha D(\theta)\right]$$

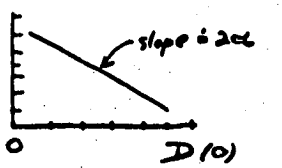

where $D \equiv \left(D_f(\theta) + D_i(\theta)\right)/2$

$\alpha \equiv (\alpha_f + \alpha_i)/2$

$\alpha_{f,i}$ = b.s. parameter

In general: ($E > E_B$ we need $P_{abs}(D)$ = absorbtion)

$$\frac{d\sigma}{dD} \propto D^3 \times \left|\text{Form factor}, F(D)\right|^2 \times \left[1 - P_{abs}(D)\right]$$

e.g. Rutherford scattering: $F(D) \propto \frac{1}{D}$

Transfer: $F(D) \propto \phi(D) \propto \frac{e^{-\alpha D}}{\alpha D}$

Fig. 28

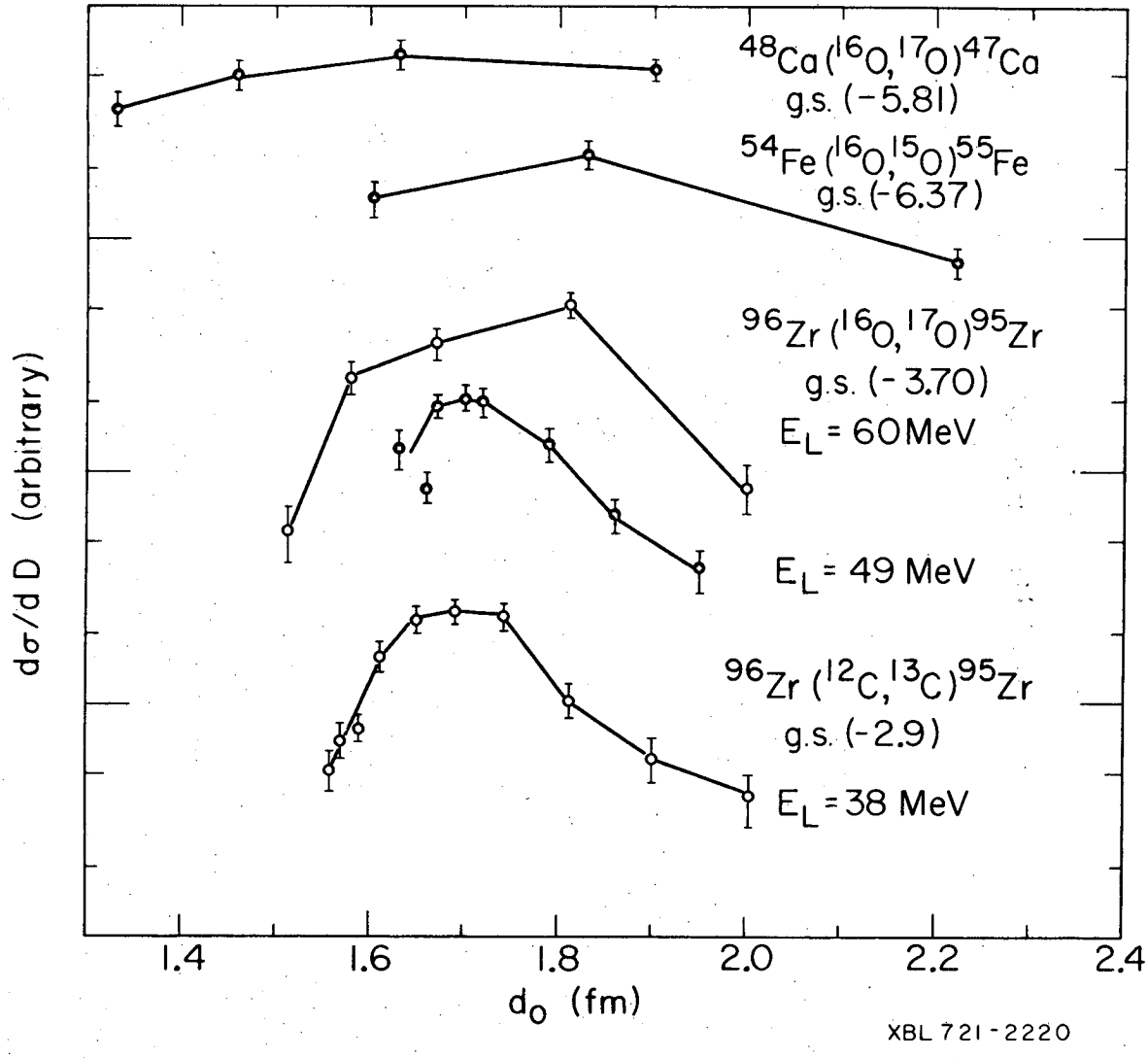
$^{48}Ca(^{16}O,^{17}O)^{47}Ca$
g.s. (-5.81)
$^{54}Fe(^{16}O,^{15}O)^{55}Fe$
g.s. (-6.37)
$^{96}Zr(^{16}O,^{17}O)^{95}Zr$
g.s. (-3.70)
E_L = 60MeV
E_L = 49 MeV
$^{96}Zr(^{12}C,^{13}C)^{95}Zr$
g.s. (-2.9)
E_L = 38 MeV
dσ/d D (arbitrary)
1.4
1.6
1.8
2.0
2.2
2.4
d_0 (fm)
XBL 721-2220

Fig. 29

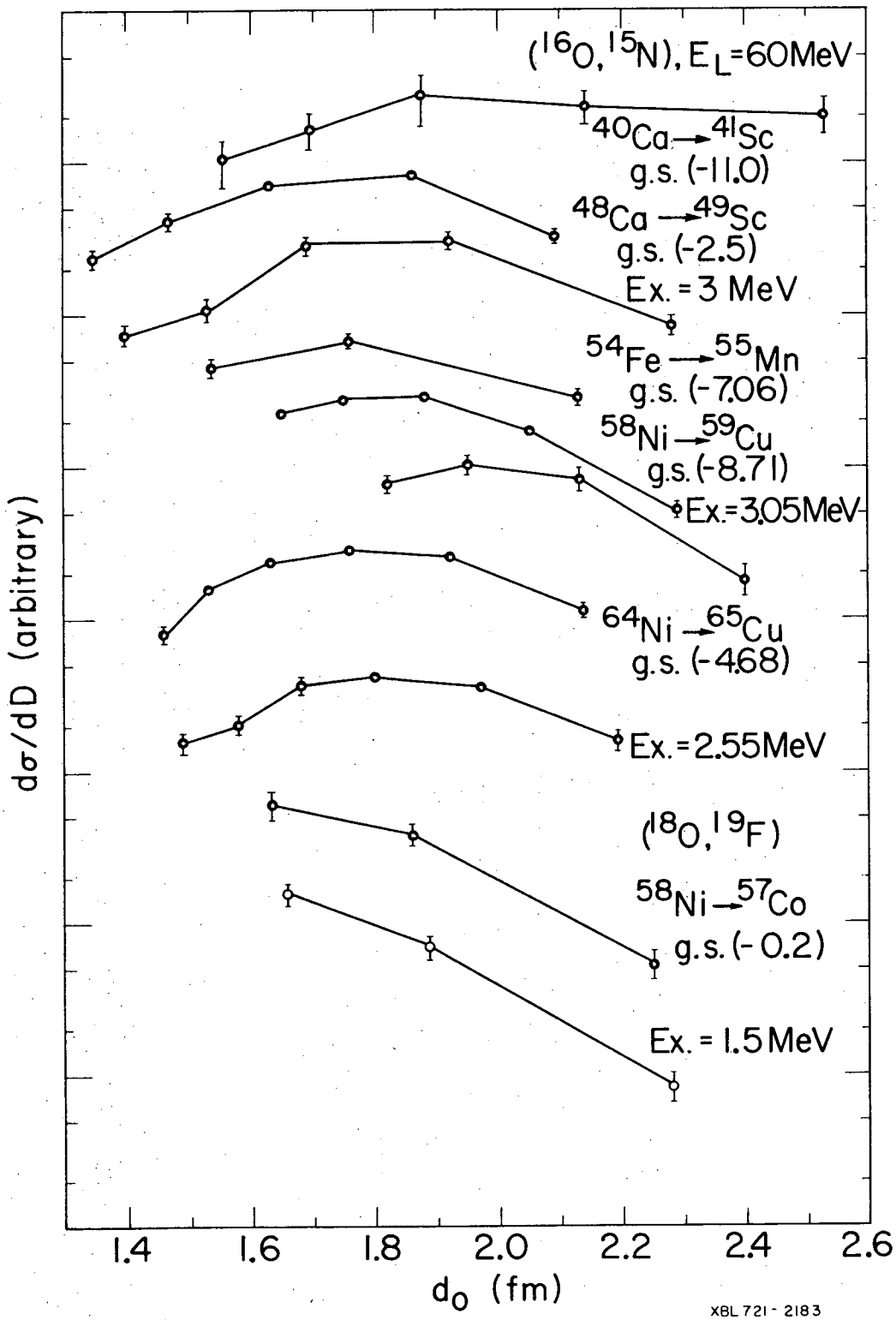
(16O, 15N), EL=60MeV
40Ca → 41Sc
g.s. (-11.0)
48Ca → 49Sc
g.s. (-2.5)
Ex. = 3 MeV
54Fe → 55Mn
g.s. (-7.06)
58Ni → 59Cu
g.s. (-8.71)
Ex.=3.05MeV
64Ni → 65Cu
g.s. (-4.68)
Ex.=2.55MeV
(18O, 19F)
58Ni → 57Co
g.s. (-0.2)
Ex. = 1.5MeV
dσ/dD (arbitrary)
1.4
1.6
1.8
2.0
2.2
2.4
2.6
d0 (fm)
XBL 721-2183

Fig. 30

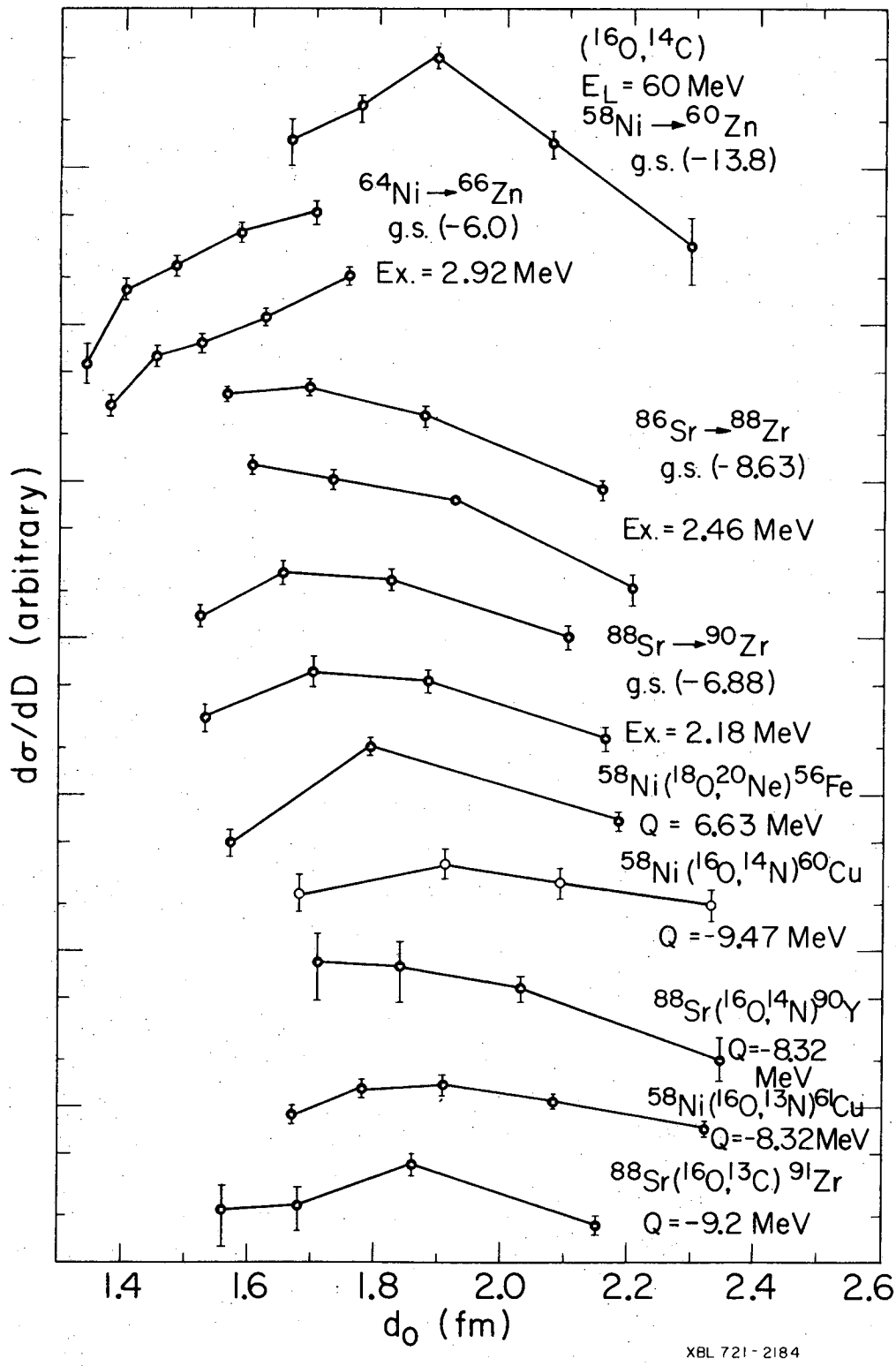
(16O,14C)
EL = 60 MeV
58Ni → 60Zn
g.s. (-13.8)
64Ni → 66Zn
g.s. (-6.0)
Ex. = 2.92 MeV
86Sr → 88Zr
g.s. (-8.63)
Ex. = 2.46 MeV
88Sr → 90Zr
g.s. (-6.88)
Ex. = 2.18 MeV
58Ni(18O,20Ne)56Fe
Q = 6.63 MeV
58Ni(16O,14N)60Cu
Q = -9.47 MeV
88Sr(16O,14N)90Y
Q=-8.32 MeV
58Ni(16O,13N)61Cu
Q=-8.32MeV
88Sr(16O,13C) 91Zr
Q = -9.2 MeV
dσ/dD (arbitrary)
1.4
1.6
1.8
2.0
2.2
2.4
2.6
d0 (fm)
XBL 721-2184

Fig. 31

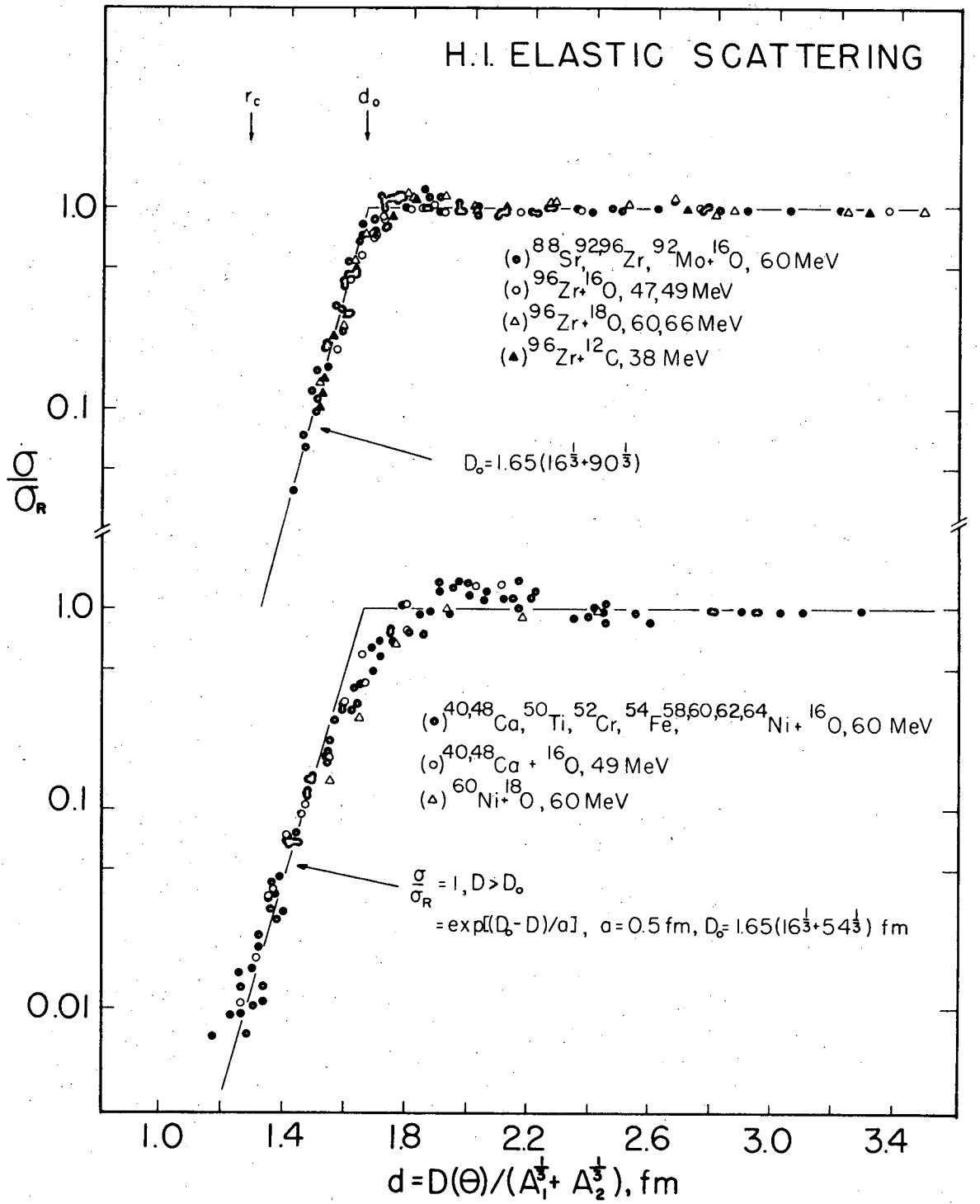
H.I. ELASTIC SCATTERING
r_c
d_o
1.0
0.1
$\frac{\sigma}{\sigma_R}$
(•) $^{88}Sr, ^{92,96}Zr, ^{92}Mo + ^{16}O$, 60 MeV
(○) $^{96}Zr + ^{16}O$, 47, 49 MeV
(△) $^{96}Zr + ^{18}O$, 60, 66 MeV
(▲) $^{96}Zr + ^{12}C$, 38 MeV
$D_o = 1.65(16^{\frac{1}{3}} + 90^{\frac{1}{3}})$
1.0
0.1
0.01
(•) $^{40,48}Ca, ^{50}Ti, ^{52}Cr, ^{54-58,60,62,64}Fe, Ni + ^{16}O$, 60 MeV
(○) $^{40,48}Ca + ^{16}O$, 49 MeV
(△) $^{60}Ni + ^{18}O$, 60 MeV
$\frac{\sigma}{\sigma_R} = 1, D > D_o$
$= \exp[(D_o - D)/a]$, $a = 0.5$ fm, $D_o = 1.65(16^{\frac{1}{3}} + 54^{\frac{1}{3}})$ fm
1.0
1.4
1.8
2.2
2.6
3.0
3.4
$d = D(\Theta)/(A_1^{\frac{1}{3}} + A_2^{\frac{1}{3}})$, fm
XBL 721-49

Fig. 32

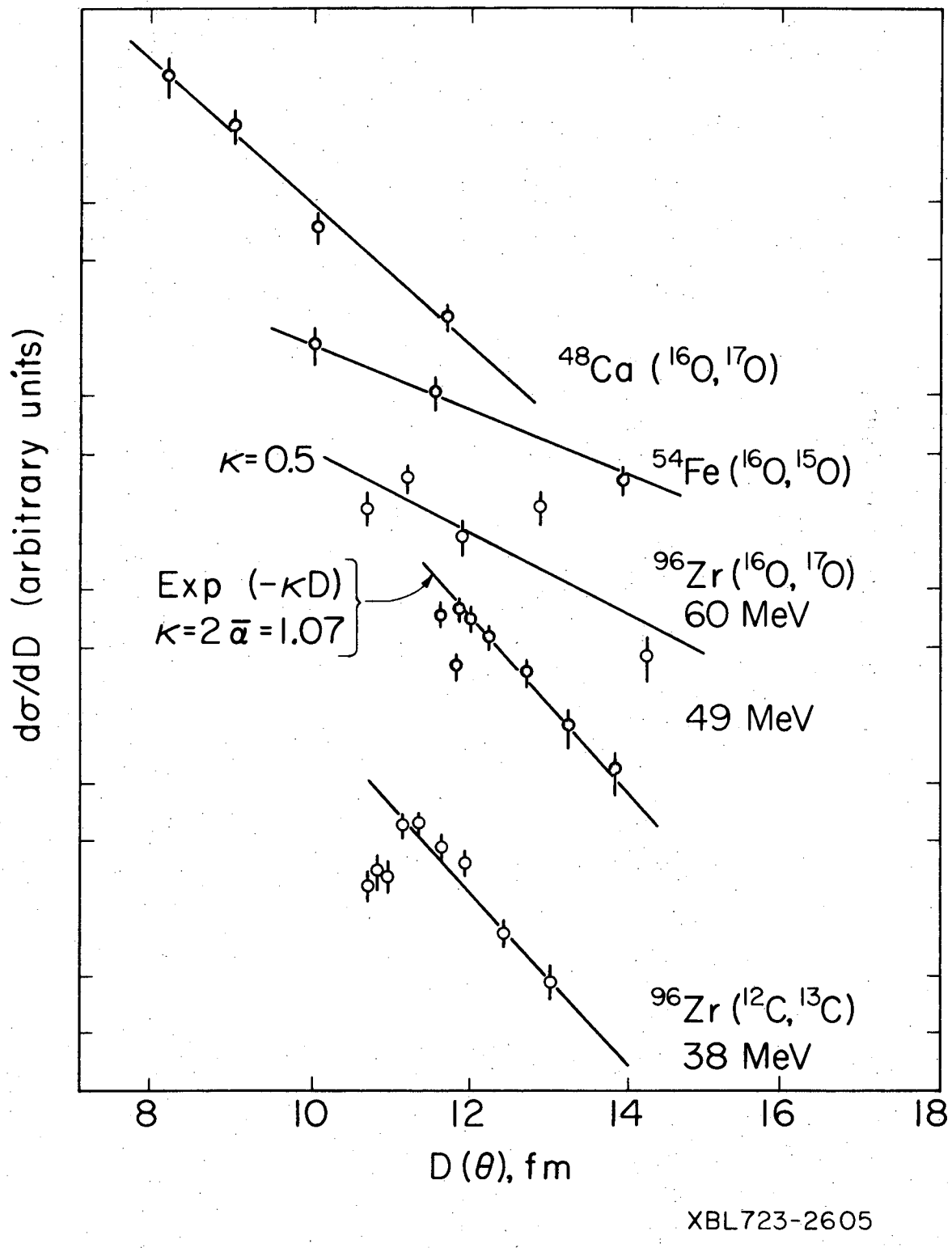
dσ/dD (arbitrary units)
D (θ), fm
8
10
12
14
16
18
48Ca (16O, 17O)
54Fe (16O, 15O)
κ=0.5
96Zr (16O, 17O)
60 MeV
Exp (-κD)
κ=2ᾱ=1.07
49 MeV
96Zr (12C, 13C)
38 MeV
XBL723-2605

Fig. 33a

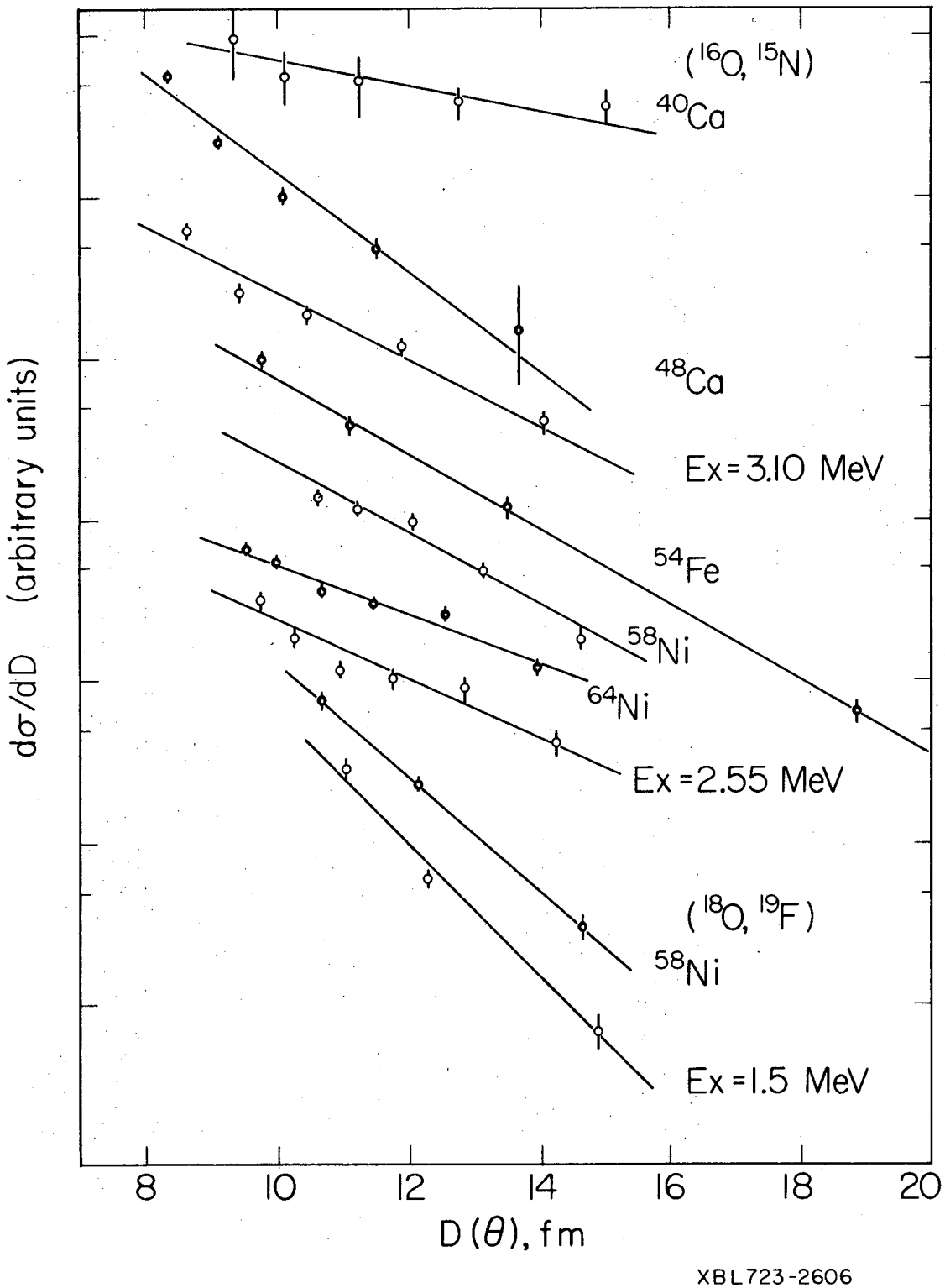
(16O, 15N)
40Ca
48Ca
Ex = 3.10 MeV
54Fe
58Ni
64Ni
Ex = 2.55 MeV
(18O, 19F)
58Ni
Ex = 1.5 MeV
dσ/dD (arbitrary units)
D(θ), fm
8
10
12
14
16
18
20
XBL723-2606

Fig. 33b

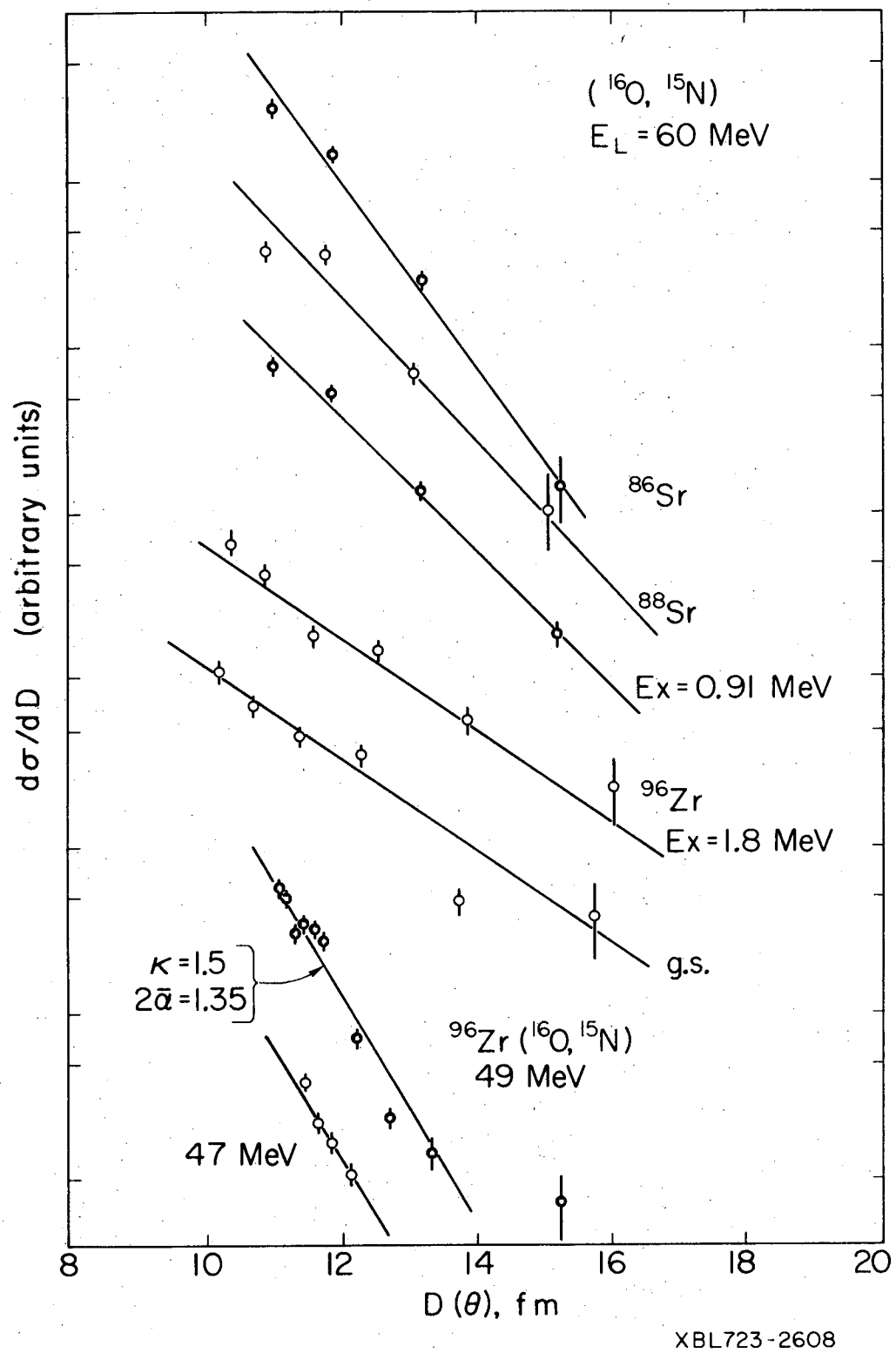
(^{16}O, ^{15}N)
E_L = 60 MeV
^{86}Sr
^{88}Sr
Ex = 0.91 MeV
^{96}Zr
Ex = 1.8 MeV
g.s.
κ = 1.5
2α̃ = 1.35
^{96}Zr (^{16}O, ^{15}N)
49 MeV
47 MeV
dσ/dD (arbitrary units)
D (θ), fm
8
10
12
14
16
18
20
XBL723-2608

Fig. 34a

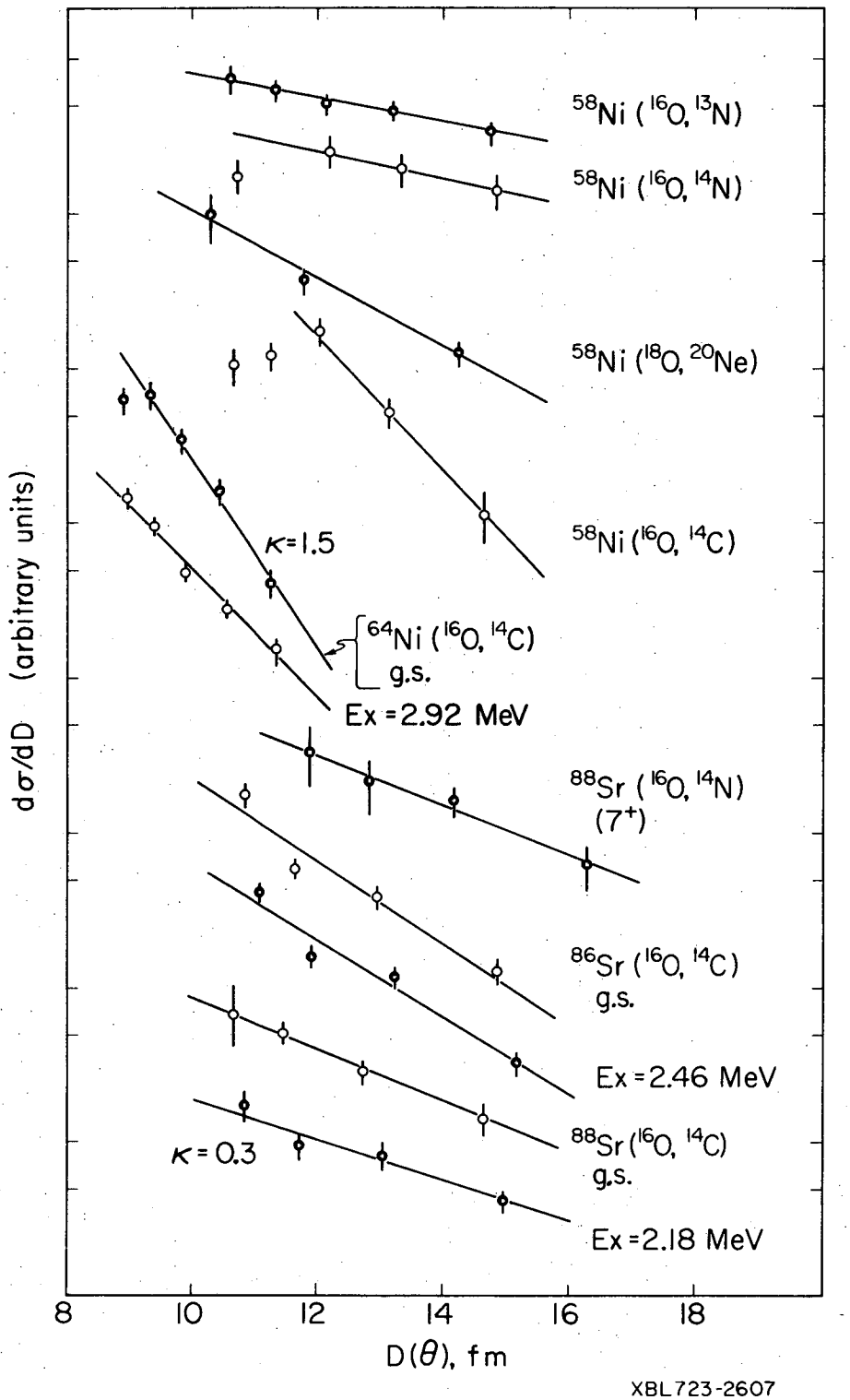
58Ni (16O, 13N)
58Ni (16O, 14N)
58Ni (18O, 20Ne)
58Ni (16O, 14C)
K=1.5
64Ni (16O, 14C)
g.s.
Ex = 2.92 MeV
88Sr (16O, 14N)
(7+)
86Sr (16O, 14C)
g.s.
Ex = 2.46 MeV
88Sr (16O, 14C)
g.s.
K = 0.3
Ex = 2.18 MeV
dσ/dD (arbitrary units)
8
10
12
14
16
18
D(θ), fm
XBL723-2607

Fig. 34b

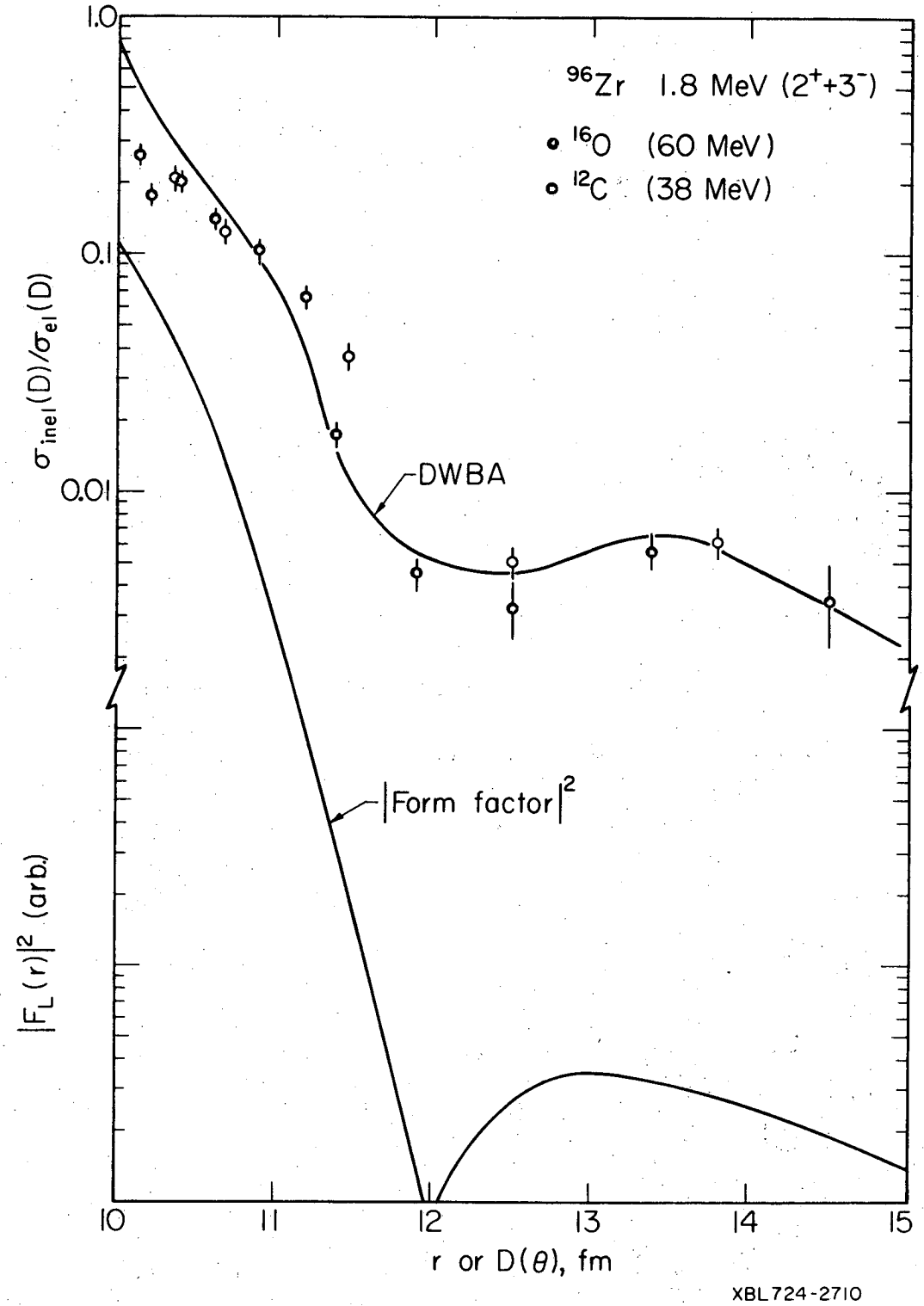
^{96}Zr 1.8 MeV (2^++3^-)
^{16}O (60 MeV)
^{12}C (38 MeV)
DWBA
|Form factor|^2
$\sigma_{inel}(D)/\sigma_{el}(D)$
$|F_L(r)|^2$ (arb.)
1.0
0.1
0.01
10
11
12
13
14
15
r or D(θ), fm
XBL724-2710

Fig. 35

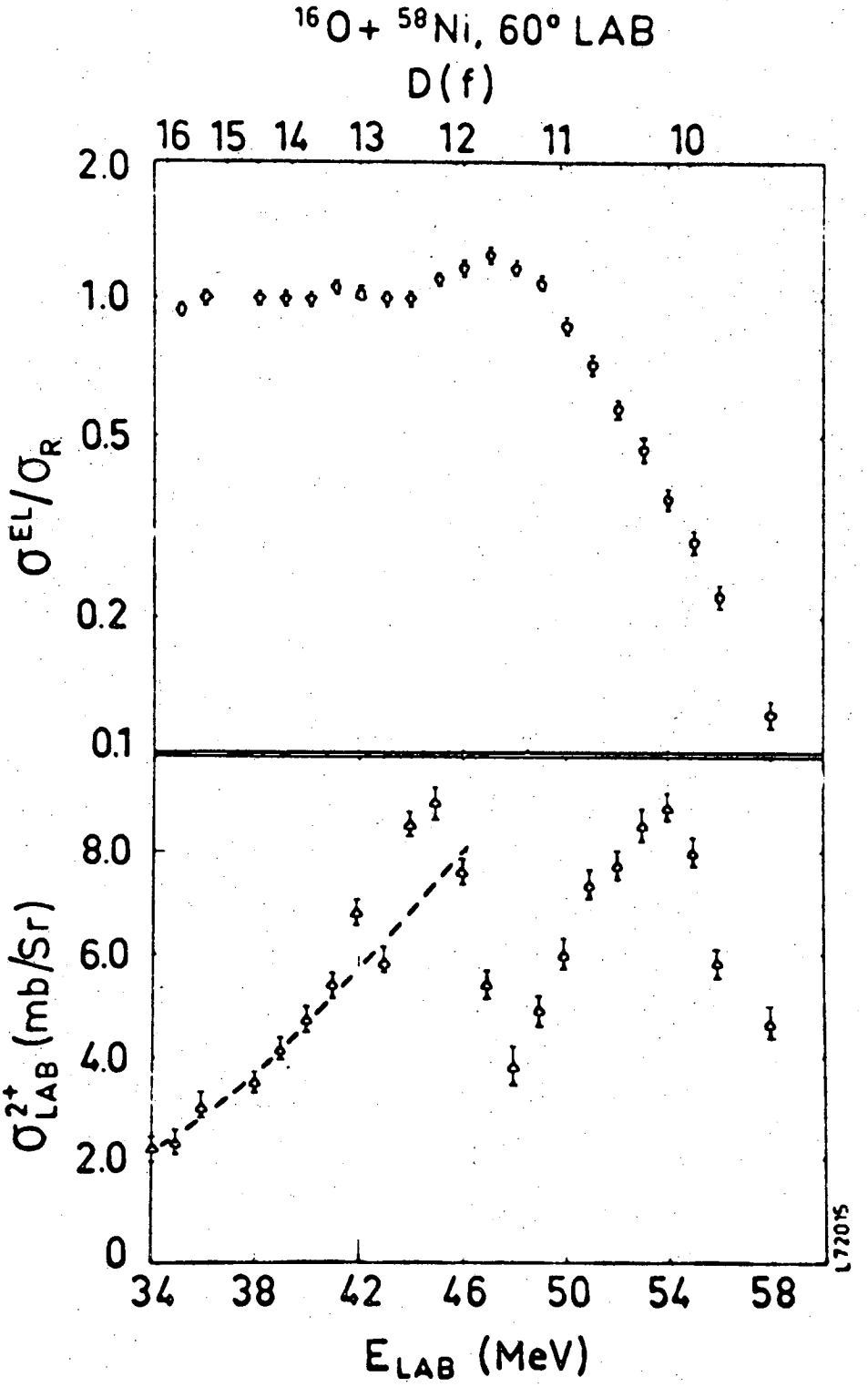
$^{16}O + ^{58}Ni$, 60° LAB
D(f)
16 15 14 13 12 11 10
2.0
1.0
0.5
0.2
0.1
σ^{EL}/σ_R
8.0
6.0
4.0
2.0
0
$\sigma^{2^+}_{LAB}$ (mb/Sr)
34 38 42 46 50 54 58
E_{LAB} (MeV)
L72015

Fig. 36

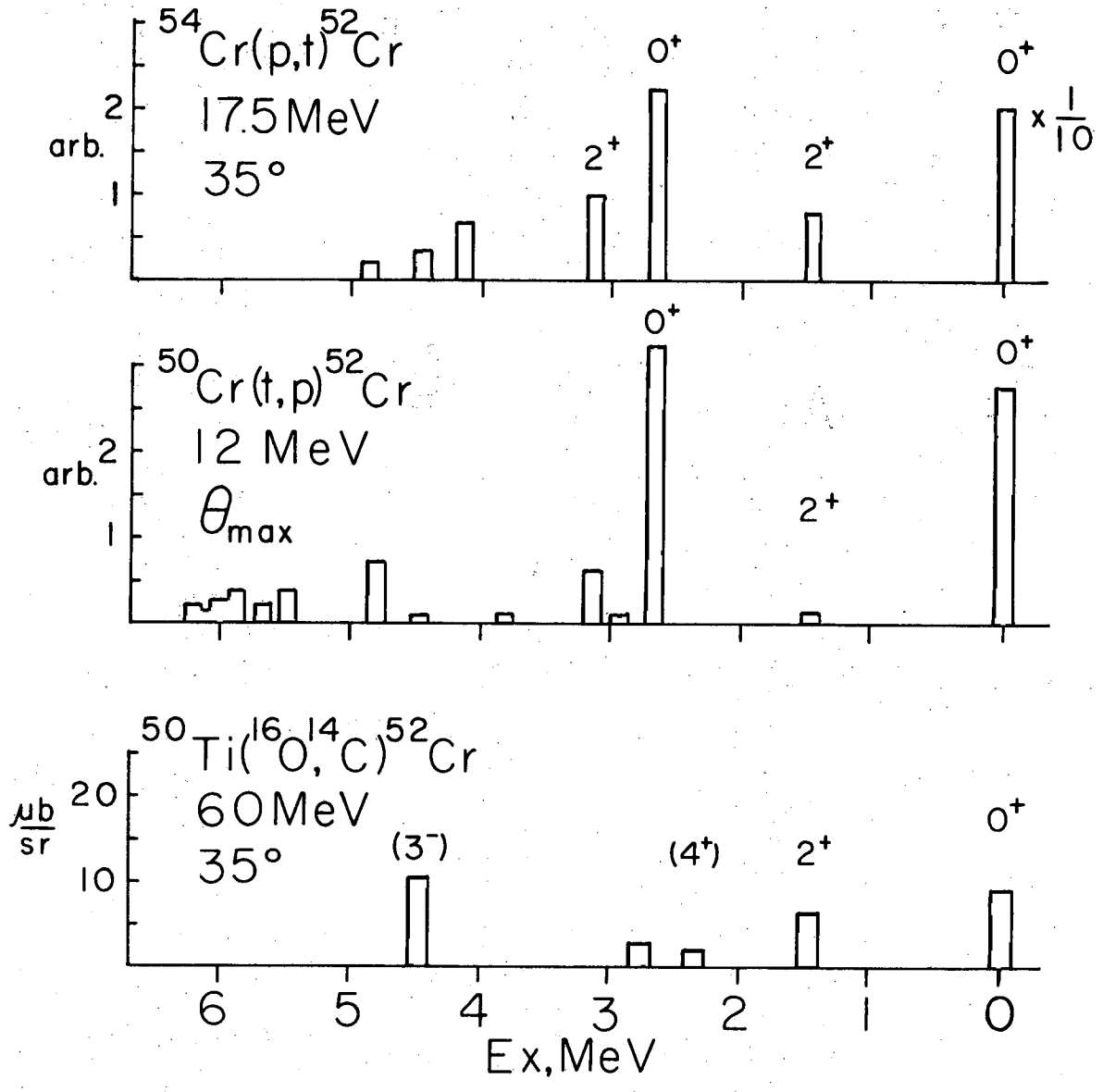

XBL 721-44

Fig. 37

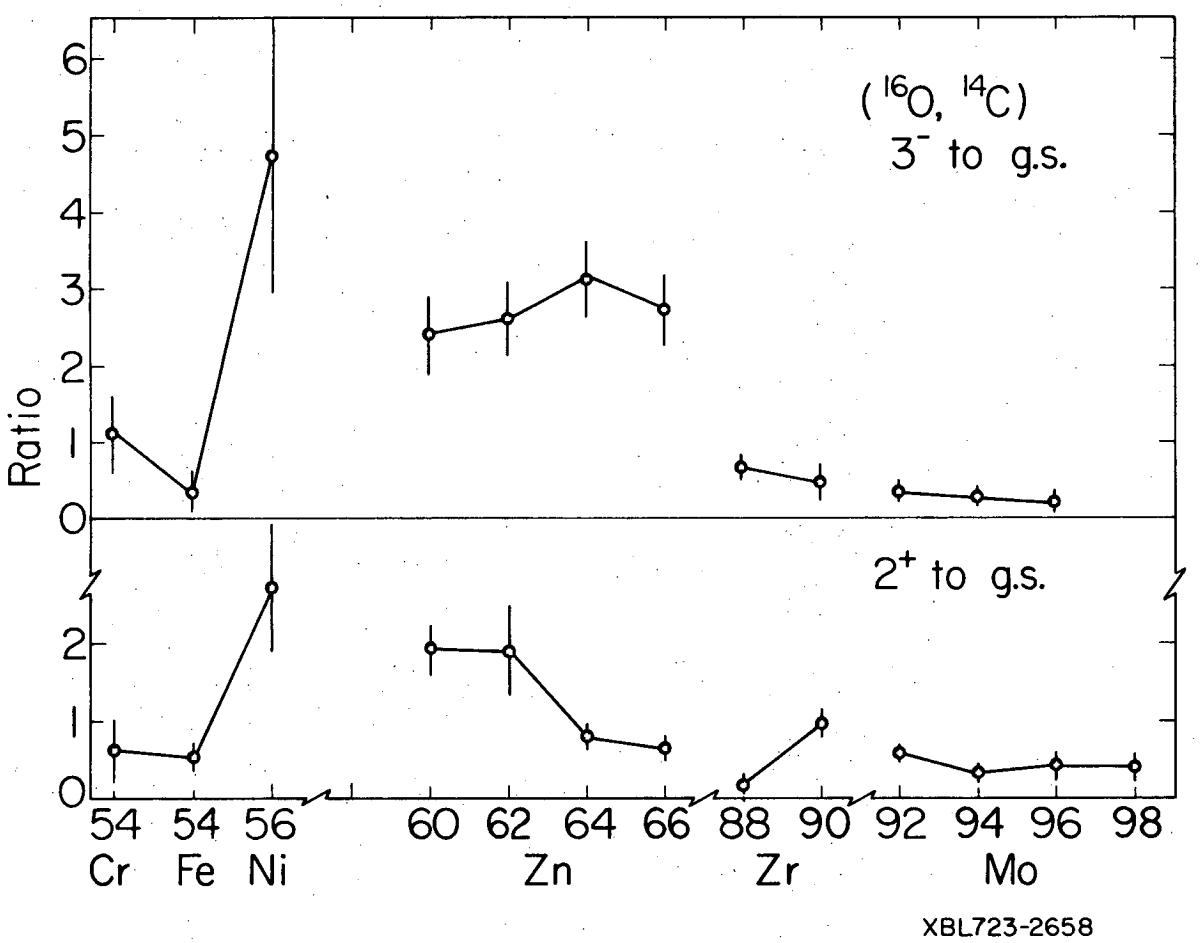
Ratio
6
5
4
3
2
1
0
(^{16}O, ^{14}C)
3$^-$ to g.s.
2$^+$ to g.s.
2
1
0
54 54 56 60 62 64 66 88 90 92 94 96 98
Cr Fe Ni Zn Zr Mo
XBL723-2658

Fig. 38

STRONG PN TRANSFERS

E_L MeV	REACTION	J^π EX	p	n
60 NBI	$^{54}Fe(^{16}O,^{14}N)^{56}Co$	5^+ (0.6)	$1f_{7/2}$	$2p_{3/2}$
60	$^{86}Sr(^{16}O,^{14}N)^{88}Y$	7^+ (0.7)	$1g_{9/2}$	$2d_{5/2}$
60	$^{88}Sr(^{16}O,^{14}N)^{90}Y$	7^+ (0.7)	$1g_{9/2}$	$2d_{5/2}$
66	$^{90}Zr(^{16}O,^{14}N)^{92}Nb$	7^+ gs	$1g_{9/2}$	$2d_{5/2}$
66	$^{92}Mo(^{16}O,^{14}N)^{94}Tc$	7^+ gs	$1g_{9/2}$	$2d_{5/2}$
114 AERL	$^{40}Ca(^{12}C,^{10}B)^{42}Sc$	7^+ (0.6)	$1f_{7/2}$	$1f_{7/2}$

⇒ pn transfer populates high spin "stretched" states (J = J max)

Fig. 39

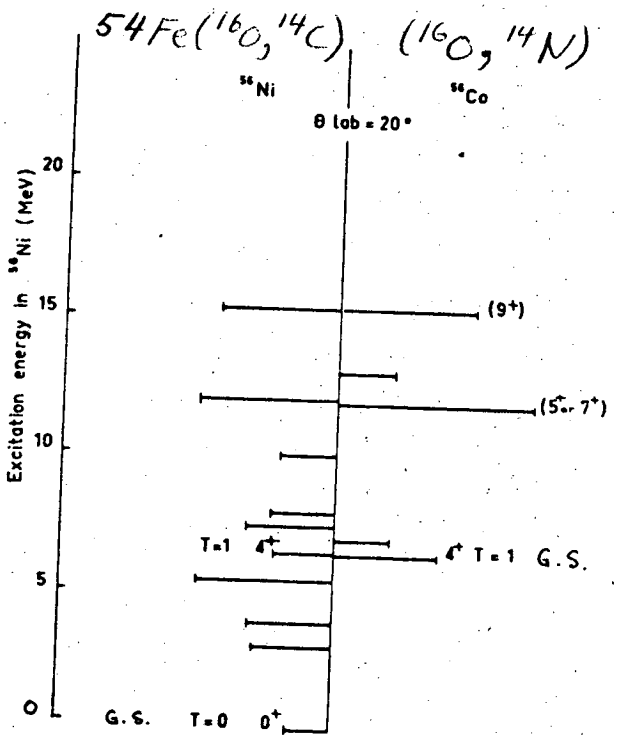

Comparison of the ^{56}Co energy levels to the ^{56}Ni ones. The ^{56}Co ground state (4^+) is aligned with the analogue 6.4 MeV (4^+) in ^{56}Ni

Fig. 40

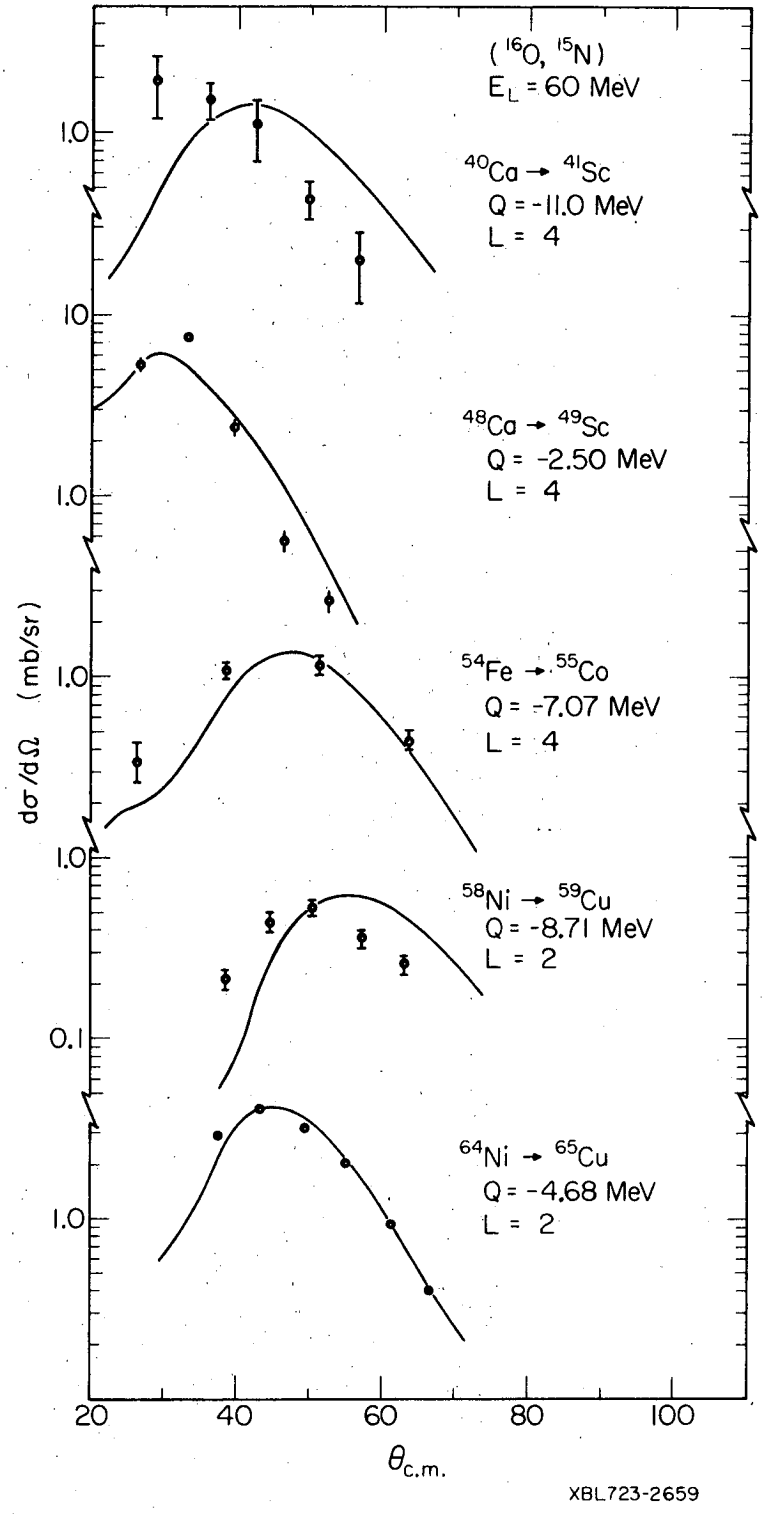
(^{16}O, ^{15}N)
E_L = 60 MeV
^{40}Ca → ^{41}Sc
Q = -11.0 MeV
L = 4
^{48}Ca → ^{49}Sc
Q = -2.50 MeV
L = 4
^{54}Fe → ^{55}Co
Q = -7.07 MeV
L = 4
^{58}Ni → ^{59}Cu
Q = -8.71 MeV
L = 2
^{64}Ni → ^{65}Cu
Q = -4.68 MeV
L = 2
dσ/dΩ (mb/sr)
1.0
10
1.0
1.0
1.0
0.1
1.0
20
40
60
80
100
$\theta_{c.m.}$
XBL723-2659

Fig. 41a

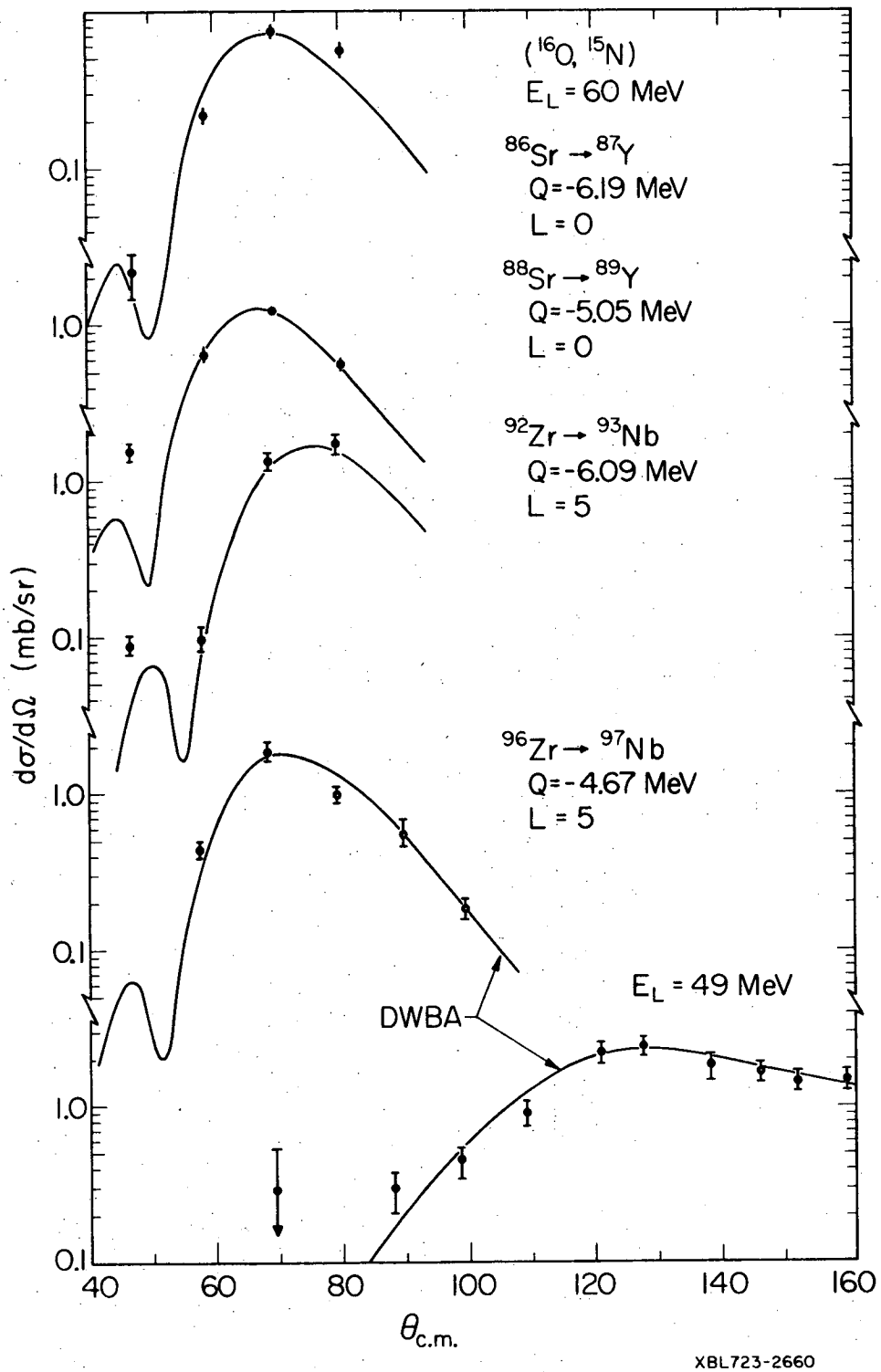
(^{16}O, ^{15}N)
E_L = 60 MeV
^{86}Sr → ^{87}Y
Q=-6.19 MeV
L = 0
^{88}Sr → ^{89}Y
Q=-5.05 MeV
L = 0
^{92}Zr → ^{93}Nb
Q=-6.09 MeV
L = 5
^{96}Zr → ^{97}Nb
Q=-4.67 MeV
L = 5
E_L = 49 MeV
DWBA
dσ/dΩ (mb/sr)
$\theta_{c.m.}$
XBL723-2660

Fig. 41b

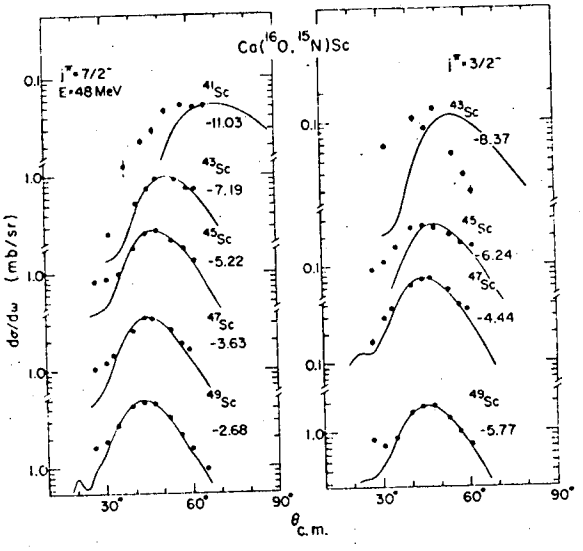

DWBA fits to the experimental Ca(^{16}O, ^{15}N)Sc angular distributions

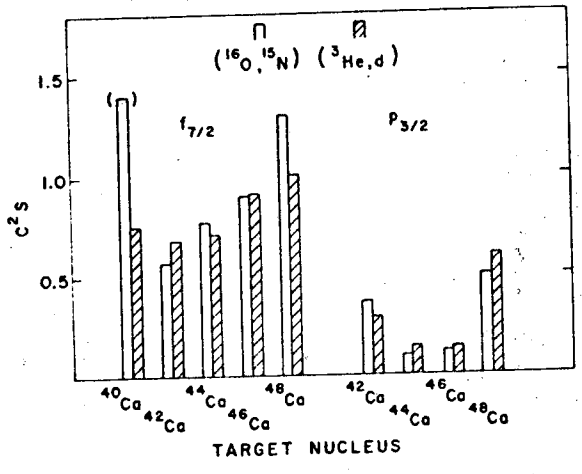

Comparison of (^{16}O, ^{15}N) and (^{3}He, d) spectroscopic factors for 1 $f_{7/2}$ and 2 $p_{3/2}$ proton transfer on the even-A Ca isotopes.

Fig. 42

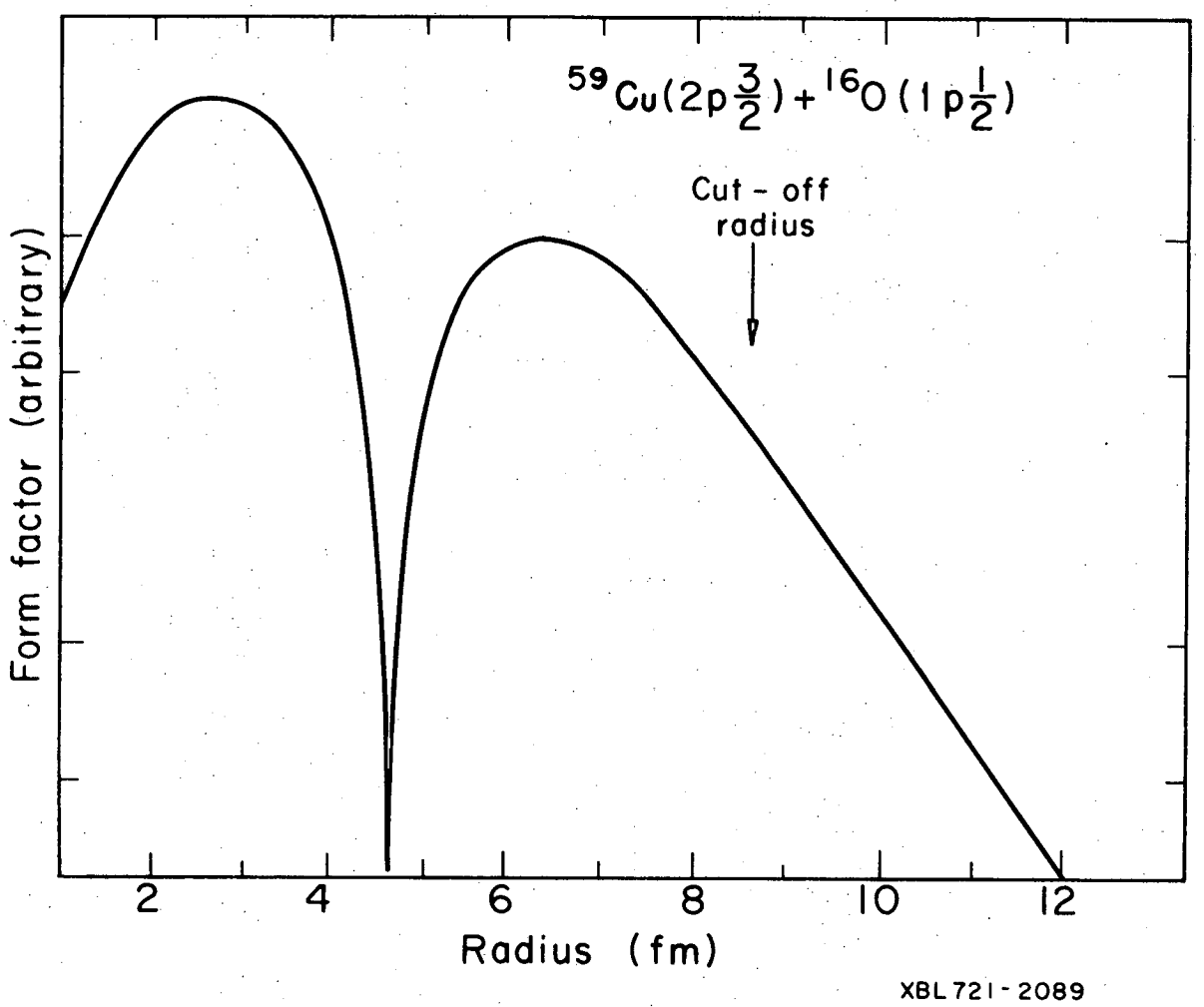
$^{59}Cu(2p\frac{3}{2}) + ^{16}O(1p\frac{1}{2})$
Cut - off radius
Form factor (arbitrary)
2
4
6
8
10
12
Radius (fm)
XBL721-2089

Fig. 43

Selection Rules

$a + A \rightarrow \underbrace{b}_{a-c} + \underbrace{B}_{A+c}$

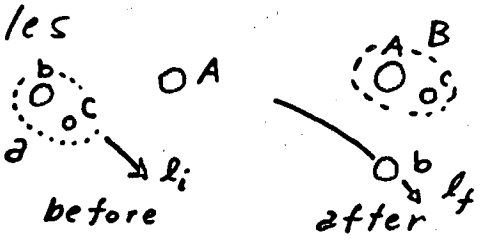

In a, c has: $n'l'j'$

In B, c has: $n\,l\,j$

Light ion reactions: $n'l'j' = 1s\frac{1}{2} \therefore l'=0, j'=\frac{1}{2}$

$(^3He,d), (\alpha,t)$ $\quad L \equiv |l_f - l_i| = l$ indep. of $j (= l \pm \frac{1}{2})$

$\sigma_{lj} \approx \sigma_{L=l}$ e.g. $nl_j = 1f_{7/2}, 1f_{5/2} \Rightarrow \sigma_{lj} = \sigma_{L=3}$

H.I. reactions: $(^{16}O,^{15}N)$: $n'l'j' = 1p\frac{1}{2}$ $\quad l'=1, j'=\frac{1}{2}$

$L = l+1$ for $j = l+\frac{1}{2}$ e.g. $L=4$ $nlj = 1f_{7/2}$

$= l-1$ for $j = l-\frac{1}{2}$ e.g. $L=2$ $nlj = 1f_{5/2}$

$\therefore \sigma_{lj} = \sigma_{L=l\pm1}$ for $j = l \pm \frac{1}{2}$

$(^{12}C,^{11}B)$: $n'l'j' = 1p\frac{3}{2}$ $\quad l'=1, j'=\frac{3}{2}$

$L = l+1, l-1$ for $j = l \pm \frac{1}{2}$ e.g. $L=4,2$ $nlj = 1f_{7/2,5/2}$

$\sigma_{lj} = \sigma_{L=l+1} + \sigma_{L=l-1}$

we find $\sigma_{L+1} \gg \sigma_{L-1}$ $\therefore \Rightarrow j$ dependence

Fig. 46

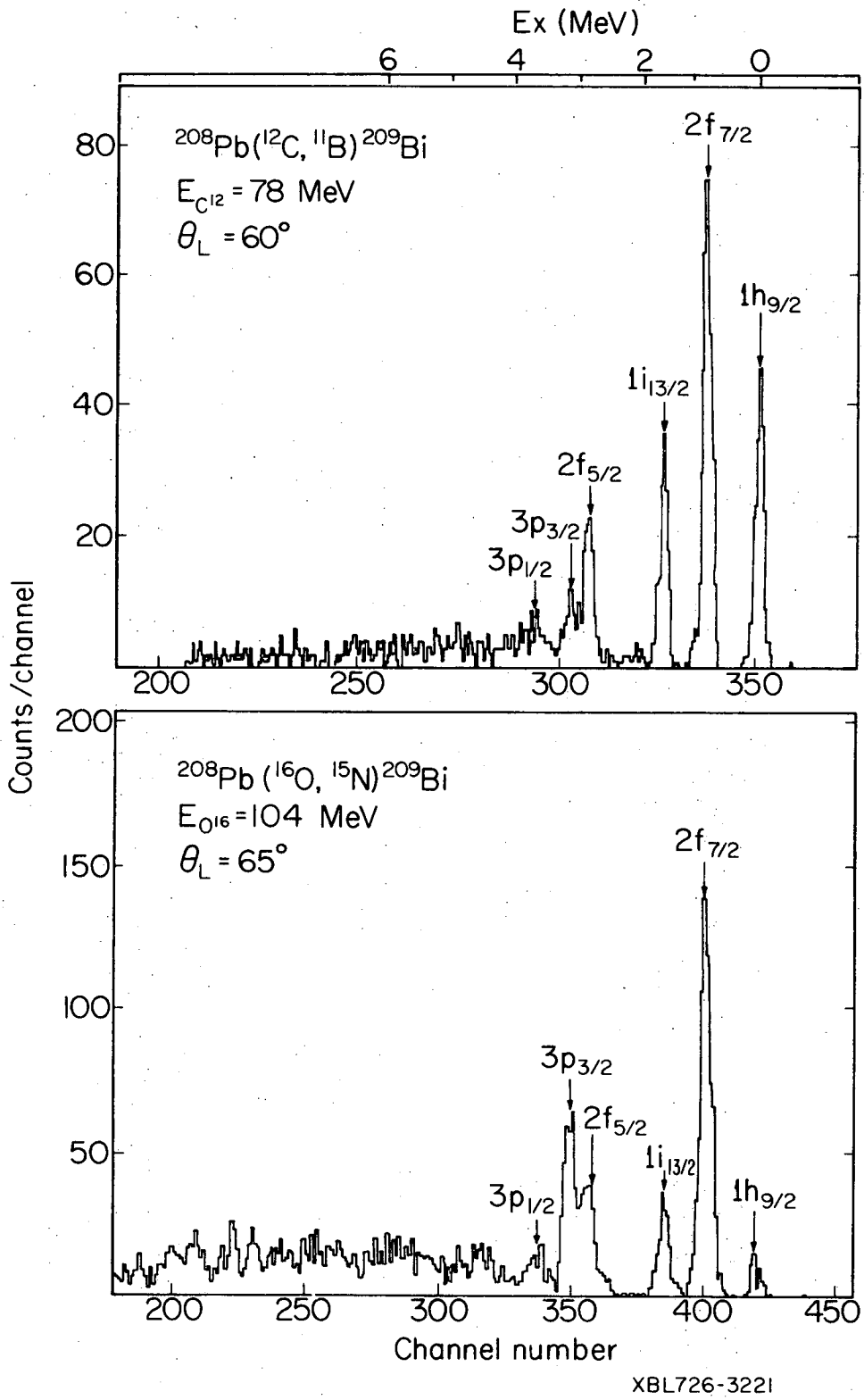
Ex (MeV)
6
4
2
0
$^{208}Pb(^{12}C, ^{11}B)^{209}Bi$
$E_{C^{12}} = 78$ MeV
$\theta_L = 60°$
$2f_{7/2}$
$1h_{9/2}$
$1i_{13/2}$
$2f_{5/2}$
$3p_{3/2}$
$3p_{1/2}$
80
60
40
20
200
250
300
350
$^{208}Pb\ (^{16}O, ^{15}N)^{209}Bi$
$E_{O^{16}} = 104$ MeV
$\theta_L = 65°$
$2f_{7/2}$
$3p_{3/2}$
$2f_{5/2}$
$1i_{13/2}$
$3p_{1/2}$
$1h_{9/2}$
200
150
100
50
200
250
300
350
400
450
Counts /channel
Channel number
XBL726-3221

Fig. 47

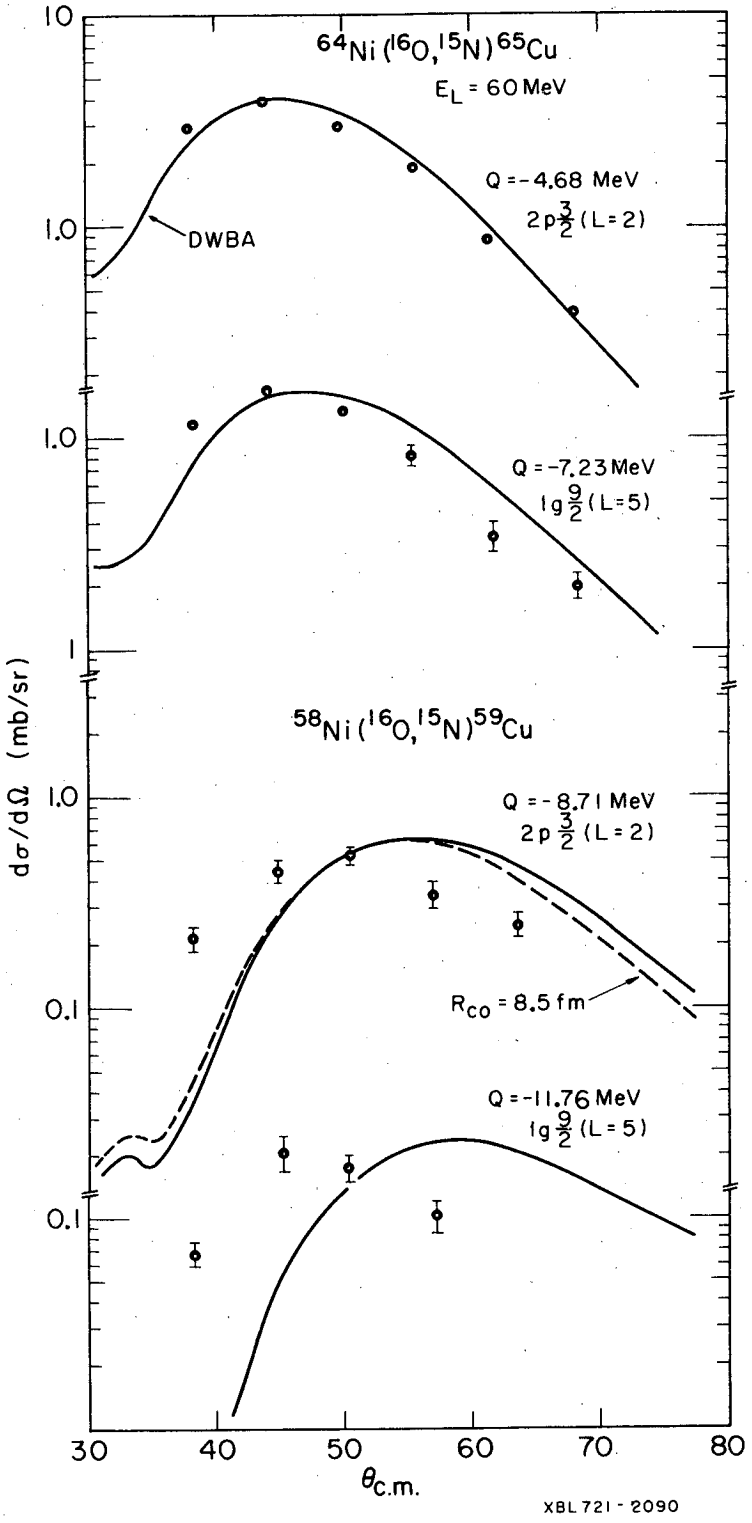
$^{64}Ni(^{16}O,^{15}N)^{65}Cu$
E_L = 60 MeV
Q = -4.68 MeV
$2p\frac{3}{2}$ (L=2)
DWBA
Q = -7.23 MeV
$1g\frac{9}{2}$ (L=5)
$^{58}Ni(^{16}O,^{15}N)^{59}Cu$
Q = -8.71 MeV
$2p\frac{3}{2}$ (L=2)
R_{co} = 8.5 fm
Q = -11.76 MeV
$1g\frac{9}{2}$ (L=5)
$d\sigma/d\Omega$ (mb/sr)
$\theta_{c.m.}$
XBL721-2090

Fig. 44

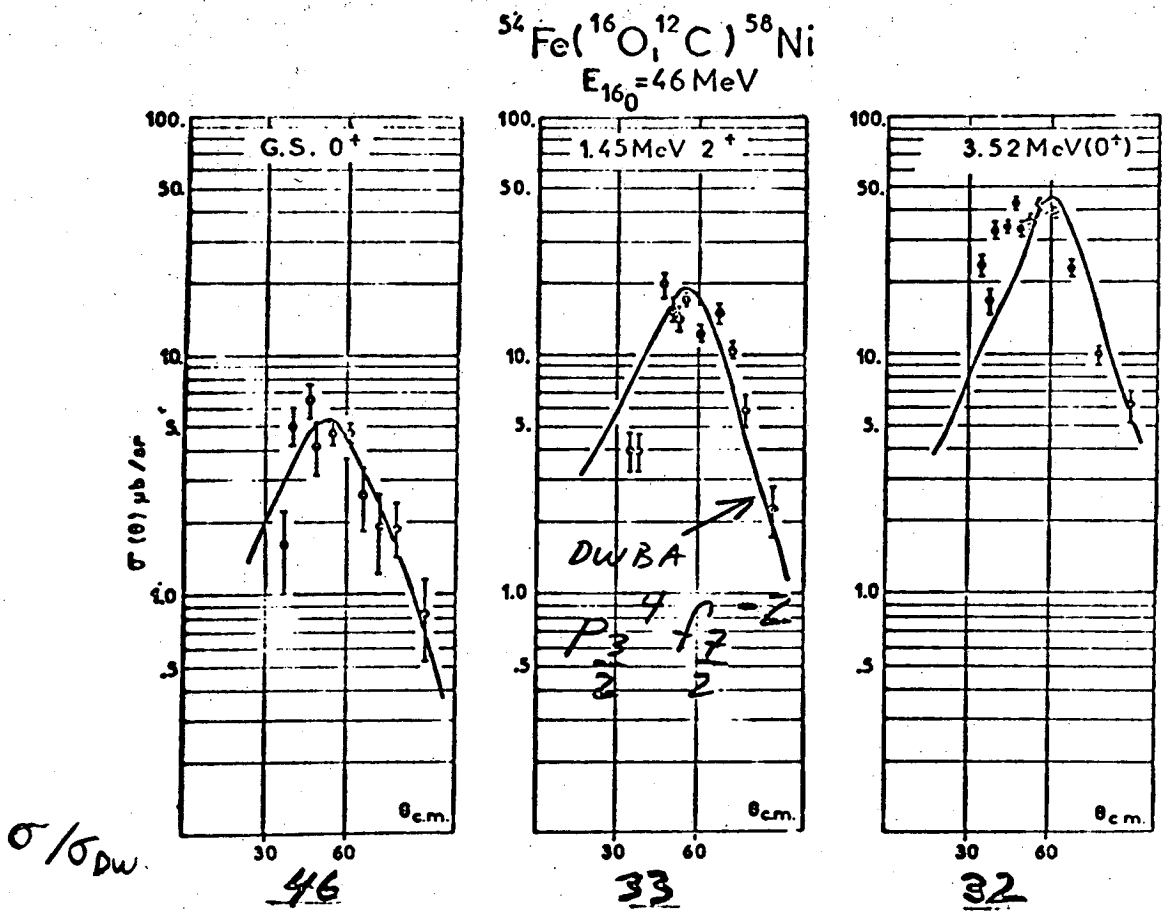
$^{54}Fe(^{16}O,^{12}C)^{58}Ni$
E_{16_O}=46 MeV
G.S. 0⁺
1.45MeV 2⁺
3.52MeV(0⁺)
σ (θ) μb/sr
θc.m.
DWBA
$p_{\frac{3}{2}}$ $f_{\frac{7}{2}}$
σ/σDW
46
33
32

Fig. 45

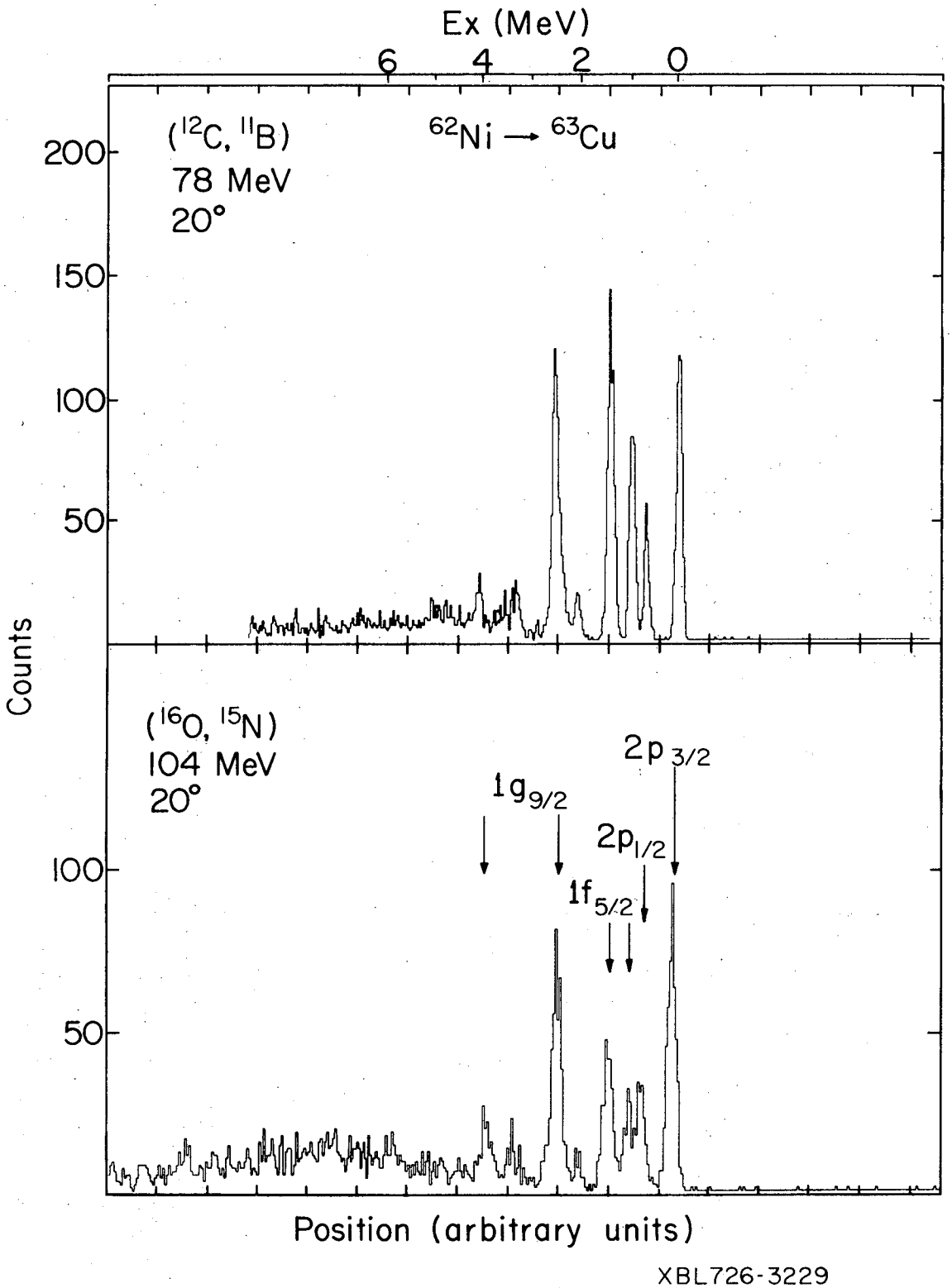
Ex (MeV)
6
4
2
0
$^{62}Ni \rightarrow {}^{63}Cu$
$(^{12}C, {}^{11}B)$
78 MeV
20°
200
150
100
50
Counts
$(^{16}O, {}^{15}N)$
104 MeV
20°
$1g_{9/2}$
$2p_{3/2}$
$2p_{1/2}$
$1f_{5/2}$
100
50
Position (arbitrary units)
XBL726-3229

Fig. 48

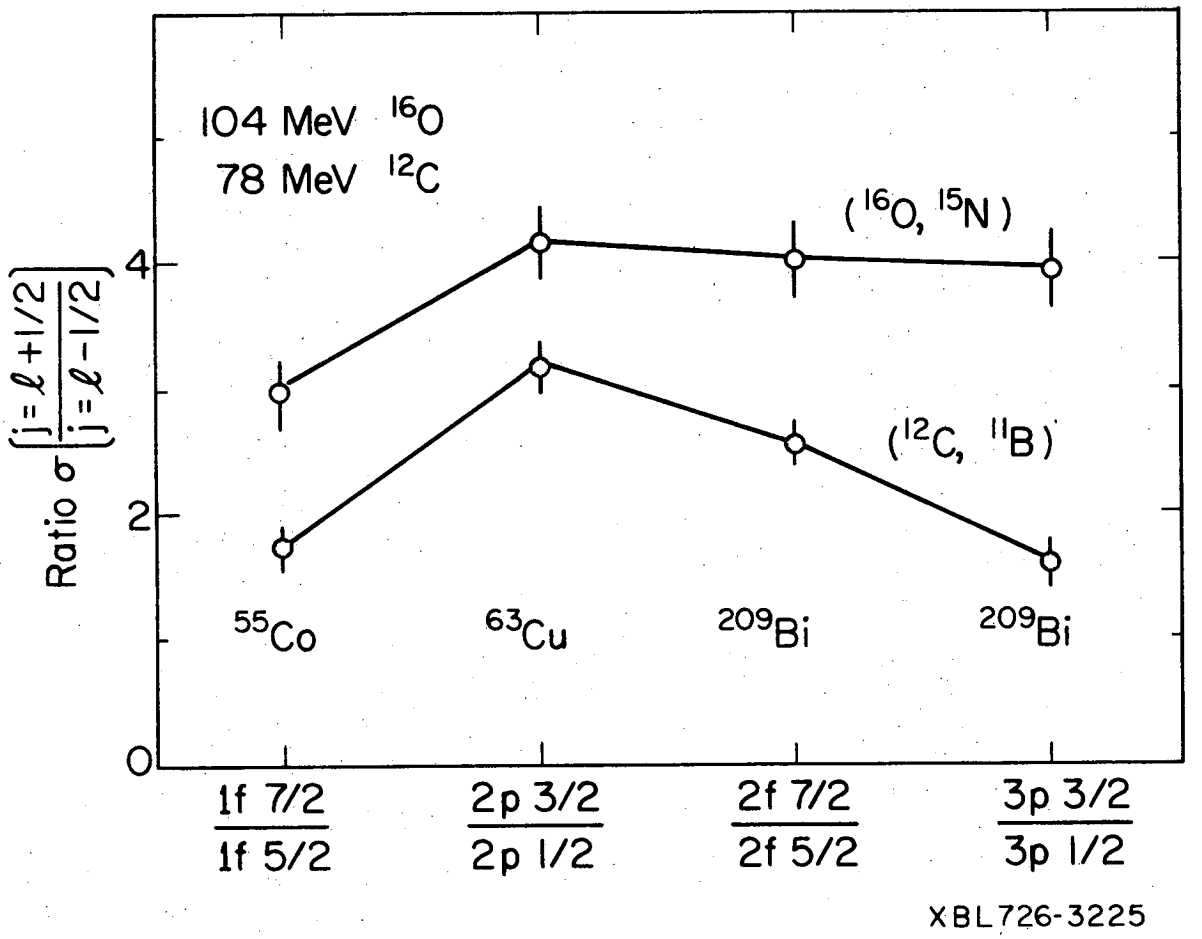
104 MeV ^{16}O
78 MeV ^{12}C
$(^{16}O, ^{15}N)$
$(^{12}C, ^{11}B)$
Ratio $\sigma \left[\frac{j=\ell+1/2}{j=\ell-1/2}\right]$
0
2
4
^{55}Co
^{63}Cu
^{209}Bi
^{209}Bi
1f 7/2 / 1f 5/2
2p 3/2 / 2p 1/2
2f 7/2 / 2f 5/2
3p 3/2 / 3p 1/2
XBL726-3225

Fig. 49

^{209}Bi SPECTROSCOPIC FACTORS

	$(^{16}O,^{15}N)$ 104 MeV		$(^{12}C,^{11}B)$ 78 MeV		$(^{16}O,^{15}N)$ 69 MeV		$(^{16}O,^{15}N)$ 69 MeV
	L	S	L	S	S	$S\frac{104}{69}$	S
$1h_{9/2}$	4	2.8	4,6	0.6	2.3	1.25	3±2.5
$2f_{7/2}$	4	0.9	2,4	<u>1.0</u>	<u>1.0</u>	0.95	1.1±0.1
$1i_{13/2}$	7	0.7	5,7	0.8	0.9	0.73	1.0±0.1
$2f_{5/2}$	2	3.1	2,4	0.5	1.3	2.43	1.0±0.3
$3p_{3/2}$	2	0.9	0,2	1.7	1.3	0.73	
$3p_{1/2}$	0	3.6	2	0.6	2.8	1.31	——
	LBL						

L rules from "no recoil" approx. (see Buttle & Goldfarb)

σ 104/69 $\sim 10^2$

Fig. 51

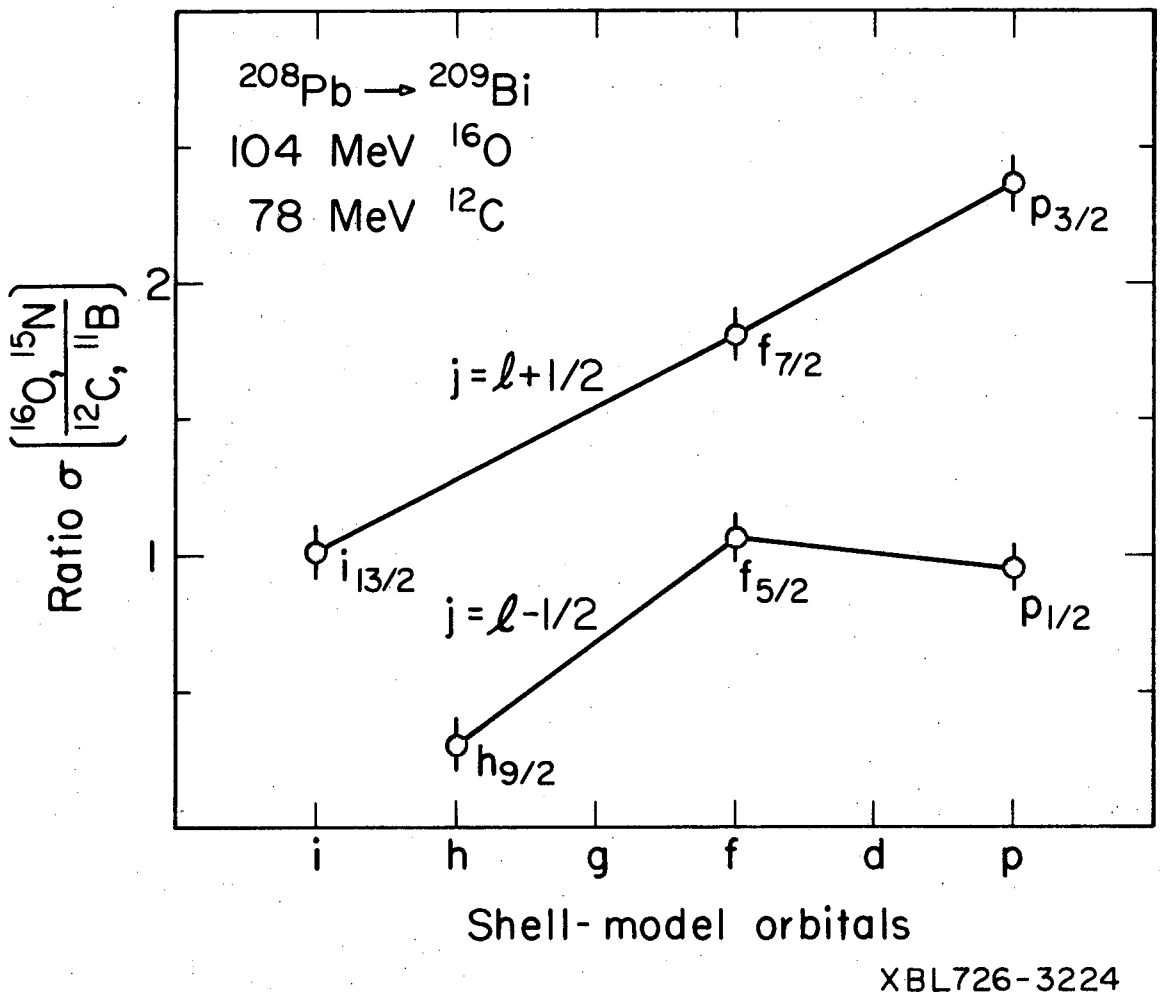
$^{208}Pb \rightarrow {}^{209}Bi$
104 MeV ^{16}O
78 MeV ^{12}C
Ratio $\sigma \left[\frac{^{16}O, ^{15}N}{^{12}C, ^{11}B}\right]$
2
1
$j = \ell + 1/2$
$j = \ell - 1/2$
$i_{13/2}$
$h_{9/2}$
$f_{7/2}$
$f_{5/2}$
$p_{3/2}$
$p_{1/2}$
i
h
g
f
d
p
Shell-model orbitals
XBL726-3224

Fig. 50

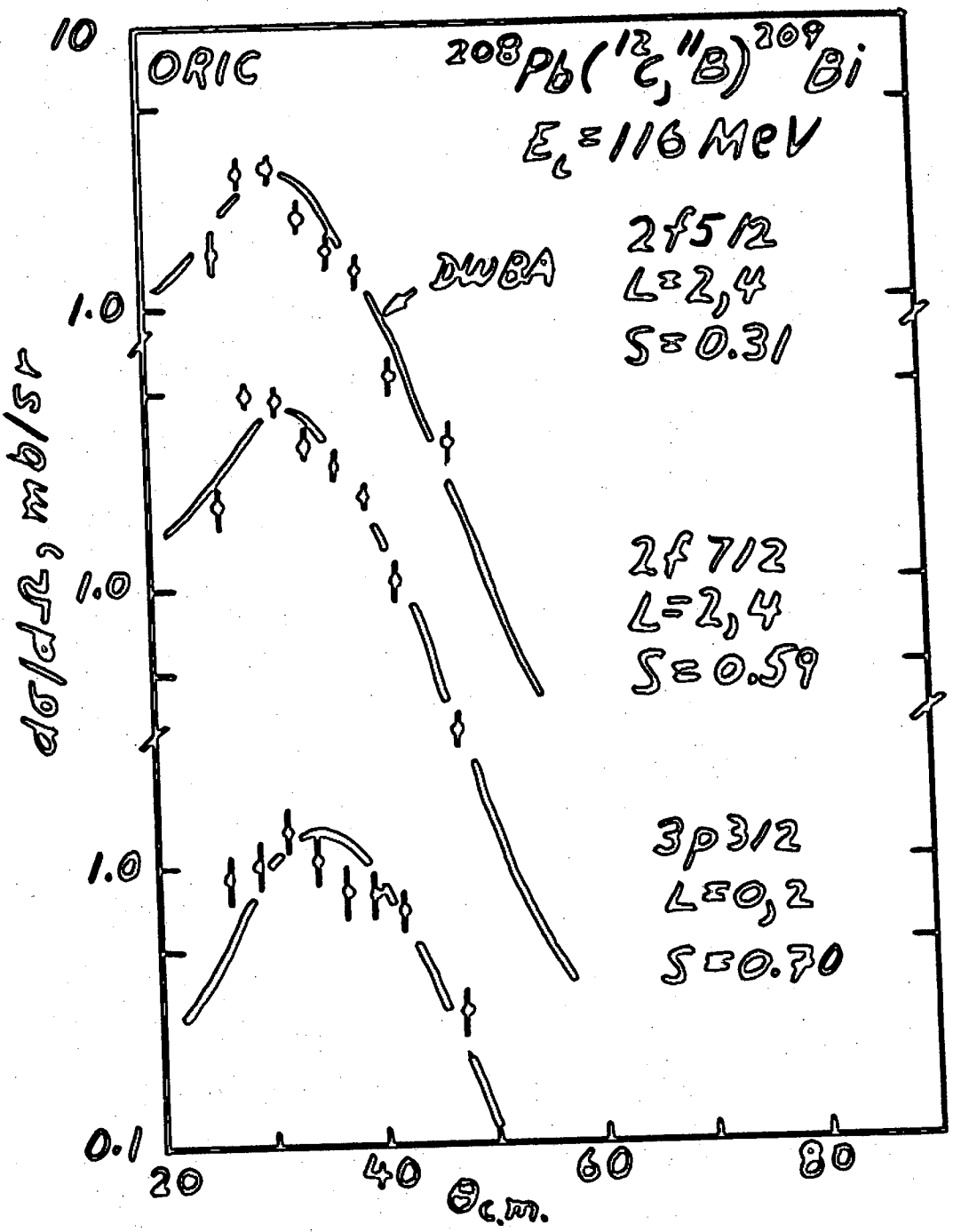
ORIC
$^{208}Pb(^{12}C,^{11}B)^{209}Bi$
E_L=116 MeV
DWBA
2f5/2
L=2,4
S=0.31
2f7/2
L=2,4
S=0.59
3p3/2
L=0,2
S=0.70
dσ/dΩ, mb/sr
10
1.0
1.0
1.0
0.1
20
40
60
80
θc.m.

Fig. 52

COULOMB + NUCLEAR EXCITATION

$$F_L(r) = \underbrace{F_L^C(r)}_{\text{Coulomb}} + \underbrace{F_L^N(r)}_{\text{Nuclear}}$$

$$F_L^C(r) = \frac{eZ_1}{2L+1}\frac{4\pi\sqrt{B(EL)}}{r^{L+1}}$$

$$F_L^N(r) = \beta_L^N\left(V_R R_R \frac{df}{dr} + iW_I R_I \frac{df}{dr}\right)$$

F_L^C, F_L^N of opposite sign $\Rightarrow$ interference

β_L^N = OM potential deformation < mass deformation of target ($=\beta_m$)

We use

$$\beta_m R_m \approx \beta_L^N R_R \quad \text{where} \quad R_m = 1.3\, A_2^{1/3}$$

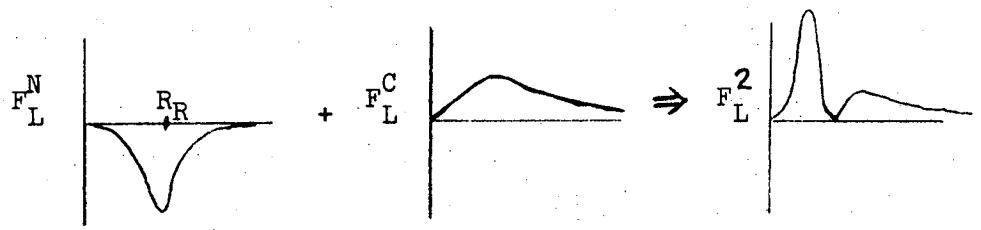

Fig. 53

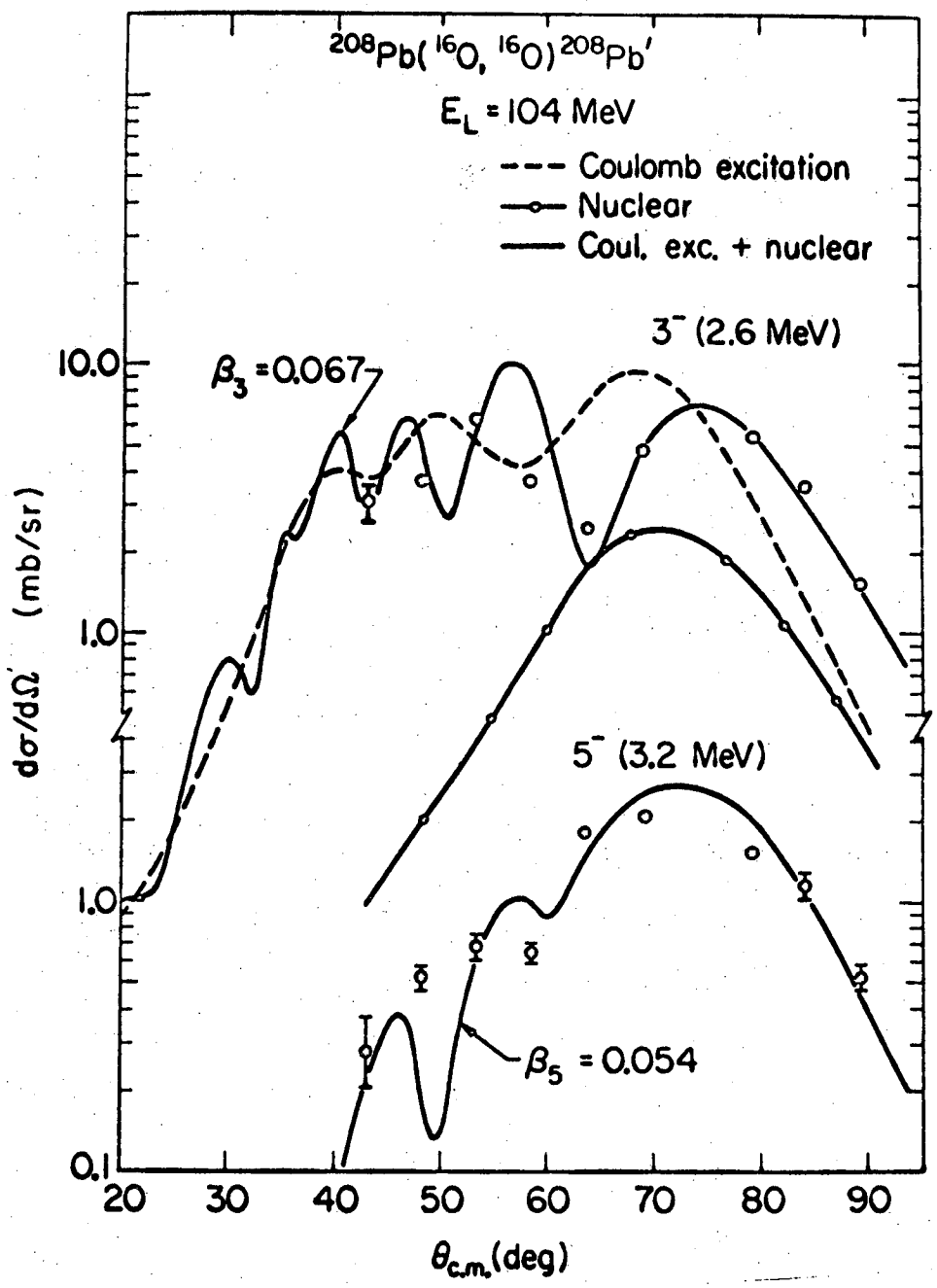
$^{208}Pb(^{16}O, ^{16}O)^{208}Pb'$
E_L = 104 MeV
Coulomb excitation
Nuclear
Coul. exc. + nuclear
3⁻ (2.6 MeV)
β_3 = 0.067
5⁻ (3.2 MeV)
β_5 = 0.054
$d\sigma/d\Omega$ (mb/sr)
10.0
1.0
1.0
0.1
20
30
40
50
60
70
80
90
$\theta_{c.m.}$(deg)

Fig. 54

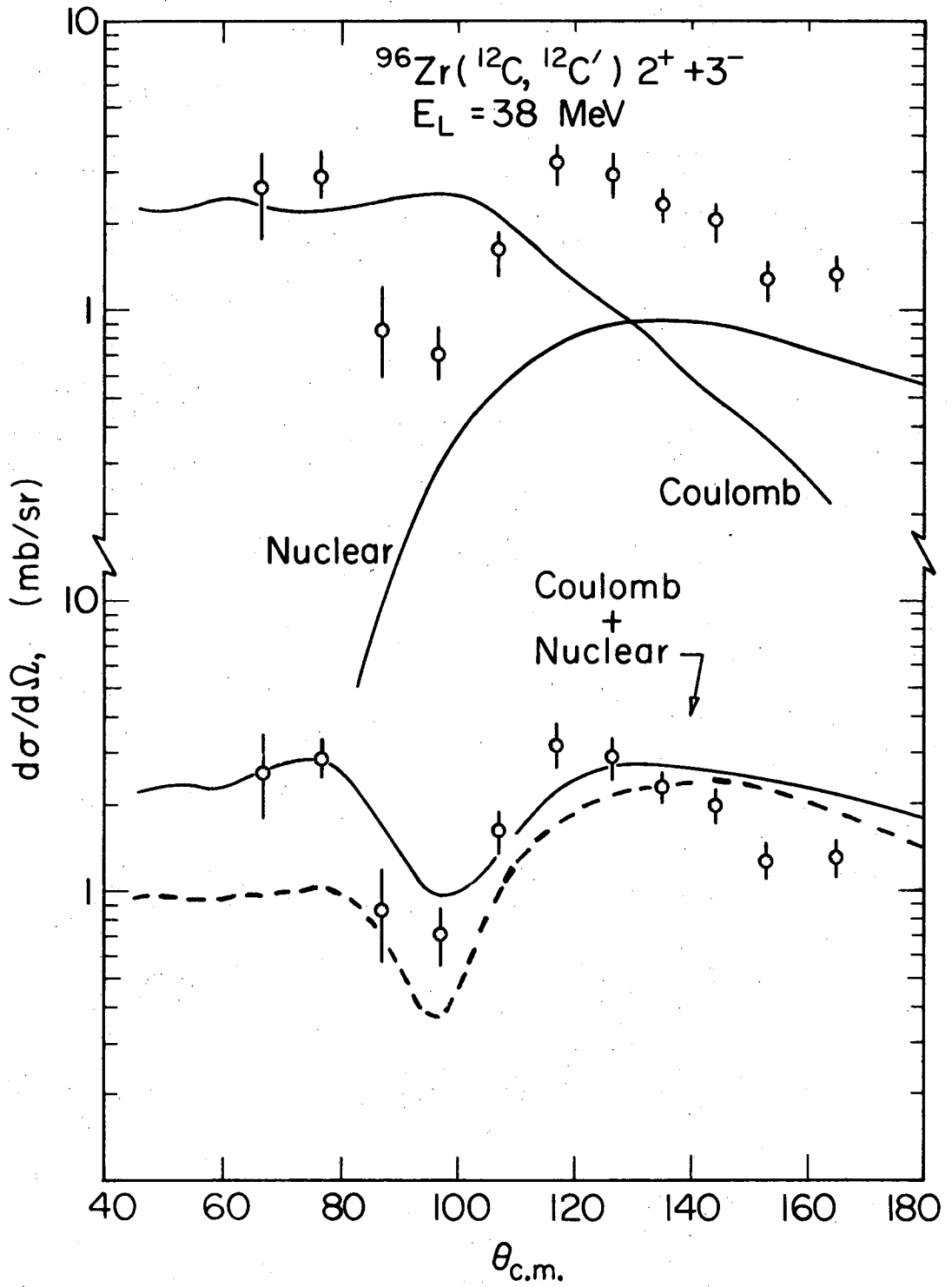
$^{96}Zr(^{12}C, ^{12}C')\ 2^+ + 3^-$
$E_L = 38$ MeV
Coulomb
Nuclear
Coulomb
+
Nuclear
10
1
10
1
40
60
80
100
120
140
160
180
$d\sigma/d\Omega$, (mb/sr)
$\theta_{c.m.}$
XBL723-2657A

Fig. 55

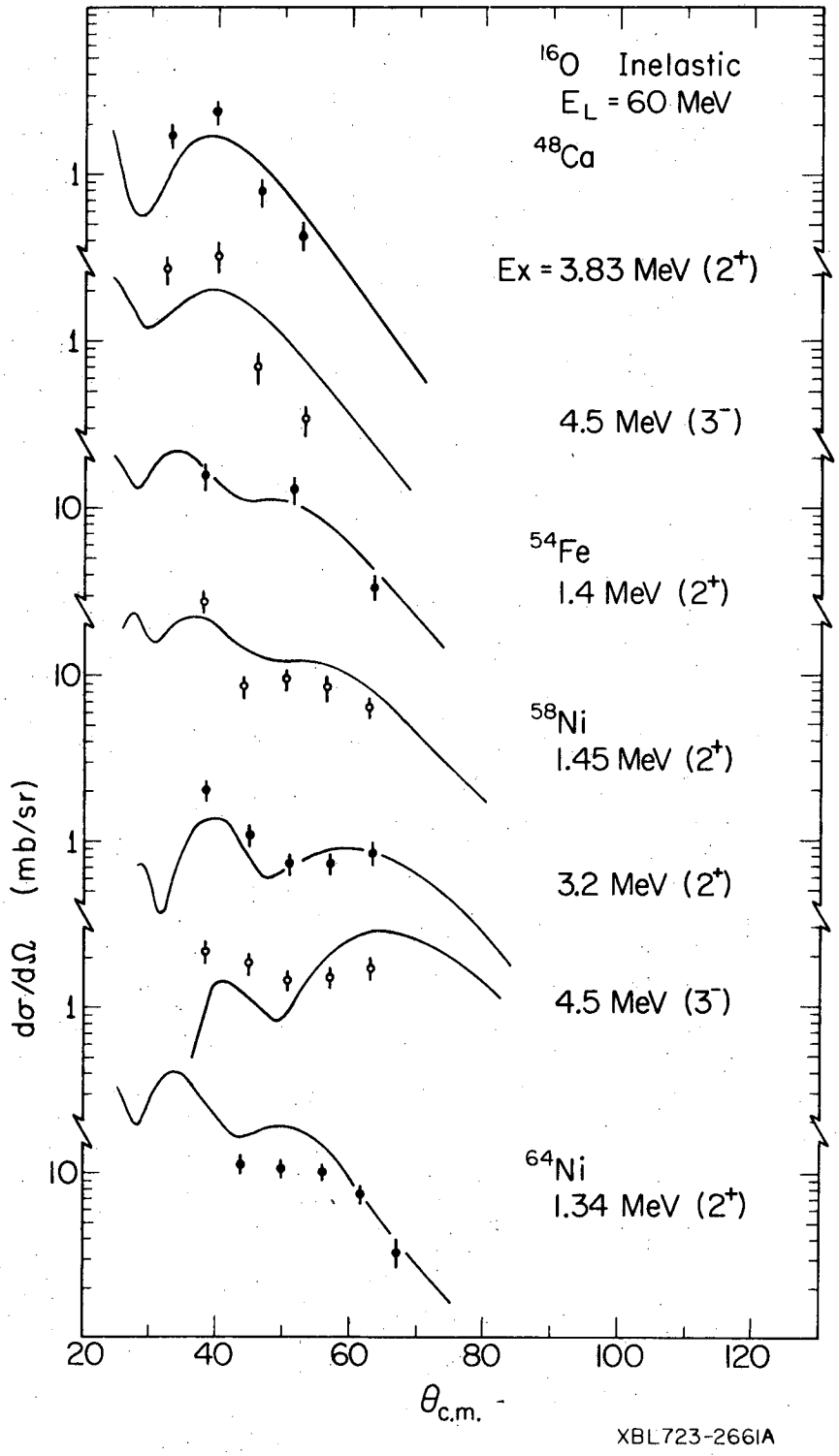
^{16}O Inelastic
E_L = 60 MeV
^{48}Ca
Ex = 3.83 MeV (2$^+$)
4.5 MeV (3$^-$)
^{54}Fe
1.4 MeV (2$^+$)
^{58}Ni
1.45 MeV (2$^+$)
3.2 MeV (2$^+$)
4.5 MeV (3$^-$)
^{64}Ni
1.34 MeV (2$^+$)
dσ/dΩ (mb/sr)
1
1
10
10
1
1
10
20
40
60
80
100
120
$\theta_{c.m.}$
XBL723-2661A

Fig. 56

Deformation Parameters

Nucleus	Ex, MeV	J^π	OM Set	B(EL) W.u.	β	β_M	Other Meas.
60 MeV ^{16}O							
^{48}Ca	3.83	2^+	II	1.7	0.06	0.10	0.13
	4.50	3^-	II	5.4	0.08	0.134	(0.18)
^{54}Fe	1.40	2^+	II	8.7	0.088	0.147	0.18
	3.00	2^+	II	3.0	0.08	0.134	0.14
^{58}Ni	1.45	2^+	II	9.9	0.092	0.152	0.187
			III	9.9	0.187	0.26	
			IV	9.9	0.044		
	3.20	2^+	II	1.2	(0.044)	0.074	0.06
		$+2^+$		+2.3			0.08
	4.50	3^-	II	13.3	(0.12)	0.198	0.16
^{64}Ni	1.34	2^+	II	(11.4)	0.112	0.182	0.192
^{88}Sr	1.84	2^+	II	8.5	0.085	0.133	(0.12)
^{96}Zr	1.8	2^+	II	(2)			0.06
		$+3^-$		(18)	0.12	0.186	0.165
		3^-	III		0.148	0.192	
		3^-	IV		0.230		
	3.2	2^+	II	(8)	0.073	0.113	0.02
38 MeV ^{12}C							
^{96}Zr	1.8	2^+	II	(2)			0.06
		$+3^-$		(18)	0.122	0.189	0.165
		2^+	II	(2)			0.06
		$+3^-$		(18)			0.165

Fig. 57

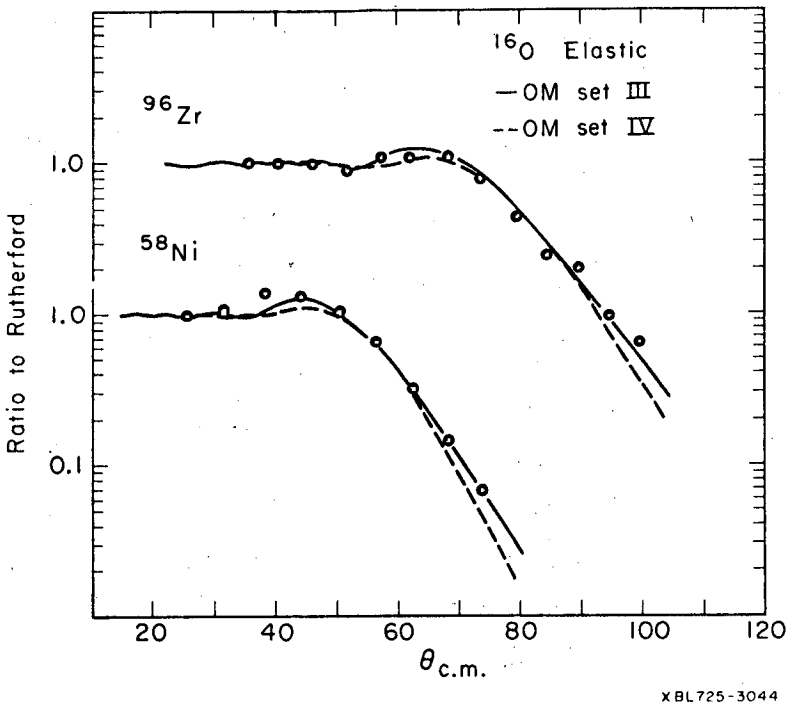
^{16}O Elastic
—OM set III
--OM set IV
^{96}Zr
^{58}Ni
1.0
1.0
0.1
Ratio to Rutherford
20
40
60
80
100
120
$\theta_{c.m.}$
XBL725-3044

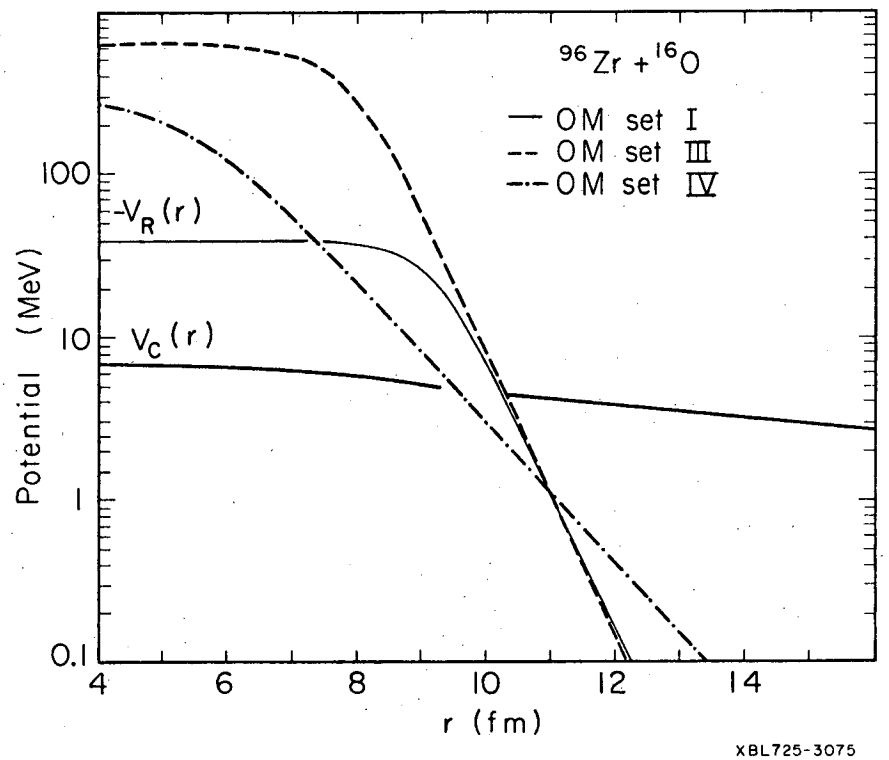
^{96}Zr + ^{16}O
— OM set I
-- OM set III
-·- OM set IV
100
$-V_R(r)$
10
$V_C(r)$
1
0.1
Potential (MeV)
4
6
8
10
12
14
r (fm)
XBL725-3075

Fig. 58

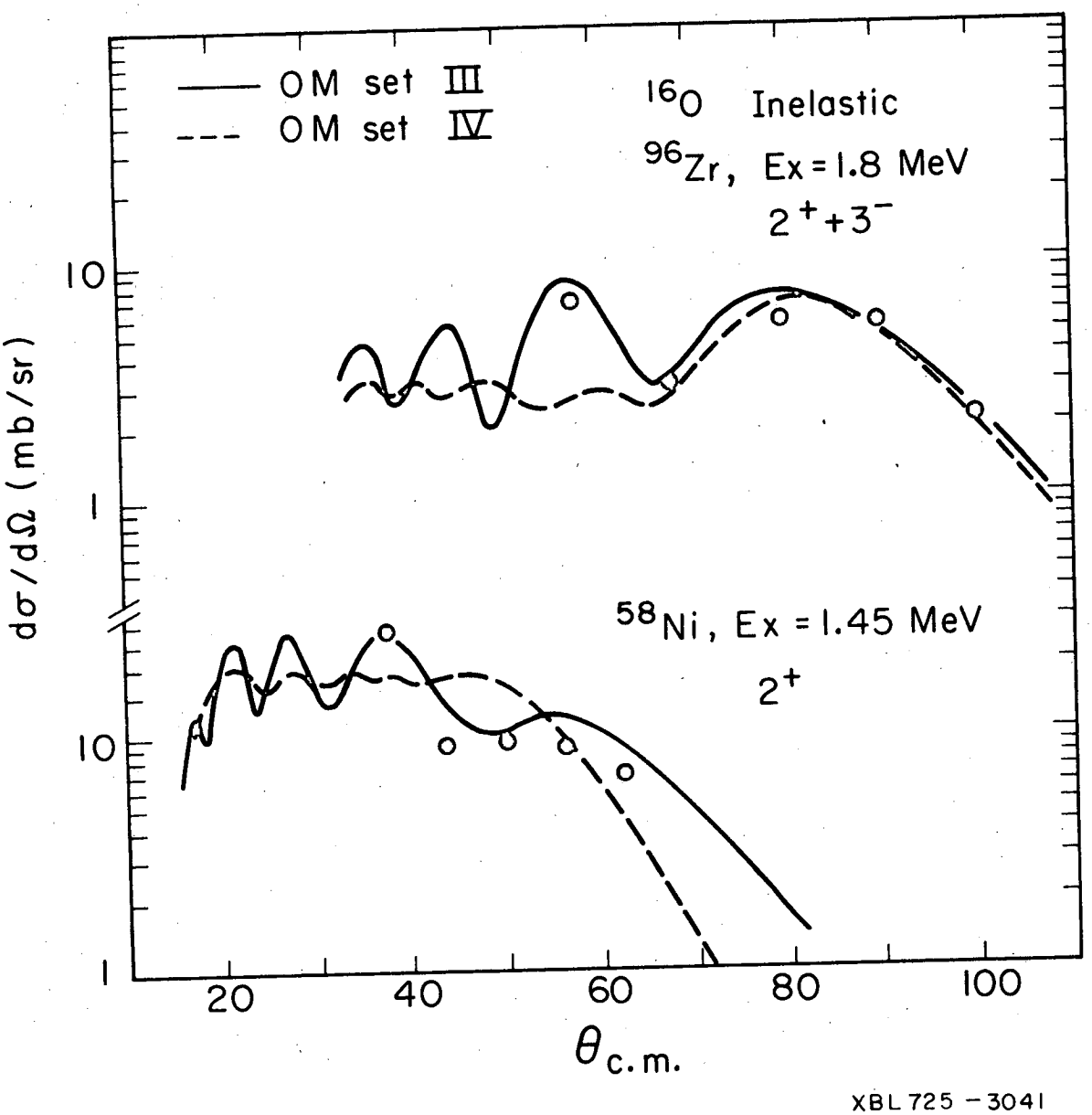
OM set III
OM set IV
^{16}O Inelastic
^{96}Zr, Ex = 1.8 MeV
$2^+ + 3^-$
^{58}Ni, Ex = 1.45 MeV
2^+
$d\sigma/d\Omega$ (mb/sr)
10
1
10
1
20
40
60
80
100
$\theta_{c.m.}$
XBL 725 - 3041

Fig. 59

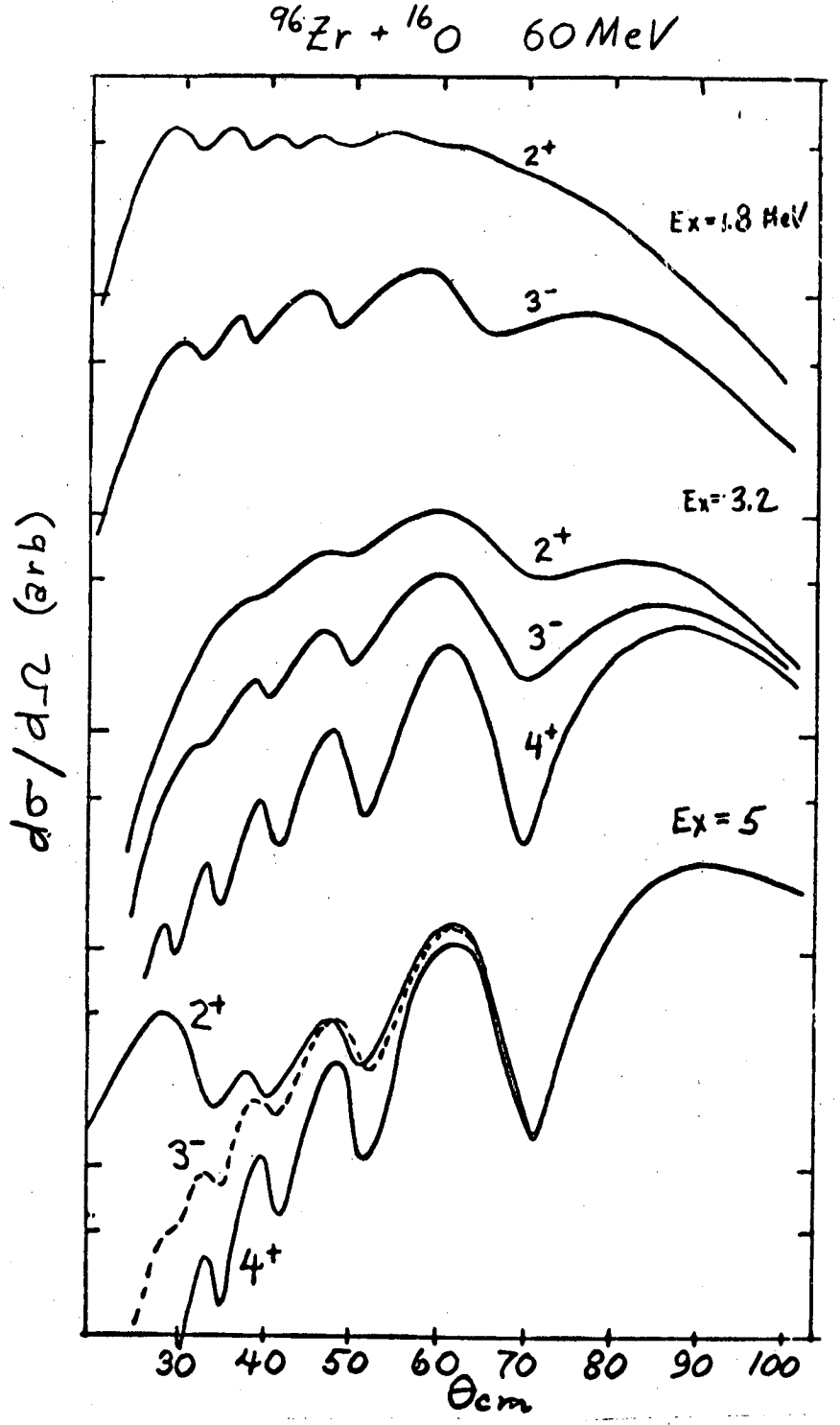
$^{96}Zr + ^{16}O$ 60 MeV
2+
Ex=1.8 MeV
3-
Ex=3.2
2+
3-
4+
Ex=5
2+
3-
4+
dσ/dΩ (arb)
30
40
50
60
70
80
90
100
θcm

Fig. 60

TECHNICAL INFORMATION DIVISION
LAWRENCE BERKELEY LABORATORY
UNIVERSITY OF CALIFORNIA
BERKELEY, CALIFORNIA 94720